BEHAVIOR OF DIAGONAL KNEE

MOMENT END-PLATE CONNECTIONS

by

Vincenza M. Italiano

Thesis submitted to the faculty of the

Virginia Polytechnic Institute and State University

In partial fulfillment of the requirements for the degree of

MASTER OF SCIENCE

in

CIVIL ENGINEERING

APPROVED:

Thomas M. Murray, Chairman

W. Samuel Easterling

Carin L. Roberts-Wollmann

May 2001

Blacksburg, Virginia

BEHAVIOR OF DIAGONAL KNEE

MOMENT END-PLATE CONNECTIONS

by
Vincenza M. Italiano

Thomas M. Murray, Chairman
Civil Engineering

ABSTRACT

An experimental and analytical investigation was conducted to study the behavior of diagonal knee moment end-plate connections and a multiple row extended moment end-plate connection. Diagonal knee moment end-plate connections differ from typical moment end-plate connections because of the large pitch distance required between the top flange and first row of tension bolts. The large pitch distance is outside of the geometric parameters of all previous research. Design solutions are presented for five moment end-plate connections with provisions added to accommodate these parameters.

The analytical investigation focused on the limit states of end-plate yielding and bolt rupture. Yield-line analysis was used to predicted end-plate yielding and a simplified Kennedy method proposed by Borgsmiller and Murray (1995) was used to predict bolt rupture including and excluding prying forces. An experimental investigation was conducted to verify the design solutions. Five knee area specimens and one plate girder specimen were tested in this study.

The analytical and experimental results are analyzed and compared. For the test specimens that failed in the connection, the predicted results proved to be conservative. Recommendations are presented at the end of the study as well as sample calculations.

ACKNOWLEDGEMENTS

The author would like to extend her sincere thanks to Dr. Thomas Murray for his unending guidance and support over the last two years. A special thanks also goes to Dr. Samuel Easterling and Dr. Carin Roberts-Wollmann for serving as committee members and to NCI Building Systems, who sponsored the reseach.

There are several individuals who provided invaluable help during the experimental reseach. They include Brett Farmer, Dennis Huffman, Ricky Woods, Clark Brown, Denson Graham, J.R. Mugajic, Jason Piotter, Tom Ramskill, and Alvin Trout. A special thanks is extended to Scott Cortese and Emmett Sumner, who assitance extended through all phases of this study.

Finally, the author would like to thank her family. Without their constant encouragement and love, none of this would be possible.

TABLE OF CONTENTS

LIST OF FIGURES

LIST OF FIGURES, Con't

LIST OF TABLES

CHAPTER I

INTRODUCTION

1.1 INTRODUCTION

Bolted moment end-plate connections are commonly used in rigid steel gable frames. This connection type can be used to join a web-tapered column to a web-tapered rafter on a diagonal to the beam flanges. The area surrounding the diagonal connection of the column to the rafter is often referred to as a "diagonal knee". Thus, this type of connection is called a diagonal knee moment end-plate connection.

A moment end-plate consists of a plate, shop-welded to the end of a beam and then bolted in the field to the connecting element. Some of the many advantages of moment end-plate connections include the elimination of field welding, ease in the erection process and the formation of a rigid moment resistant connection. Moment end-plate connections can be classified as either flush or extended. Flush end-plates are level with the beam flanges and all bolts are contained between the beam flanges. Extended end-plates extend beyond the beam flanges and allow for bolts to be placed in the extension. In general, flush end-plates are used for smaller loads or near the inflection points of gable frames (Murray 1988). Extended end-plates are used for heavier loads and are more resistant to rotation than flush end-plates (Bond 1989). Extended end-plates are more common in multi-story buildings for beam-to-column connections and beam-to-beam, or "splice" connections. Both flush and extended end-plates can be stiffened. In

stiffened flush end-plates, a gusset plate is welded to the beam web and the end-plate near the bolt rows. In stiffened extended end-plates, a gusset plate is welded to the outer tension flange and the end-plate extension.

In recent years, much research has been done on the study of moment end-plate connections for use in beam-to-beam connections and beam-to-column connections. The establishment of a unified method for the design of numerous end-plate configurations has been ongoing based on the limit states of end-plate yielding and bolt rupture. This method has been expanded and improved over the last fifteen years (Mays 2000a). Currently, the yield line pattern developed by Mays (2000a) is used to predict the end-plate yield strength, while the simplified Kennedy method proposed by Borgsmiller and Murray (1995) is used to predict bolt rupture. To the author's knowledge, no research has been conducted to apply the unified method to the design of diagonal knee moment end-plate connections for tapered steel members in rigid gable frames.

The design of diagonal knee moment end-plate connections differs slightly from the design used in prismatic steel members. Because the connection is at a diagonal to the beam flange as opposed to a right angle, the first row of bolts on the tension side must be placed further away from the tension flange to allow for a bolt to be inserted and properly tightened. Thus, the diagonal knee connections have a larger distance between the tension flange and the first line of bolts. This pitch distance, p_f, is outside the parameters of all other moment end-plate connections previously tested. Therefore, current design procedures must be adjusted to accommodate these new parameters.

This study continues the unification process in two ways. First, it adds provisions to account for an excessive pitch distance, allowing the design procedures to be applied

to diagonal knee moment end-plate connections. Secondly, it provides design solutions for two connection configurations not previously analyzed: the eight-bolt flush unstiffened connection and the multiple row extended ¼ (one row outside and four rows inside) unstiffened connection.

1.2 LITERATURE REVIEW

A unification of the procedures used for the design of moment end-plate connections has been ongoing for approximately 15 years (Mays 2000). The design procedures concentrate on the limit states of end-plate yielding and bolt rupture. All design procedures to be discussed below use yield-line analysis to predict the design strength of the end-plate, and some variation of the split tee analogy proposed by Kennedy *et al* (1981).

Kennedy *et al* (1981) used a split-tee analogy to predict bolt forces in bolted splices and beam column connections. As shown in Figure 1.1, a tee stub with two bolts was used as the model for the analysis in which the stem or web of the tee is equivalent to the beam flange, and where 2F = the applied flange force, B = the bolt force per bolt, and Q = the prying force per bolt. The contribution of the web to the moment capacity of the section is ignored in the analysis and thus, is not included in the model. The split-tee analogy assumes that the design of an end-plate is controlled by the stresses that develop around the tension flange and the neighboring bolts. It also assumes that the end-plate deforms about the beam tension flange.

Kennedy *et al* (1981) used the split tee analogy to define three cases of end-plate behavior based on the thickness of the end-plate and the load applied through the beam

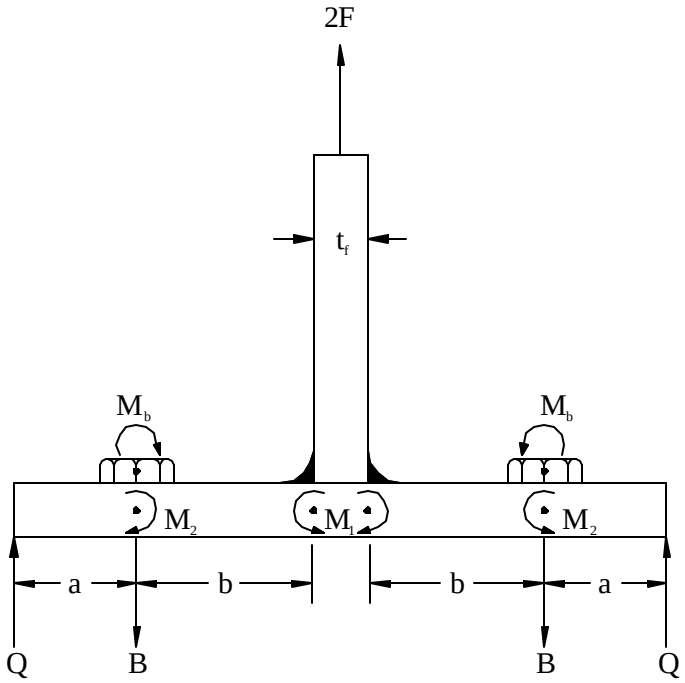

Figure 1.1 Kennedy Split Tee Analogy Model (Kennedy *et al* 1981)

tension flange. In each case, equations are formulated for the required end-plate thickness, associated prying force and bolt force per bolt. The three cases of plate behavior are thick plate behavior, intermediate plate behavior, and thin plate behavior. Each case is illustrated in Figure 1.2.

Thick plate behavior, shown in Figure 1.2a, occurs in all end-plates at low applied loads. During this stage of plate behavior, no plastic hinges have formed in the end-plate. Thus, the prying forces are equal to zero. The upper limit of thick plate behavior occurs when plastic hinges develop at each face of the beam tension flange and is found by the iteration of

$$t_1 = \sqrt{\frac{2(2F)b}{w\sqrt{F_{py}^2 - 3\left(\frac{F}{wt_1}\right)^2}}} \qquad (1.1)$$

where b = the distance from the face of the beam flange to the nearest bolt centerline, w = the width of the end-plate per bolt pair, F_{py} = the yield stress of the end-plate material, and t_1 = the thick plate limit. If the thickness of the end plate, t_p, is greater than or equal to the thick plate limit, $t_p < t_1$, then the end-plate is exhibiting thick plate behavior. During this stage, the force in each bolt is equal to half of the flange force

$$B = F \qquad (1.2)$$

Intermediate plate behavior, shown in Figure 1.2b, exists once plastic hinges have formed at each face of the beam flange. Once the initiation of intermediate plate behavior occurs, prying forces develop in the bolts. The prying forces during intermediate plate behavior are calculated from

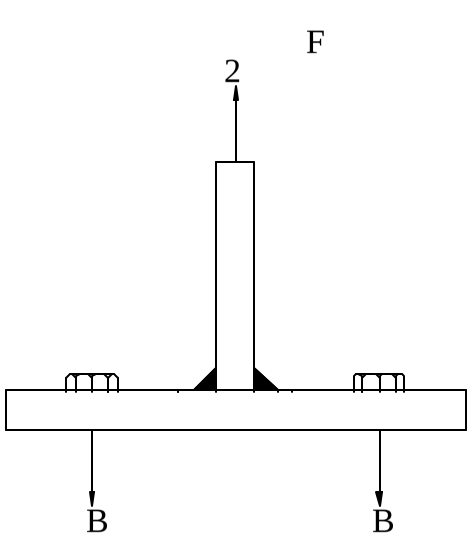

(a) Thick Plate Behavior

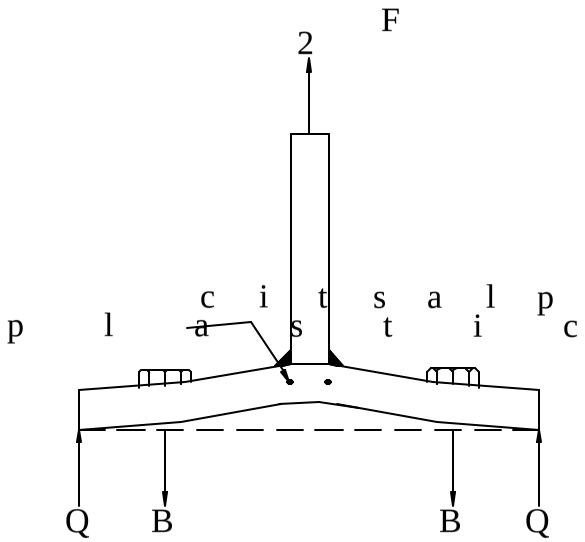

(b) Intermediate Plate Behavior

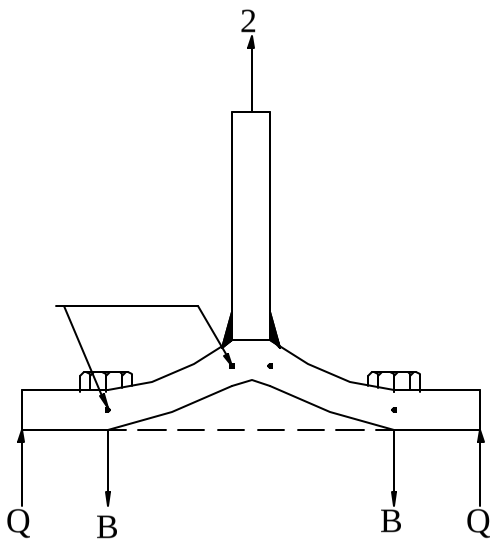

(c) Thin Plate Behavior

$$Q = \frac{Fb}{a} - \frac{\pi d_b^3 F_{yb}}{32a} - \frac{wt_p^2}{4a}\sqrt{F_{py}^2 - 3\left(\frac{F}{wt_p}\right)^2} \qquad (1.3)$$

Figure 1.2 Kennedy Plate Behavior (after Morrison *et al* 1985, 1986)

where a = the distance from the bolt centerline to the point of application of the prying force, d_b = the bolt diameter, F_{yb} = the design strength of the bolt (taken from Table J3.2, AISC, 1995), and Q = the prying force in one bolt during intermediate plate behavior. Kennedy *et al* (1981) defines a range for the value of "a" to be $2d_b<a<3d_b$. The force in each bolt during intermediate plate behavior is equal to

$$B = F + Q \tag{1.4}$$

The upper limit of intermediate plate behavior is reached when plastic hinges form at each bolt line and is found by the iteration of

$$t_{11} = \sqrt{\frac{2\left(2Fb - \frac{\eth d_b^3}{16} F_{yb}\right)}{w\sqrt{F_{py}^2 - 3\left(\frac{F}{wt_{11}}\right)^2} + w'\sqrt{F_{py}^2 - 3\left(\frac{F}{w't_{11}}\right)^2}}} \tag{1.5}$$

where w' = the width of the end plate per bolt at the bolt line minus the bolt hole and t_{11} = the thin plate limit. Thus, if $t_1 > t_p > t_{11}$, then the end-plate is exhibiting intermediate plate behavior.

Thin plate behavior, shown in Figure 1.2c, begins at the thin plate limit. Thus, if $t_p < t_{11}$, then the end-plate exhibits thin plate behavior. In this final state, the prying forces have reached their maximum value, Q_{max}, which is calculated from

$$Q_{max} = \frac{w't_p^2}{4a}\sqrt{F_{py}^2 - 3\left(\frac{F'}{w't_p}\right)^2} \tag{1.6}$$

where

$$F' = \frac{t_p^2 F_{py}\left(0.85w + 0.80w'\right) + \delta d_b^3 F_{yb}/8}{4b} \qquad (1.7)$$

The force in each bolt during thin plate behavior is calculated from

$$B = F + Q_{max} \qquad (1.8)$$

Kennedy *et al* (1981) provide guidelines for an ideal design using the split tee analogy. Under service loads the end-plate should function as a thick plate, under factored loads the end-plate should function as an intermediate plate and under ultimate loads the end-plate should function as a thin plate. From this point forward, the method discussed above will be referred to as the Kennedy method.

Srouji *et al* (1983) developed a methodology for the design of four different end-plate configurations using yield-line analysis to determine the end-plate strength criteria and the Kennedy method to determine the bolt strength requirements. The four end-plate configurations studied are the one- and two-bolt row flush end-plates and the stiffened and unstiffened extended end-plates with two bolts on either side of the tension flange. For the two-bolt row flush end-plate connection, the Kennedy method was modified to account for the additional bolt row. It was determined that the two bolts in the innermost bolt row carried $1/6^{th}$ of the total applied flange force for "thin" end-plates. A total of fourteen specimens were tested for this study, eight one-row flush end-plates and six two-row flush end-plates, and the results were compared to the predicted design strengths. It was concluded that yield-line analysis adequately predicts the strength of one- and two-bolt row flush end plates and of the unstiffened extended end-plate connection. It was also concluded that the modified Kennedy method adequately predicts the bolt forces.

Hendrick *et al* (1985) continued the work started by Srouji *et al* (1983) in an effort to unify the design of flush moment end-plate connections. Hendrick *et al* (1985)

developed design procedures for four flush end-plate configurations: the two-bolt flush unstiffened end-plate, the four-bolt flush unstiffened end-plate, the four-bolt flush end-plate stiffened between the tension bolt rows, and the four-bolt flush end-plate stiffened outside the tension bolt rows. The authors made two improvements to the design procedures develop by Srouji *et al* (1983). The distance from the bolt centerline to the point of application of the prying force, a, was determined by an empirical equation based on test data from twenty-one tests to be

$$a = 3.682\left(\frac{t_p}{d_b}\right)^3 - 0.085 \qquad (1.9)$$

In addition, the innermost row bolt force, B_2, was modified to account for the change in the location of the prying force. For the four-bolt unstiffened configuration and the four-bolt stiffened configuration with the stiffener outside the tension bolt rows, B_2 was changed from $1/6^{th}$ to $1/8^{th}$ the applied flange force for "thin" end-plates. For the four-bolt configuration stiffened between bolt rows, B_2 was determined to be equal to $1/5^{th}$ the applied flange force. Among other findings from this study, it was concluded that the stiffened end-plate connection is stronger when the stiffener is placed between the bolt rows rather than when it is placed outside the bolt rows, and all four connections are suitable to be used in Type I construction (rigid framing).

Morrison *et al* (1985) and Morrison *et al* (1986) continued the unification of design procedures begun by Hendrick *et al* (1985) with the four-bolt extended stiffened moment end-plate connection and the multiple row extended 1/3 (one row outside and three rows inside) unstiffened moment end-plate connection, respectively. Morrison *et al* (1985) and Morrison *et al* (1986) used yield-line theory and a modified Kennedy method to develop design procedures for the two connections. The modified Kennedy method

was further altered from the changes made by Hendrick *et al* (1985) by dividing the end-plate into two inner and outer end-plates, separated at the center of the beam tension flange. Empirical factors, α and β, were developed from experimental test results to proportion the tension flange force to the inner and outer end-plates and were incorporated into the design procedures. From experimental testing, it was concluded that the outer end-plate did not make contact at the outer edge of the end-plate, and thus, prying forces cannot develop in the outer end-plate. Six tests were performed for each connection to verify the design procedures. All connections tested were determined suitable for Type I construction.

Murray (1988) provides a review of then recent developments in the design of moment end-plate connections. For the two- and four-bolt flush end-plate connections, stiffened and unstiffened, yield-line analysis is recommended to determine the required end-plate thickness combined with the modified Kennedy method developed by Hendrick *et al* (1985) to predict the bolt forces including prying forces. For extended end-plates, various methods were recommended, including a method proposed by Krishnamurthy (1978), which is currently included in the AISC Manual (1995), and a procedure based on finite element/regression analysis. It was recommended that more research be directed at unification of moment end-plate design procedures, and "at developing criteria for other configurations, such as the multiple row flush end-plate configuration".

Bond (1989) conducted an analytical and experimental investigation of the six-bolt flush unstiffened moment end-plate connection. Five tests were performed and compared to the analytical predictions computed using yield-line theory and the modified Kennedy method. To distribute the bolt force among the three bolt rows, empirical

factors, α_1, α_2, and α_3, were derived from the experimental results. Also, a regression equation was created to express the moment-rotation relationship for the six-bolt configuration and to determine whether a six-bolt configuration can be used for Type I construction for a specific loading.

Abel (1993) developed a design procedure for the four-bolt extended unstiffened moment end-plate connection to be consistent with the unified design procedures established by Hendrick *et al* (1985). The analytical investigation was verified by four full-scale experimental tests. Following the modified Kennedy method established by Morrison *et al* (1985), the author determined the α and β empirical factors for the outer and inner end-plates to both be equal to 0.5. It was also concluded that the four-bolt extended unstiffened connection could be used for Type I or FR (fully restrained) construction.

Murray and Borgsmiller (1995) provide a design method for the multiple row extended 1/3 unstiffened moment end-plate connection. Ten previously conducted full-scale tests were used to verify the design procedures. The plate thickness was determined using the yield-line pattern proposed by Morrison *et al* (1986) and the bolt size was determined using a modified Kennedy method. The authors determined that the bolt force calculations could be significantly reduced by using two simplifying assumptions. The first assumption states that bolts that have reached their proof load will continue to yield without rupture until all bolts have reached their proof load. The second assumption states that when a bolt has reached its proof load, the plate is assumed to be "thin" and the prying forces are at a maximum, Q_{max}. From these simplifying assumptions, the bolts in a connection are classified as "load-carrying" or "non-load

carrying". A load-carrying bolt is one that has been experimentally proven to carry load. Conversely, a non-load carrying bolt is one that has been proven to not carry any load in a specific moment end-plate configuration. Using this information, equations are formulated and compared to determine the predicted connection strength, M_{pred}. It was concluded that for the multiple row extended 1/3 unstiffened connection the method developed by Murray and Borgsmiller (1995) appeared to produce accurate results.

Borgsmiller and Murray (1995) continued the work started by Murray and Borgsmiller (1995) by applying the simplified method for the design of moment-end plate connections to nine different end-plate configurations. The nine connections discussed are a compilation of all connection configurations discussed in this literature review thus far. Borgsmiller and Murray (1995) analyzed fifty-two previously conducted full-scale tests to verify the proposed design procedures and concluded that the procedures are appropriate for the design of the nine moment end-plate configurations presented

Mays (2000a) provided a study of a sixteen bolt extended end-plate with bolt rows containing four bolts across. The purpose of the study was to develop design procedures for large moment end-plates and determine their effectiveness under seismic loading. Mays (2000a) developed a yield-line pattern that produced lower end-plate stresses than those presented in Borgsmiller and Murray (1995). This yield-line pattern will be discussed further in Chapter III.

1.2 OBJECTIVE AND SCOPE OF RESEARCH

The objective of this study is to develop design solutions for five moment end-plate configurations; one extended end-plate and four flush end-plates with large pitch distances. The design solutions will provide equations for the determination of the end-plate thickness using yield-line theory and bolt forces using the simplified Kennedy method (Borgsmiller and Murray 1995) given the geometric and material properties of the end-plate and bolts.

These objectives are accomplished in the following manner. In Chapter II, the experimental investigation is described in detail. The test setups are illustrated and described, as well as the instrumentation used to record the test data. The testing procedure is discussed followed by a summary of the experimental results. Chapter III describes the analytical investigation. Yield-line theory is discussed first and equations are formulated to apply to the five moment end-plate connections. A simplified version of the Kennedy method (Borgsmiller and Murray 1995) is then formulated and applied. In Chapter IV, the analytical and experimental results are compared. In Chapter V, the study is summarized, conclusions are drawn, and recommendations for further research are provided. Sample calculations are presented for the analysis of a flush and an extended moment end-plate connection. A detailed appendix of the experimental work follows the text.

CHAPTER II

EXPERIMENTAL INVESTIGATION

2.1 SCOPE OF TESTING

Five knee area tests and one plate girder test were conducted at the Virginia Tech Structures and Materials Laboratory located in Blacksburg, Virginia. The research was sponsored by NCI Building Systems, located in Houston Texas.

The knee area specimens were sections of a gable frame, as shown in Figure 2.1. The knee area consisted of the entire length of a column and a portion of the rafter. Each knee was connected by a bolted flush moment end-plate connection. One of the five knee area specimens was stiffened at the connection. The remaining four knee area specimens were unstiffened at the connection. A typical test setup for the knee area test is shown in Figure 2.2. Lateral bracing was provided to each specimen to prohibit lateral movement. The specimens were instrumented and loaded to failure using a hydraulic ram.

The plate girder test consisted of two built-up sections connected by an extended moment end-plate connection. The specimen was loaded at two equally spaced load-points along the top flange of the plate girder. The specimen was tested as shown in Figure 2.3. Again, lateral bracing was provided to prohibit lateral movement of the test specimen. The specimen was instrumented and loaded to failure using two hydraulic rams.

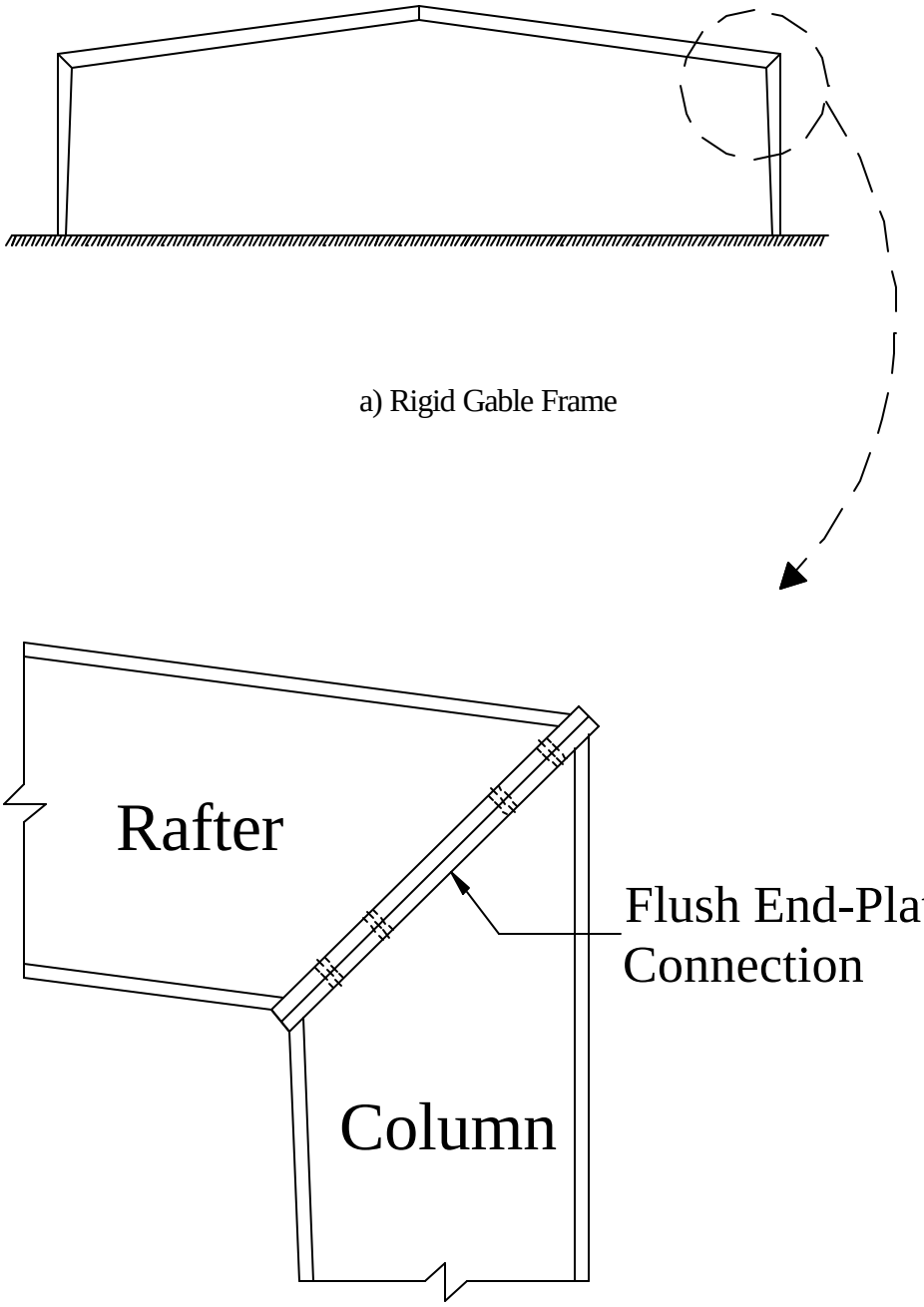

a) Rigid Gable Frame

b) Knee Area Details

Figure 2.1 Typical Rigid Gable Frame and Knee Area Detail

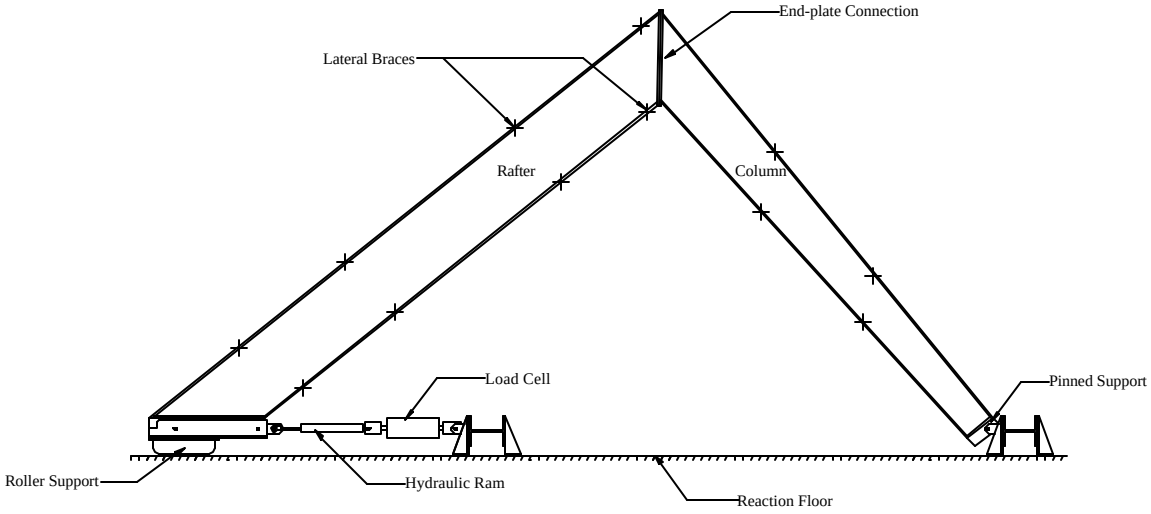

Figure 2.2 Knee Area Test Setup

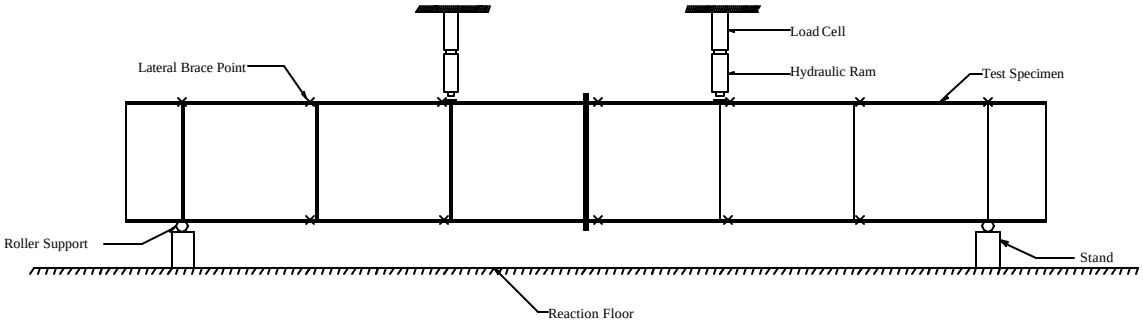

Figure 2.3 Plate Girder Test Setup

2.2 TESTING PROGRAM

2.2.1 Test Specimens

All test specimens were designed by NCI Building Systems and fabricated by Metallic Building Company. The test specimens were built-up sections composed of steel plates with a nominal yield stress of 50 ksi. Each test specimen had a unique moment end-plate configuration, as shown in Figure 2.4. All of the connections used ASTM A325 high strength steel bolts. Prior to testing, the dimensions of each specimen were measured and recorded. The average connection dimensions for each specimen can be found in Appendices B through G. The nominal connection dimensions for each test specimen are shown in Table 2.1. An illustration of the terms used in the table is found in Figure 2.5.

Each test is given a specific designation based on the bolt diameter, the connection configuration, the thickness of the end-plate and the beam depth. The following designations are used to classify each connection configuration:

F2 – Four-Bolt Flush Unstiffened Moment End-Plate

F3 – Six-Bolt Flush Unstiffened Moment End-Plate

F4 – Eight-Bolt Flush Unstiffened Moment End-Plate

F5 – Ten-Bolt Flush Unstiffened Moment End-Plate

F5S – Ten-Bolt Flush Stiffened Moment End-Plate

MRE$^{1}/_{4}$ – Multiple Row Extended Unstiffened Moment End-plate

The test designation is written as follows:

Connection Configuration–d_b-t_p-h

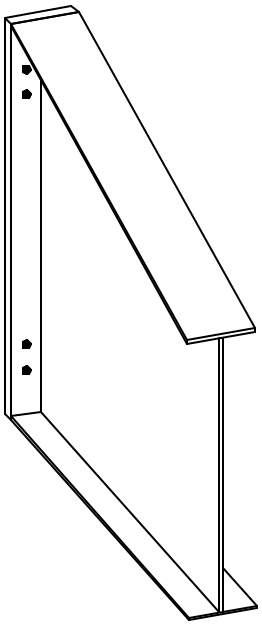

a) Four-Bolt Flush Unstiffened (F2)

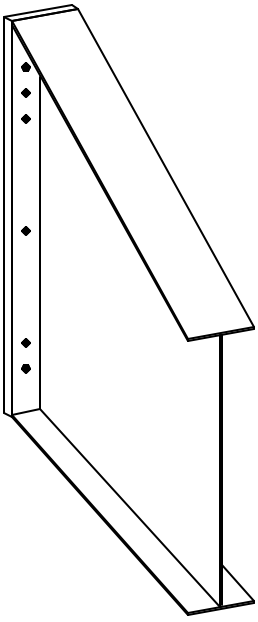

b) Six-Bolt Flush Unstiffened (F3)

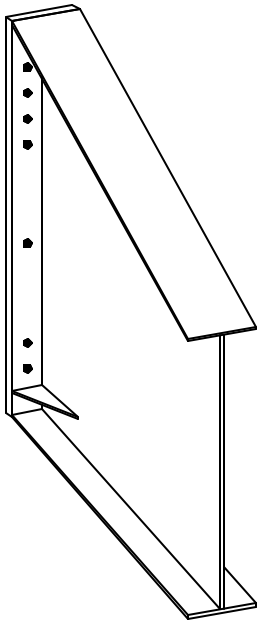

c) Eight-Bolt Flush Unstiffened (F4)

Figure 2.4 End-Plate Configurations

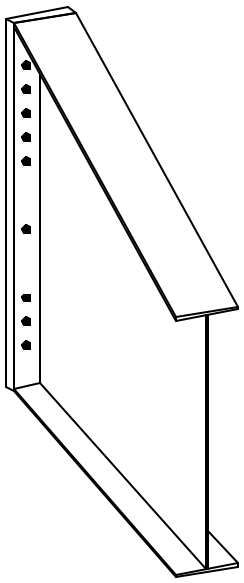

d) Ten-Bolt Flush Unstiffened (F5)

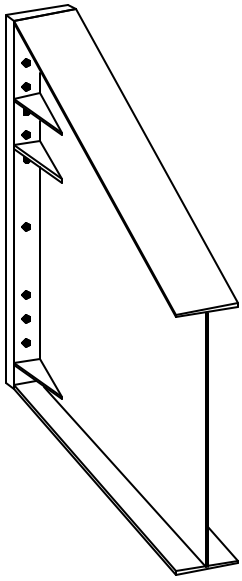

e) Ten-Bolt Flush Stiffened (F5)

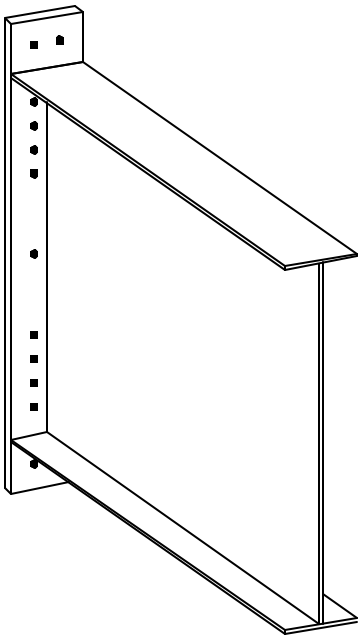

f) Multiple Row Extended (MRE$^{1}/_{4}$)

Figure 2.4 Con't End-Plate Configurations

Table 2.1

Nominal Connection Dimensions

Test Designation	Bolt Diameter d_b (in)	Hole Diameter ϕ (in)	Beam Width b_p (in)	Beam Depth h (in)	p_{ext} (in)	$p_{f,o}$ (in)	p_f (in)	p_b (in)	Gage g (in)	Top Flange Thickness t_{fl} (in)	Bottom Flange Thickness t_{f2} (in)	End-Plate Thickness t_p (in)
F2-5/8-1/2-28	5/8	11/16	6	28	-	-	4 9/16	4	3	3/16	1/4	1/2
F3-3/4-3/4-50	3/4	13/16	8	50	-	-	4 3/4	4	3	1/4	3/8	3/4
F4-7/8-3/4-67	7/8	15/16	8	67	-	-	5 5/8	4	3 1/2	3/8	3/4	3/4
F5-1 1/4-3/4-84	1 1/4	21/16	12	84	-	-	7 1/2	4	4 1/2	1/2	1	3/4
F5S-1 1/4-3/4-84	1 1/4	21/16	12	84	-	-	7 1/2	4	4 1/2	1/2	1	3/4
MRE 1/4-1 1/4-1-70 1/2	1 1/4	21/16	12	61 1/2	4 1/2	2 1/4	2	4	4 1/2	3/4	3/4	1

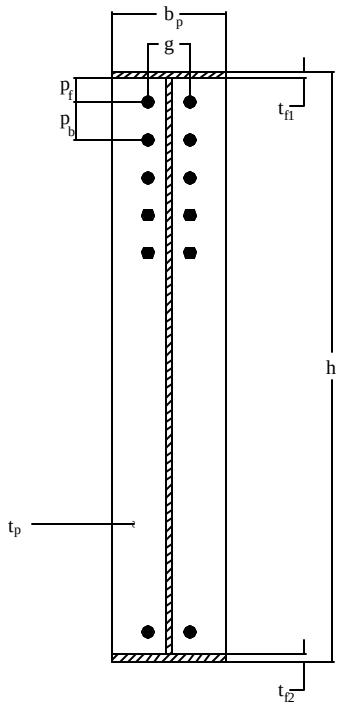

a) Flush End-Plate Connection

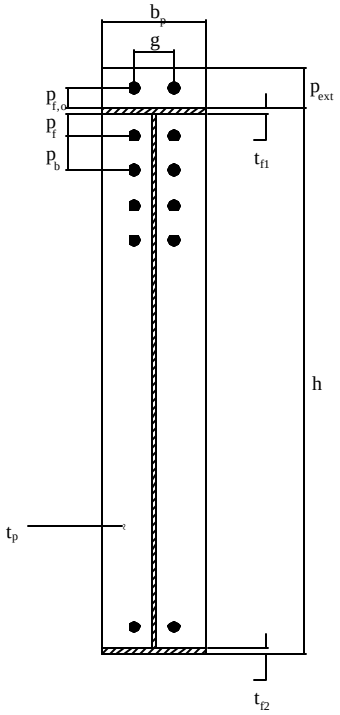

a) Extended Moment End-Plate Connection

Figure 2.5 End-Plate Connection Dimensions

An example of this test designation is F5-$1^1/_4$-$^3/_4$-84 that corresponds to a ten-bolt flush unstiffened moment end-plate connection with $1^1/_4$ in. diameter bolts, a ¾ in. thick end-plate and a beam depth of 84 in.

2.2.2 Test Setups

All test setups were constructed so that the connection was subjected to pure moment. Lateral bracing was provided to prohibit lateral movement, thus, simulating actual building conditions. The lateral bracing mechanisms were bolted to the testing frames, which were connected to a reaction floor. All test setups were simply supported.

The knee area test setup was pin-connected at the column end and roller-connected at the rafter end, as shown in Figure 2.2. The column was connected directly to a support stand, which was bolted to the reaction floor. A link connected the roller end of the rafter to a reaction beam. The link was composed of a hydraulic ram to apply the load and a load cell to measure the load. The hydraulic ram pulled the rafter inward, causing tension in the outside flange and compression in the inside flange.

The plate girder specimen was supported by two test stands, as shown in Figure 2.3. Lateral bracing was provided at each web stiffener to prohibit lateral movement. A hydraulic ram was used to apply load and a load cell was used to measure the load at the two load points. The hydraulic ram pushed the specimen down at the two load points causing compression in the top flange and tension in the bottom flange.

2.2.3 Instrumentation

Instrumentation was added to each test setup to measure specific parameters during testing. All instrumentation was connected to a PC-based data acquisition system that monitored and recorded all instrumentation data during testing.

All tests were instrumented with calibrated bolts. To instrument a bolt, a small hole was drilled into the shank of the bolt. A strain gage was then inserted into the hole and filled with epoxy. The bolts were then calibrated using a 300 kip capacity universal testing machine to determine the relationship between strain and load. The instrumented bolts were placed in the connection in an alternating pattern beginning at the top of the tension side. The exact locations of the calibrated bolts for each test are included in the Appendices. Prior to testing, most bolts were tightened to the minimum bolt tension listed in Table J3.1 of the *LRFD Specification for Structural Steel Buildings* (1995). In some cases, the bolts were not tightened to the minimum bolt tension, but to an amount that could be safely attained with the equipment available.

All test specimens were instrumented with displacement transducers to measure deflections. Each knee area test employed two displacement transducers. One transducer was placed at the bottom of the rafter support to measure horizontal movement. Another transducer was placed at the bottom of the column to measure any horizontal movement due to movement of the pinned support. The plate girder test used five displacement transducers to measure vertical deflections: at the mid-span end-plate connection, at each load point, and at each support. The transducers placed at the supports measured support settlements.

All test specimens were instrumented with gauged calipers to measure the plate separation between the edges of the adjacent end-plates in each connection. In all knee area tests, the calipers were placed above the first row of bolts on the tension side of each connection as close as possible to the inside of the top flange. In the plate girder test, two calipers were placed on the tension side of the connection, one just inside the bottom

flange and one just outside the bottom flange on the extended portion of the end-plates. The locations of the gauged calipers for each test are included in the corresponding appendix.

Strain gages were attached to the web of specimens MRE$^{1}/_{4}$-$1^{1}/_{4}$-1-$70^{1}/_{2}$ and F5-$1^{1}/_{4}$-$^{3}/_{4}$-84. The gages were attached to both sides of the tension portion of the web and were used to determine when the web of the specimen yielded. The approximate locations of the strain gages for these two tests are shown in Figure 2.6.

All specimens were whitewashed prior to testing. This presented a clear sign of yielding marked by the flaking of mill scale from the specimen.

2.2.4 Test Procedure

Prior to testing, each specimen was loaded to approximately 20% of its predicted ultimate load to "seat" all of the specimen and test frame components. Prior to the initiation of each test, all instrumentation was zeroed with the exception of the pretensioned bolt strains. Each specimen was loaded at a prescribed load interval. First yield was noted as well as the load or deflection at which subsequent yielding occurred. The test was continued until failure occurred. Failure was defined as the point at which the specimen was no longer able to hold load or was no longer functional.

Two specimens, F5-$1^{1}/_{4}$-$^{3}/_{4}$-84 and F5S-$1^{1}/_{4}$-$^{3}/_{4}$-84, were tested in a series of cycles. Each specimen was loaded to its predicted ultimate load, provided by NCI Building Systems. If failure had not initiated, the specimen was unloaded, bolts were removed from the moment end-plate connection, and the test was resumed. This pattern was repeated until failure ensued. Further details of each cycle are provided in the corresponding Appendices.

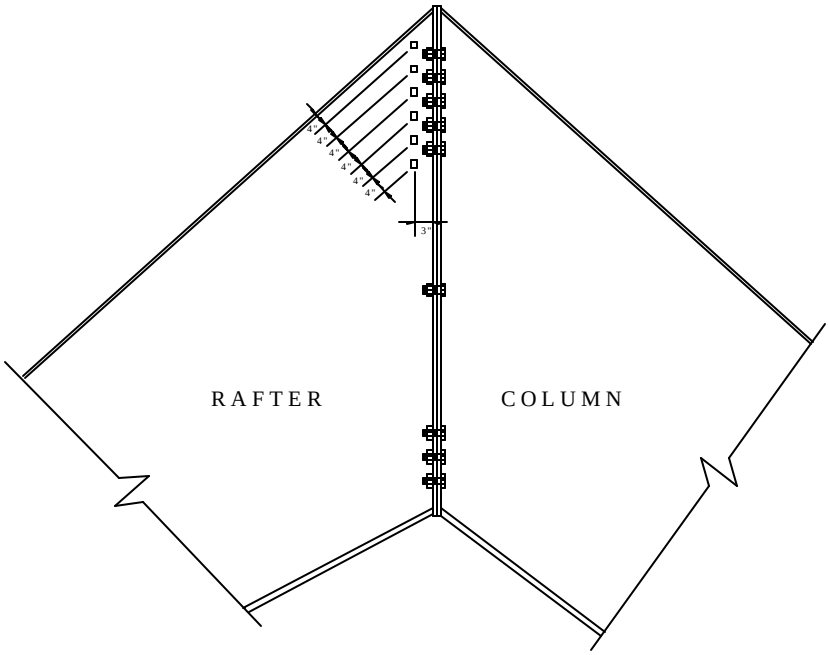

a) F5-$1^1/_4$-$^3/_4$-84 Strain Gage Locations

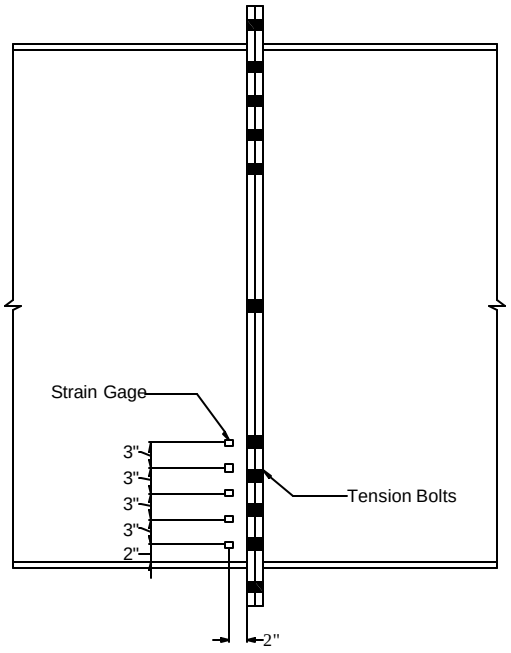

b) MRE$^1/_4$-$1^1/_4$-1-$70^1/_2$ Strain Gage Locations

Figure 2.6 Web Strain Gage Locations

2.3 EXPERIMENTAL RESULTS

Detailed results for each test specimen are provided in Appendices B through G. Table 2.2 is a summary of the test results.

The knee area test results are listed first in the Appendices in order of smallest to largest moment end-plate connection. The plate girder test results follow. For each test specimen, the results include a test summary sheet, a drawing of the nominal specimen dimensions, a table of the geometric and material properties of each specimen, a drawing of the measured connection details, pictures of the specimen after testing, and the following plots: applied moment vs. deflection, applied moment vs. plate separation, and bolt force vs. applied moment. The test results for F5-$1^1/_4$-$^3/_4$-84 and MRE$^1/_4$-$1^1/_4$-1-$70^1/_2$ also include a plot of load vs. strains in the web of the test specimen.

The relationship between the applied moment and deflection is plotted for each specimen. Each plot shows both the theoretical relationship between moment and deflection in the elastic range as well as the experimental results up to the ultimate failure moment. The knee specimens have the applied moment plotted against the chord deflection. The chord deflection is a measure of the horizontal change in length between the pinned-end of the column and the roller-end of the rafter. The theoretical deflection for the knee area specimens is computed using a stiffness analysis computer program. The applied moment vs. deflection plot for the plate girder specimen is a comparison of the average vertical deflection at the load points vs. the applied moment on the specimen. The theoretical deflection for this specimen was computed using the elastic deflection equation for a simply supported beam with two equal, concentrated loads symmetrically placed:

Table 2.2

Summary of Test Results

Test Designation	Maximum Applied Load (kips)	Maximum End-Plate Moment (kip-ft)	Failure Mode	Failure Location
F2-5/8-1/2-28	13.4 kips	150 kip-ft	Local Flange Buckling	Column Flange
F3-3/4-3/4-50	41.25 kips	552 kip-ft	Lateral Torsional Buckling	Column and Rafter Sections
F4-7/8-3/4-67	84.6 kips	1160 kip-ft	Local web buckling	Rafter Web
F5-1 1/4-3/4-84	196.5 kips	2529 kip-ft	End-plate yielding with high bolt strains	End-Plates
F5S-1 1/4-3/4-84	202.5 kips	2606 kip-ft	End-plate yielding with high bolt strains	End-Plates
MRE 1/4-1 1/4-1-70 1/2	265 kips	3044 kip-ft	Specimen did not fail	Specimen did not fail

$$\Ä = \frac{Pa}{6EI}\left(3la - 4a^2\right) \quad (2.1)$$

where a = the horizontal distance from the support to the nearest load point, l = the total length from support to support, and P = the load applied at each load point. The experimental yield moment and maximum moment are presented in each plot where applicable. The predicted connection failure moment is also included in applicable plots. This value is computed for each specimen using the proposed method to be discussed in detail in Chapter III.

The relationship between plate separation and applied moment is plotted for each test specimen. The plate separation is the product of the strain measured by the gauged calipers and a conversion factor. The predicted connection failure moment is provided for comparison in each plot where applicable.

Bolt force vs. applied moment plots are included for all test specimens. The bolt force is a measure of the bolt strain in the calibrated bolts multiplied by a conversion factor. Since this relationship is only valid in the elastic region, it was necessary to apply and adjustment factor to the bolts that were loaded beyond their proof load. Once the bolts reached their proof load, the bolt force was determined using the following relationship from Abel (1993):

$$BF_{plastic} = P_y + (\varepsilon_{plastic}\text{-}\varepsilon_y)*(m_{elastic}*R) \quad (2.2)$$

where P_y = bolt proof load,

$$m_{elastic} = \frac{P_y}{\mathring{a}_y} \quad (2.3)$$

and

$$R = \frac{\left[\frac{\text{strain}}{\text{load}}\right]_{\text{elastic}}}{\left[\frac{\text{strain}}{\text{load}}\right]_{\text{plastic}}} \qquad (2.4)$$

The bolt proof load shown on the plot was calculated using a value of 90 ksi as the nominal strength of an A325 bolt (taken from Table J3.2, AISC 1995) multiplied by the nominal cross-sectional area of each bolt. The bolt pretension value was taken directly from Table J3.1 in the AISC Manual (1995).

Web strain on the tension side vs. applied load is plotted for test specimens F5-$1^1/_4$-$^3/_4$-84 and MRE$^1/_4$-$1^1/_4$-1-$70^1/_2$.

2.4 COUPON TESTS

Test specimens were cut from the web and flanges of the rafter and column of each steel member following testing. Blank end-plate material was provided by NCI Building Systems for coupon specimens. In accordance with ASTM E8 *Standard Test Methods for Tension Testing of Metallic Materials,* the specimens were machined into coupons and tested with a 300 kip capacity universal testing machine. Using the data compiled, the tensile properties were determined according to ASTM A370 standards for the following parameters: ultimate strength, yield strength, and percent elongation. The results of the coupon tests are summarized in Table 2.3.

Test specimens were not taken from the web and flanges of MRE$^1/_4$-$1^1/_4$-1-$70^1/_2$ because of possible additional testing of the specimen.

Table 2.3

Tensile Coupon Test Results

Specimen	Member	Element	Yield Strength (ksi)	Ultimate Strength (ksi)	Percent Elongation (%)
F2-5/8-1/2-28	Column	Top Flange	70.0	82.7	17.0
		Web	59.0	69.5	23.0
		Bottom Flange	62.2	74.8	24.0
	Rafter	Top Flange	70.0	83.1	19.0
		Web	60.8	71.6	21.0
		Bottom Flange	64.4	75.0	22.0
	End-Plate		58.1	88.2	32.3
F3-3/4-3/4-50	Column	Top Flange	55.0	68.1	24.0
		Web	67.0	78.6	21.5
		Bottom Flange	59.3	78.8	22.0
	Rafter	Top Flange	56.1	68.4	24.0
		Web	67.6	77.8	21.5
		Bottom Flange	59.2	77.6	22.0
	End-Plate		55.7	84.7	24.5
F4-7/8-3/4-67	Column	Top Flange	61.0	91.3	23.0
		Web	52.0*	68.7*	23.0*
		Bottom Flange	56.2	85.5	24.0
	Rafter	Top Flange	61.0	91.3	23.0
		Web	52.0	68.7	23.0
		Bottom Flange	55.0	82.0	28.0
	End-Plate		55.0	84.8	25.5
F5-1 1/4-3/4-84	Column	Top Flange	57.9	81.4	25.0
		Web	50.4	69.0	24.0
		Bottom Flange	55.4	84.0	27.0
	Rafter	Top Flange	57.1	81.4	25.0
		Web	47.1	67.0	29.5
		Bottom Flange	56.1	84.1	27.0
	End-Plate		55.6	84.3	25.0
F5S-1 1/4-3/4-84	Column	Top Flange	56.6	80.8	27.0
		Web	49.2	68.3	26.0
		Bottom Flange	56.1	84.7	27.0
	Rafter	Top Flange	56.0	80.6	26.0
		Web	46.0	66.3	27.5
		Bottom Flange	55.6	84.3	25.8
	End-Plate		55.2	83.3	26.0
MRE1/4-1 1/4-1-70 1/2	End-Plate		54.9	85.4	26.0

*All values were assumed to be the same as those for the rafter web. No coupons were tested from the column web.

CHAPTER III

ANALYTICAL INVESTIGATION

3.1 OVERVIEW

There are two limit states for bolted moment end-plate connections; end-plate yielding and bolt rupture. In this study, yield-line analysis is used to predict the end-plate yield strength, and a simplified version of the Kennedy method (Borgsmiller and Murray 1995) is used to predict bolt rupture including prying action. The method used to predict bolt rupture without prying action is discussed in Chapter IV.

In this chapter, a yield-line mechanism is developed for each moment end-plate in the study. Following the yield-line analysis, the simplified version of the Kennedy method is discussed and applied to each moment end-plate connection in the study.

3.2 END-PLATE STRENGTH PREDICTIONS

3.2.1 General Theory

K. W. Johansen (1962) first introduced yield-line theory for use in reinforced concrete slabs. Since then, the principles behind the theory have been applied toward the analysis of steel moment end-plate connections. A yield line is defined as the continuous formation of plastic hinges along a straight or curved line. The moment at which the plastic hinges form remains relatively constant as the deformations increase, thus forming

a visible yield line. Since the plastic deformations at the yield lines are significantly larger than the elastic deformations in the regions between yield lines, it is assumed that these elastic regions behave as rigid plates. In yield-line theory, failure occurs when the formation of successive yield lines in a slab or plate form a kinematically valid collapse mechanism. This succession of yield lines is referred to as a yield-line pattern.

According to Srouji *et al* (1983) there are three guidelines that should be followed in order to establish the location of a yield line;

1. Axes of rotation generally lie along lines of support.
2. Yield lines pass through the intersection of the axes of rotation of adjacent plate segments.
3. Along every yield line, the bending moment is assumed to be constant and is taken as the plastic moment of the plate.

There are two methods that can be used to analyze a yield-line pattern. They are the equilibrium method and the virtual work method. The virtual work method is preferred based on the ease of application and is the method that will be used for the analysis of moment end-plates in this study. The virtual work method is based on the principle of conservation of energy (Hibbeler 1995). The external work done by the applied loads from a unit virtual displacement is set equal to the internal work done to accommodate these displacements as the plate rotates about the yield lines. For a known set of applied loads, each unique yield-line pattern will result in a different required plastic moment capacity. The pattern that requires the largest plastic moment capacity is the controlling yield-line pattern. Conversely, if the plastic moment capacity of the end-plate is known, the pattern that yields the lowest failure load is the controlling pattern.

Therefore, yield-line theory is an upper bound solution and the objective is to determine the least upper bound.

The following discussion is taken directly from Srouji *et al* (1983).

The internal work stored in a particular yield-line mechanism is the sum of the internal energy stored in each yield line forming the mechanism. The internal energy stored in any given yield line is obtained by multiplying the normal moment on the yield line with the normal rotation of the yield line. Thus, the energy stored in the n-th line of length L_n is

$$W_{in} = \int_{L_n} m_p \grave{e}_n \, ds \tag{3.1}$$

where θ_n is the relative rotation of line n, ds is the elemental length of line n. The internal energy stored by a yield-line mechanism can be written as

$$W_i = \sum_{n=1}^{N} \int_{L_n} m_p \grave{e}_n \, ds \tag{3.2}$$

$$= \sum_{n=1}^{N} m_p \grave{e}_n L_n$$

where N is the number of yield lines in the mechanism.

In complicated yield-line patterns, the values of the relative rotation are tedious to obtain, therefore, it is more convenient to resolve the slopes and moments in the x- and y- directions. This results in the following form of Equation 3.2

$$W_i = \sum_{n=1}^{N} (m_{px} \grave{e}_{nx} L_x + m_{py} \grave{e}_{ny} L_y) \tag{3.3}$$

in which m_{px} and m_{py} are the x- and y- components of the normal moment capacity per unit length, L_x and L_y are the x- and y- components of the relative normal rotation of yield line n.

The moment capacity per unit length for steel plates is

$$m_{px} = m_{py} = m_p = \frac{F_{py} t_p^2}{4} \tag{3.4}$$

where F_{py} is the yield stress of the end-plate material and t_p is the thickness of the end-plate.

The external work is the product of an applied moment and the angle through which it rotates. For all end-plate configurations, the equation for external work is identical. It is assumed that the two end-plates rotate about the outside face of the compression flanges of each member. Thus, the equation for external work is

$$W_e = M_u \theta = M_u \left(\frac{1}{h} \right) \tag{3.5}$$

where M_u equals the ultimate moment at the end-plate and θ equals the virtual rotation of the end-plate connection. Using small angle theory and a virtual deflection equal to unity at the outside face of the tension flange, θ is set equal to $\frac{1}{h}$, where h is the total depth of the beam.

3.2.2 Four-Bolt Flush Unstiffened Moment End-Plate

A study on the behavior of four-bolt flush unstiffened moment end-plates was conducted by Mays (2000b). Based on the study, the two controlling yield-line mechanisms for the four-bolt flush unstiffened moment end-plate were derived, as shown in Figure 3.1. The controlling mechanism depends on the pitch distance, p_f, and the distance s. The distance "s" is defined as the maximum possible distance between a bolt

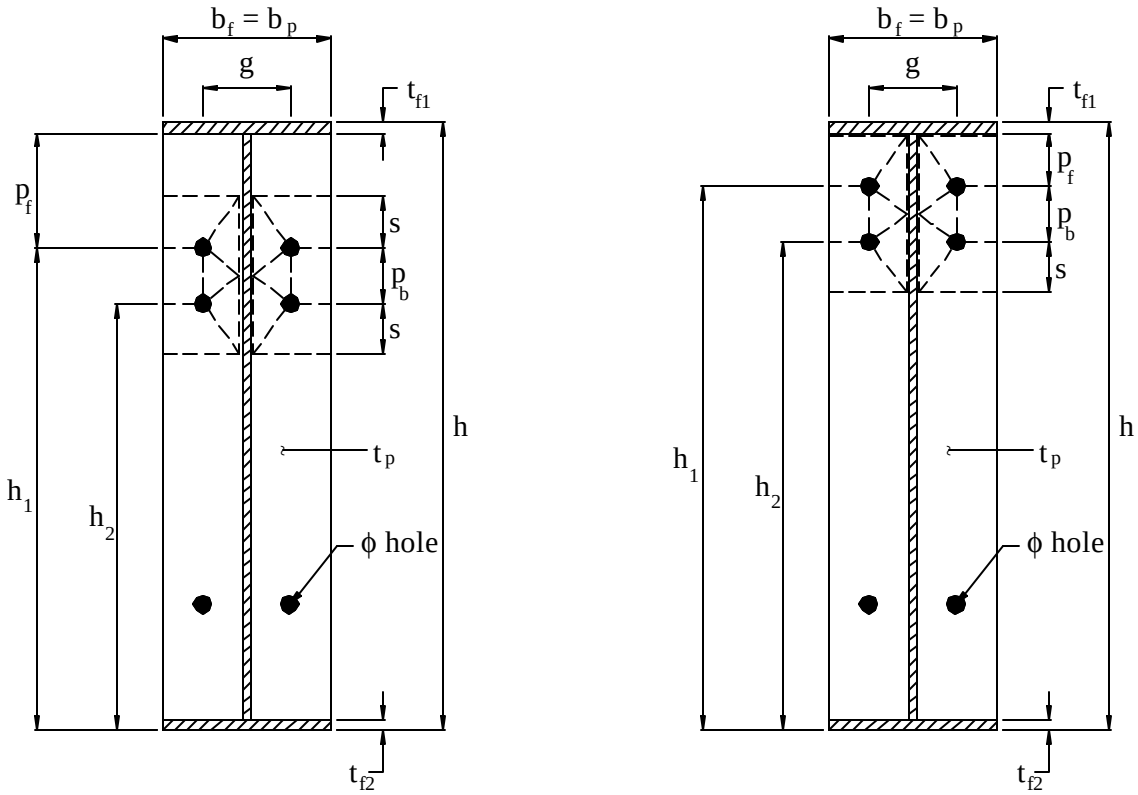

a) Case I: $p_f > s$ b) Case II: $p_f < s$

Figure 3.1 Yield-Line Mechanisms for a Four-Bolt Flush Unstiffened Moment End-Plate

centerline and the formation of a yield line. Thus, when the pitch distance, p_f, is greater than s, a yield line will develop at a distance "s" from the outermost bolt row centerline, and Case I is the controlling mechanism. This case is typical of diagonal knee moment end-plate connections. If the pitch distance, p_f, is less than the distance s, then the uppermost horizontal yield line will form at the inner face of the beam tension flange and Case II is the controlling mechanism. The equations for each case are presented below.

Case I: $p_f > s$

The internal work for this yield line pattern is

$$W_i = \frac{4m_p}{h}\left[\frac{b_p}{2}\left[h_1\left(\frac{1}{s}\right)+h_2\left(\frac{1}{s}\right)\right]+\frac{2}{g}\left[h_1\left(s+0.75p_b\right)+h_2\left(s+0.25p_b\right)\right]+\frac{g}{2}\right] \tag{3.6}$$

where m_p is defined in Equation 3.4 and the remaining parameters are defined in Figure 3.1a. The connection strength based on yielding of the end-plate is found by equating the external energy from Equation 3.5 with the internal energy calculated in Equation 3.6, resulting in

$$M_{pl} = 4m_p\left[\frac{b_p}{2}\left[h_1\left(\frac{1}{s}\right)+h_2\left(\frac{1}{s}\right)\right]+\frac{2}{g}\left[h_1\left(s+0.75p_b\right)+h_2\left(s+0.25p_b\right)\right]+\frac{g}{2}\right] \tag{3.7}$$

The required end-plate thickness is computed by replacing m_p with Equation 3.4 and solving for t_p, resulting in

$$t_p = \left[\frac{M_u / F_{py}}{\left[\frac{b_p}{2} \left[h_1 \left(\frac{1}{s} \right) + h_2 \left(\frac{1}{s} \right) \right] + \frac{2}{g} \left[h_1 (s + 0.75 p_b) + h_2 (s + 0.25 p_b) \right] + \frac{g}{2} \right]} \right]^{1/2} \tag{3.8}$$

The distance, s, is found by differentiating the internal work equation with respect to s and setting the resulting equation equal to zero, giving

$$s = \frac{1}{2} \sqrt{b_p g} \tag{3.9}$$

Case II: $p_f < s$

The internal work for this yield line pattern is

$$W_i = \frac{4 m_p}{h} \left[\frac{b_p}{2} \left[h_1 \left(\frac{1}{p_f} \right) + h_2 \left(\frac{1}{s} \right) \right] + \frac{2}{g} \left[h_1 (p_f + 0.75 p_b) + h_2 (s + 0.25 p_b) \right] + \frac{g}{2} \right] \tag{3.10}$$

where m_p is defined in Equation 3.4 and the remaining parameters are defined in Figure 3.1b. The connection strength based on yielding of the end-plate is found by equating the external energy from Equation 3.5 with the internal energy calculated in Equation 3.10, resulting in

$$M_{pl} = 4 m_p \left[\frac{b_p}{2} \left[h_1 \left(\frac{1}{p_f} \right) + h_2 \left(\frac{1}{s} \right) \right] + \frac{2}{g} \left[h_1 (p_f + 0.75 p_b) + h_2 (s + 0.25 p_b) \right] + \frac{g}{2} \right] \tag{3.11}$$

The required end-plate thickness is computed by replacing m_p with Equation 3.4 and solving for t_p, resulting in

$$t_p = \left[\frac{M_u / F_{py}}{\left[\frac{b_p}{2} \left[h_1 \left(\frac{1}{p_f} \right) + h_2 \left(\frac{1}{s} \right) \right] + \frac{2}{g} \left[h_1 (p_f + 0.75 p_b) + h_2 (s + 0.25 p_b) \right] + \frac{g}{2} \right]} \right]^{1/2} \tag{3.12}$$

The distance, s, is found by differentiating the internal work equation with respect to s and setting the resulting equation equal to zero, giving

$$s = \frac{1}{2} \sqrt{b_p g} \tag{3.13}$$

3.2.3 Six-Bolt Flush Unstiffened Moment End-Plate

A study on the behavior of six-bolt flush unstiffened moment end-plates was conducted by Mays (2000b). From this study, the two controlling yield-line mechanisms for the six-bolt flush unstiffened moment end-plate were derived as shown in Figure 3.2. The geometric parameters are also defined in the figure. The controlling mechanism is determined by comparing the pitch distance, p_f, and the distance s Case I applies to moment end-plates with a large inner pitch distance, p_f, such that p_f is greater than the distance s. This case often occurs in diagonal knee moment end-plate connections. Case II applies to moment end-plates where p_f is less than s. The equations for the internal work, W_i, moment end-plate strength, M_{pl}, end-plate thickness, t_p, and the distance s are presented below for each case.

Case I: $p_f > s$

$$W_i = \frac{4 m_p}{h} \left[\frac{b_p}{2} \left[h_1 \left(\frac{1}{s} \right) + h_3 \left(\frac{1}{s} \right) \right] + \frac{2}{g} \left[h_1 (s + 1.5 p_b) + h_3 (s + 0.5 p_b) \right] + \frac{g}{2} \right] \tag{3.14}$$

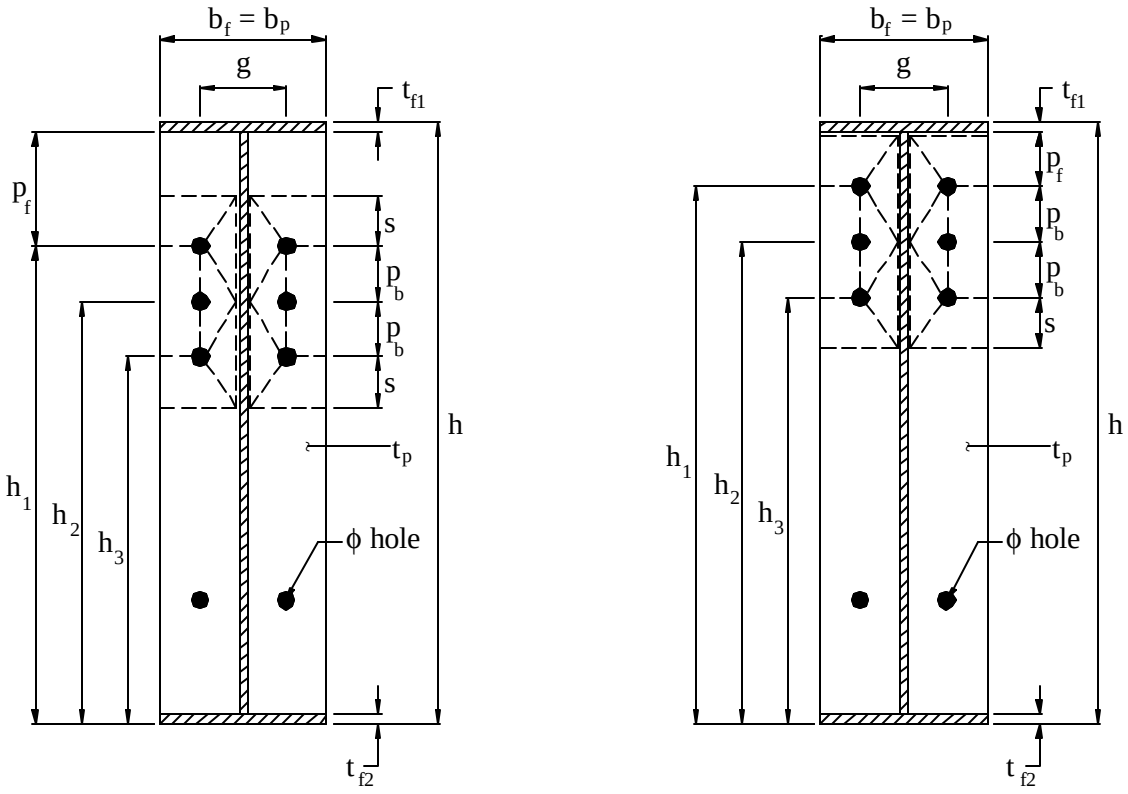

a) Case I: $p_f > s$

b) Case II: $p_f < s$

Figure 3.2 Yield-Line Mechanisms for a Six-Bolt Flush Unstiffened Moment End-Plate

$$M_{pl} = 4m_p\left[\frac{b_p}{2}\left[h_1\left(\frac{1}{s}\right)+h_3\left(\frac{1}{s}\right)\right]+\frac{2}{g}\left[h_1\left(s+1.5p_b\right)+h_3\left(s+0.5p_b\right)\right]+\frac{g}{2}\right] \tag{3.15}$$

$$t_p = \left[\frac{M_u/F_{py}}{\left[\frac{b_p}{2}\left[h_1\left(\frac{1}{s}\right)+h_3\left(\frac{1}{s}\right)\right]+\frac{2}{g}\left[h_1\left(s+1.5p_b\right)+h_3\left(s+0.5p_b\right)\right]+\frac{g}{2}\right]}\right]^{1/2} \tag{3.16}$$

$$s = \frac{1}{2}\sqrt{b_p g} \tag{3.17}$$

Case II: $p_f < s$

$$W_i = \frac{4m_p}{h}\left[\frac{b_p}{2}\left[h_1\left(\frac{1}{p_f}\right)+h_3\left(\frac{1}{s}\right)\right]+\frac{2}{g}\left[h_1\left(p_f+1.5p_b\right)+h_3\left(s+0.5p_b\right)\right]+\frac{g}{2}\right] \tag{3.18}$$

$$M_{pl} = 4m_p\left[\frac{b_p}{2}\left[h_1\left(\frac{1}{p_f}\right)+h_3\left(\frac{1}{s}\right)\right]+\frac{2}{g}\left[h_1\left(p_f+1.5p_b\right)+h_3\left(s+0.5p_b\right)\right]+\frac{g}{2}\right] \tag{3.19}$$

$$t_p = \left[\frac{M_u/F_{py}}{\left[\frac{b_p}{2}\left[h_1\left(\frac{1}{p_f}\right)+h_3\left(\frac{1}{s}\right)\right]+\frac{2}{g}\left[h_1\left(p_f+1.5p_b\right)+h_3\left(s+0.5p_b\right)\right]+\frac{g}{2}\right]}\right]^{1/2} \tag{3.20}$$

$$s = \frac{1}{2}\sqrt{b_p g} \tag{3.21}$$

3.2.4 Eight-Bolt Flush Unstiffened Moment End-Plate

The two controlling yield-line mechanisms for the eight-bolt flush unstiffened moment end-plate configuration are shown in Figure 3.3. This pattern was derived from a study conducted by Mays (2000b). Case I applies to moment end-plates where the pitch distance, p_f, is larger than the distance s, while Case II applies to moment end-plates where the pitch distance p_f, is less than the distance s. The equations for the internal work, W_i, moment end-plate strength, M_{pl}, end-plate thickness, t_p, and the distance s are listed for each case as follows

Case I: $p_f > s$

$$W_i = \frac{4m_p}{h}\left[\frac{b_p}{2}\left[h_1\left(\frac{1}{s}\right)+h_4\left(\frac{1}{s}\right)\right]+\frac{2}{g}\left[h_1\left(s+2.25p_b\right)+h_4\left(s+0.75p_b\right)\right]+\frac{g}{2}\right] \tag{3.22}$$

$$M_{pl} = 4m_p\left[\frac{b_p}{2}\left[h_1\left(\frac{1}{s}\right)+h_4\left(\frac{1}{s}\right)\right]+\frac{2}{g}\left[h_1\left(s+2.25p_b\right)+h_4\left(s+0.75p_b\right)\right]+\frac{g}{2}\right] \tag{3.23}$$

$$t_p = \left[\frac{M_u/F_{py}}{\left[\frac{b_p}{2}\left[h_1\left(\frac{1}{s}\right)+h_4\left(\frac{1}{s}\right)\right]+\frac{2}{g}\left[h_1\left(s+2.25p_b\right)+h_4\left(s+0.75p_b\right)\right]+\frac{g}{2}\right]}\right]^{1/2} \tag{3.24}$$

$$s = \frac{1}{2}\sqrt{b_p g} \tag{3.25}$$

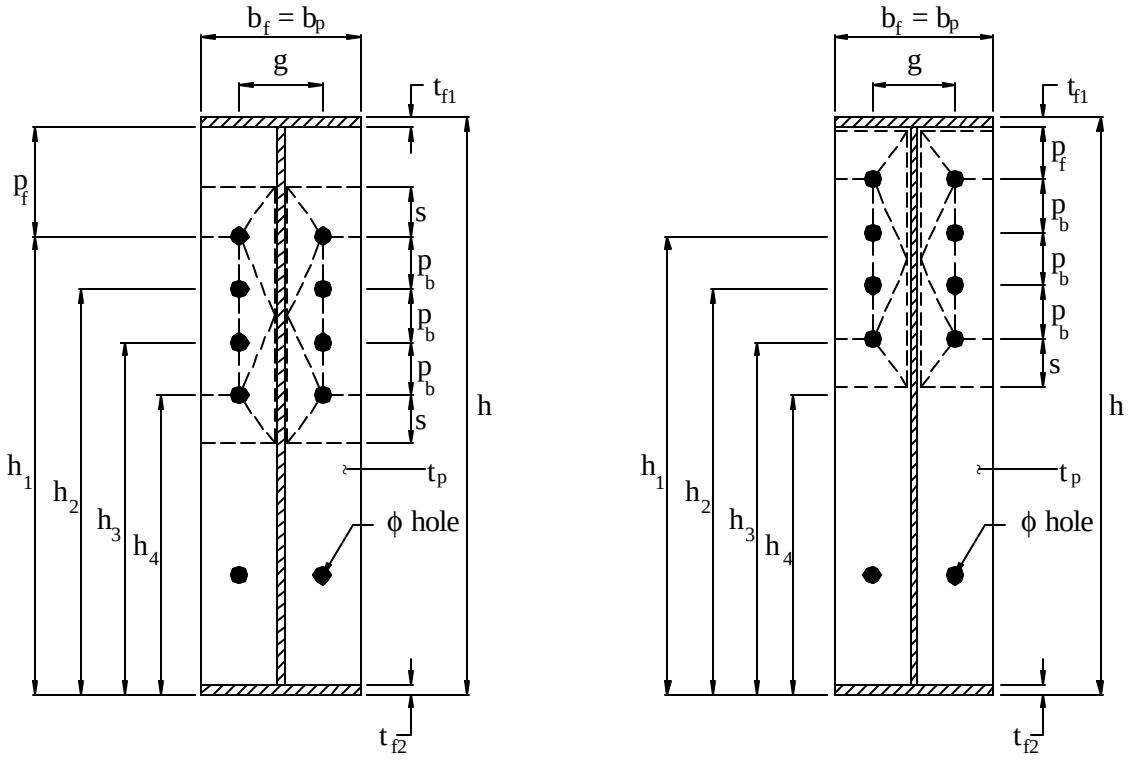

a) Case I: $p_f > s$ b) Case II: $p_f < s$

Figure 3.3 Yield-Line Mechanisms for an Eight-Bolt Flush Unstiffened Moment End-Plate

Case II: $p_f < s$

$$W_i = \frac{4m_p}{h}\left[\frac{b_p}{2}\left[h_1\left(\frac{1}{p_f}\right)+h_4\left(\frac{1}{s}\right)\right]+\frac{2}{g}\left[h_1\left(p_f+2.25p_b\right)+h_4\left(s+0.75p_b\right)\right]+\frac{g}{2}\right] \tag{3.26}$$

$$M_{pl} = 4m_p\left[\frac{b_p}{2}\left[h_1\left(\frac{1}{p_f}\right)+h_4\left(\frac{1}{s}\right)\right]+\frac{2}{g}\left[h_1\left(p_f+2.25p_b\right)+h_4\left(s+0.75p_b\right)\right]+\frac{g}{2}\right] \tag{3.27}$$

$$t_p = \left[\frac{M_u/F_{py}}{\left[\frac{b_p}{2}\left[h_1\left(\frac{1}{p_f}\right)+h_4\left(\frac{1}{s}\right)\right]+\frac{2}{g}\left[h_1\left(p_f+2.25p_b\right)+h_4\left(s+0.75p_b\right)\right]+\frac{g}{2}\right]}\right]^{1/2} \tag{3.28}$$

$$s = \frac{1}{2}\sqrt{b_p g} \tag{3.29}$$

3.2.5 Four-Bolt Flush Moment End-Plate Stiffened Outside Tension Bolt Rows

A study on the behavior of four-bolt flush stiffened moment end-plates was conducted by Mays (2000b). From this study, the two controlling yield-line mechanisms for the four-bolt flush stiffened moment end-plate connection were derived as shown in Figure 3.4. Case I applies to moment end-plates where the pitch distance, p_f, is larger than the distance s, while Case II applies to moment end-plates where the pitch distance p_f, is less than the distance s. In both cases, if the pitch distance from the second row of bolts to the face of the stiffener, p_s, is larger than the distance s, then the connection is treated as if it were unstiffened, and the equations for a four-bolt flush unstiffened moment end-plate apply. For the four-bolt flush stiffened moment end-plate, the

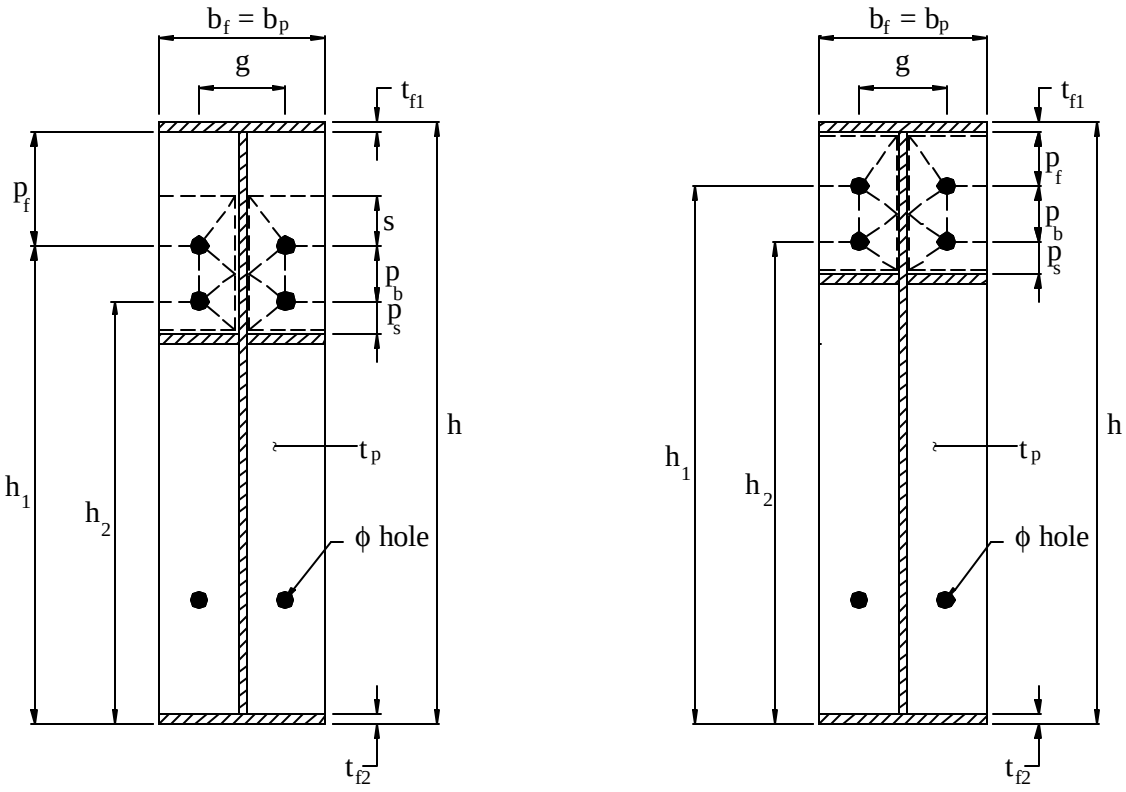

a) Case I: $p_f > s$

b) Case II: $p_f < s$

Figure 3.4 Yield-Line Mechanisms for a Four-Bolt Flush Moment End-Plate with Stiffener Outside the Tension Bolt Rows

equations for the internal work, W_i, moment end-plate strength, M_{pl}, end-plate thickness, t_p, and the distance s are listed for each case as follows

Case I: $p_f > s$

$$W_i = \frac{4m_p}{h}\left[\frac{b_p}{2}\left[h_1\left(\frac{1}{s}\right)+h_2\left(\frac{1}{p_s}\right)\right]+\frac{2}{g}\left[h_1\left(s+0.75p_b\right)+h_2\left(p_s+0.25p_b\right)\right]+\frac{g}{2}\right] \tag{3.30}$$

$$M_{pl} = 4m_p\left[\frac{b_p}{2}\left[h_1\left(\frac{1}{s}\right)+h_2\left(\frac{1}{p_s}\right)\right]+\frac{2}{g}\left[h_1\left(s+0.75p_b\right)+h_2\left(p_s+0.25p_b\right)\right]+\frac{g}{2}\right] \tag{3.31}$$

$$t_p = \left[\frac{M_u/F_{py}}{\left[\frac{b_p}{2}\left[h_1\left(\frac{1}{s}\right)+h_2\left(\frac{1}{p_s}\right)\right]+\frac{2}{g}\left[h_1\left(s+0.75p_b\right)+h_2\left(p_s+0.25p_b\right)\right]+\frac{g}{2}\right]}\right]^{1/2} \tag{3.32}$$

$$s = \frac{1}{2}\sqrt{b_p g} \tag{3.33}$$

Case II: $p_f < s$

$$W_i = \frac{4m_p}{h}\left[\frac{b_p}{2}\left[h_1\left(\frac{1}{p_f}\right)+h_2\left(\frac{1}{p_s}\right)\right]+\frac{2}{g}\left[h_1\left(p_f+0.75p_b\right)+h_2\left(p_s+0.25p_b\right)\right]+\frac{g}{2}\right] \tag{3.34}$$

$$M_{pl} = 4m_p\left[\frac{b_p}{2}\left[h_1\left(\frac{1}{p_f}\right)+h_2\left(\frac{1}{p_s}\right)\right]+\frac{2}{g}\left[h_1\left(p_f+0.75p_b\right)+h_2\left(p_s+0.25p_b\right)\right]+\frac{g}{2}\right] \tag{3.35}$$

$$t_p = \left[\frac{M_u/F_{py}}{\left[\frac{b_p}{2}\left[h_1\left(\frac{1}{p_f}\right)+h_2\left(\frac{1}{p_s}\right)\right]+\frac{2}{g}\left[h_1\left(p_f+0.75p_b\right)+h_2\left(p_s+0.25p_b\right)\right]+\frac{g}{2}\right]}\right]^{1/2} \tag{3.36}$$

$$s = \frac{1}{2}\sqrt{b_p g} \tag{3.37}$$

3.2.6 Multiple Row Extended Unstiffened ¼ Moment End-Plate

The controlling yield-line mechanism for the multiple row extended unstiffened ¼ moment end-plate connection is shown in Figure 3.5. This pattern was derived from a study done by Mays (2000b). For the multiple row extended unstiffened ¼ moment end-plate connection, the equations for the internal work, W_i, moment end-plate strength, M_{pl}, end-plate thickness, t_p, and the distance s are as follows

$$W_i = \frac{4m_p}{h}\left[\begin{array}{l}\frac{b_p}{2}\left[h_1\left(\frac{1}{p_{f,i}}\right)+h_4\left(\frac{1}{s}\right)+h_0\left(\frac{1}{p_{f,o}}\right)-\frac{1}{2}\right]+\\ \frac{2}{g}\left[h_1\left(p_{f,i}+2.25p_b\right)+h_4\left(s+0.75p_b\right)\right]+\frac{g}{2}\end{array}\right] \tag{3.38}$$

$$M_{pl} = 4m_p\left[\begin{array}{l}\frac{b_p}{2}\left[h_1\left(\frac{1}{p_{f,i}}\right)+h_4\left(\frac{1}{s}\right)+h_0\left(\frac{1}{p_{f,o}}\right)-\frac{1}{2}\right]+\\ \frac{2}{g}\left[h_1\left(p_{f,i}+2.25p_b\right)+h_4\left(s+0.75p_b\right)\right]+\frac{g}{2}\end{array}\right] \tag{3.39}$$

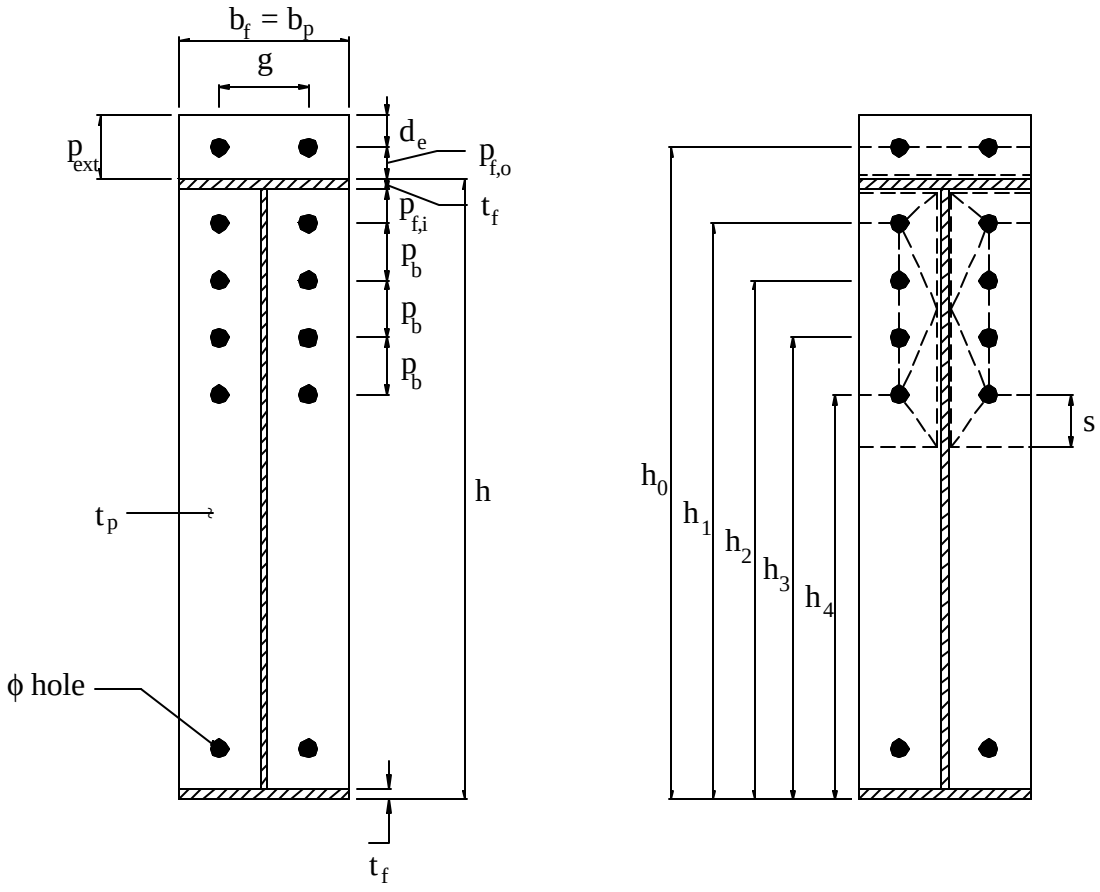

Figure 3.5 Yield-Line Mechanism for a Multiple Row Extended Unstiffened ¼ Moment End-Plate

$$t_p = \left[\frac{M_u / F_{py}}{\left[\frac{b_p}{2}\left[h_1\left(\frac{1}{p_{f,i}}\right) + h_4\left(\frac{1}{s}\right) + h_0\left(\frac{1}{p_{f,o}}\right) - \frac{1}{2}\right] + \frac{2}{g}\left[h_1\left(p_{f,i} + 2.25p_b\right) + h_4\left(s + 0.75p_b\right)\right] + \frac{g}{2}\right]} \right]^{1/2} \tag{3.40}$$

$$s = \frac{1}{2}\sqrt{b_p g} \tag{3.41}$$

3.3 CONNECTION STRENGTH USING SIMPLIFIED BOLT ANALYSIS

3.3.1 General Theory

Since yield-line theory only predicts the moment strength of the connection based on end-plate yielding, a method must be employed to analyze the moment strength of the connection based on bolt forces. As a moment end-plate connection yields, it deforms from its original shape, inducing prying action in the bolts. Thus, prying action is included in the bolt-force analysis. In this study, a simplified version of the Kennedy method (Borgsmiller and Murray 1995) is used to predict the moment strength of the end-plate connection based on the limit state of bolt rupture with prying action.

The Kennedy Split Tee Analogy (Kennedy *et al* 1981) predicts bolt forces in a connection by defining the stage of plate behavior based on the plate thickness and applied load. Once the stage of plate behavior is determined, prying forces are calculated from the corresponding equations. This method has been modified to apply to the analysis of flush end-plates and multiple row extended end-plates (Srouji *et al* 1983). The Kennedy method and the modified Kennedy method require several iterations and

tedious calculations. The simplified method substantially reduces the amount of calculations required.

According to Borgsmiller and Murray (1995), there are two basic assumptions behind the simplified method:

1. Bolts that have reached their proof load can continue yielding without rupture until the other bolts reach their proof load as well.
2. When a bolt reaches its proof load, the plate behaves as a thin plate and the maximum prying force, Q_{max}, can be incorporated into the bolt analysis.

The proof load, P_t, is defined as the product of the design strength listed in Table J3.2 (AISC 1995) and the cross-sectional area of the bolt

$$P_t = A_b F_{yb} \tag{3.42}$$

The bolts in a specific configuration are divided into two categories, load-carrying bolts and non-load-carrying bolts. A load-carrying bolt is one that has been proven experimentally to carry load in an end-plate configuration. In the simplified method, Borgsmiller and Murray (1995) set all load-carrying bolts equal to the proof load, P_t, calculated from Equation 3.42. All non-load-carrying bolts are set equal to the minimum bolt pretension values, T_b, given in Table J3.1 (AISC 1995).

To illustrate the simplified method, Borgsmiller and Murray (1995) use a two-bolt flush unstiffened moment end-plate connection, as shown in Figure 3.6. In the figure, M_q equals the moment strength of the connection based on bolt rupture with prying action and B equals the bolt force per bolt. The subscript q in M_q indicates that prying action is

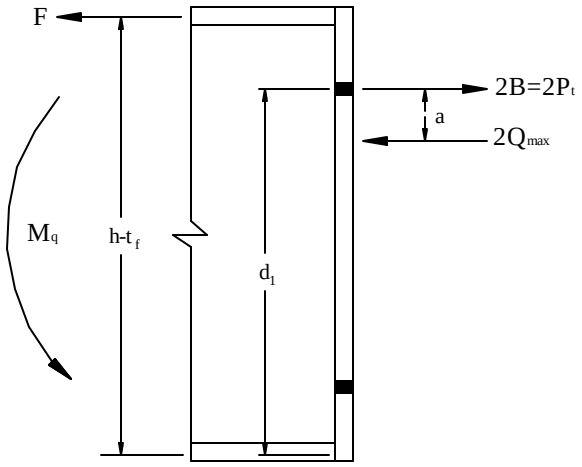

Figure 3.6 Bolt Analysis for a Two-Bolt Flush Unstiffened Moment End-Plate

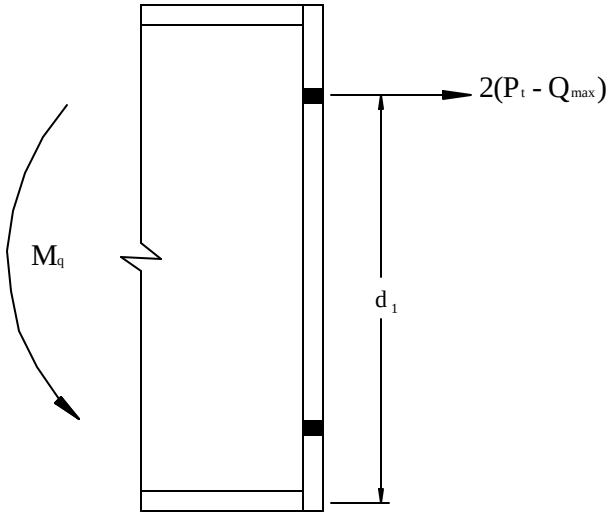

Figure 3.7 Simplified Bolt Force Model for a Two-Bolt Flush Unstiffened Moment End-Plate

included. Summing the moments yields the following

$$\begin{aligned} M_q &= 2Bd_1 - 2Q_{max}(d_1 - a) \\ &= 2\left[(P_t - Q_{max})d_1 + Q_{max}a\right] \end{aligned} \tag{3.43}$$

Borgsmiller and Murray (1995) report that the term $(Q_{max}a)$ only accounts for approximately 2% of the total connection strength, thus it is neglected. Equation 3.43 is reduced to

$$M_q = 2(P_t - Q_{max})d_1 \tag{3.44}$$

From this analysis, it is assumed that all load-carrying bolts hold a load of $(P_t - Q_{max})$, as shown in Figure 3.7. However, it is necessary to ensure that this load is never below the minimum bolt pretension load, T_b. Therefore, M_q can be expressed as

$$M_q = \max \begin{vmatrix} 2(P_t - Q_{max})d_1 \\ 2(T_b)d_1 \end{vmatrix} \tag{3.45}$$

The procedure described above can be generalized to include any configuration as

$$M_q = \max \begin{vmatrix} \sum_{i=1}^{N_i} 2(P_t - Q_{max})_i d + \sum_{j=1}^{N_j} 2(T_b)_j d \\ \sum_{n=1}^{N} 2(T_b)_n d \end{vmatrix} \tag{3.46}$$

where N_i = the number of load-carrying bolt rows, N_j = the number of non-load-carrying bolt rows, N = the total number of bolt rows, and d = the distance from the respective bolt row to the compression flange centerline. The maximum prying force is calculated from (Kennnedy *et al* 1981)

$$Q_{max} = \frac{w' t_p^{\,2}}{4a}\sqrt{F_{py}^2 - 3\left(\frac{F'}{w' t_p}\right)^2} \tag{1.6}$$

where F' equals (Kennedy *et al* 1981)

$$F' = \frac{t_p^2 F_{py}\left(0.85 b_f / 2 + 0.80 w'\right) + \eth d_b^3 F_{yb}/8}{4 p_f} \tag{3.47}$$

Kennedy *et al* (1981) cautioned that the quantity under the radical might be negative. If this occurs, then the end-plate fails in shear and the connection is inadequate to hold the applied load. The distance "a" in Equation 1.6 is different for interior and exterior bolts. For interior bolts (Hendrick *et al* 1985)

$$a_i = 3.682\left(\frac{t_p}{d_b}\right)^3 - 0.085 \tag{3.48}$$

For exterior bolts (Borgsmiller and Murray 1995)

$$a_o = \min \left| \begin{array}{l} 3.682\left(\frac{t_p}{d_b}\right)^3 - 0.085 \\ p_{ext} - p_{f,o} \end{array} \right. \tag{3.49}$$

where p_{ext}= the distance from the outer face of the beam tension flange to the edge of the extended end-plate and $p_{f,o}$= the distance from the outer face of the beam tension flange to the center of the exterior bolt holes (Figure 2.5b). To avoid confusion, the maximum prying force is labeled $Q_{max,i}$ and $Q_{max,o}$, where the subscript "i" stands for interior bolts and the subscript "o" designates outer or exterior bolts.

3.3.2 Four-Bolt Flush Unstiffened Moment End-Plate

The connection strength predictions presented here are taken from a study conducted by Borgsmiller and Murray (1995).

Based on testing done by Srouji *et al* (1983), it was determined that all four bolts in the four-bolt-flush moment end-plate connection are load-carrying bolts. The model

used for this analysis is shown in Figure 3.8. The moment strength of the four-bolt flush connection based on bolt rupture with prying forces is calculated from

$$M_q = \max \begin{vmatrix} 2(P_t - Q_{max})(d_1 + d_2) \\ 2(T_b)(d_1 + d_2) \end{vmatrix} \quad (3.50)$$

where Q_{max} is calculated from Equation 1.6 and P_t is calculated from Equation 3.42.

3.3.3 Six-Bolt Flush Unstiffened Moment End-Plate

The connection strength predictions presented here are taken from a study done by Borgsmiller and Murray (1995).

Based on testing done by Srouji *et al* (1983), it was determined that the first and third rows of bolts in the six-bolt flush moment end-plate connection are composed of load-carrying bolts and the middle row of bolts is composed of non-load-carrying bolts. The model used for this analysis is shown in Figure 3.9. The moment strength of the six-bolt flush connection based on bolt rupture with prying forces is calculated from

$$M_q = \max \begin{vmatrix} 2(P_t - Q_{max})(d_1 + d_3) + 2(T_b)d_2 \\ 2(T_b)(d_1 + d_2 + d_3) \end{vmatrix} \quad (3.51)$$

3.3.4 Eight-Bolt Flush Unstiffened Moment End-Plate

Based on testing performed for this study, the determination of load-carrying and non-load carrying bolts in the eight-bolt flush moment end-plate connection was inconclusive. From Figure 3.10, it is apparent that the outermost bolt row (bolt #6 and #1) consists of load-carrying bolts. It is also clear that the third and fourth outermost tension bolt rows (bolt #2 and #4) and the row of stitch bolts (bolt #5) consist of non-load carrying bolts. The uncertainty arises from the second outermost row (bolt #3) of tension bolts. The second outermost row of tension bolts shows some increase in bolt

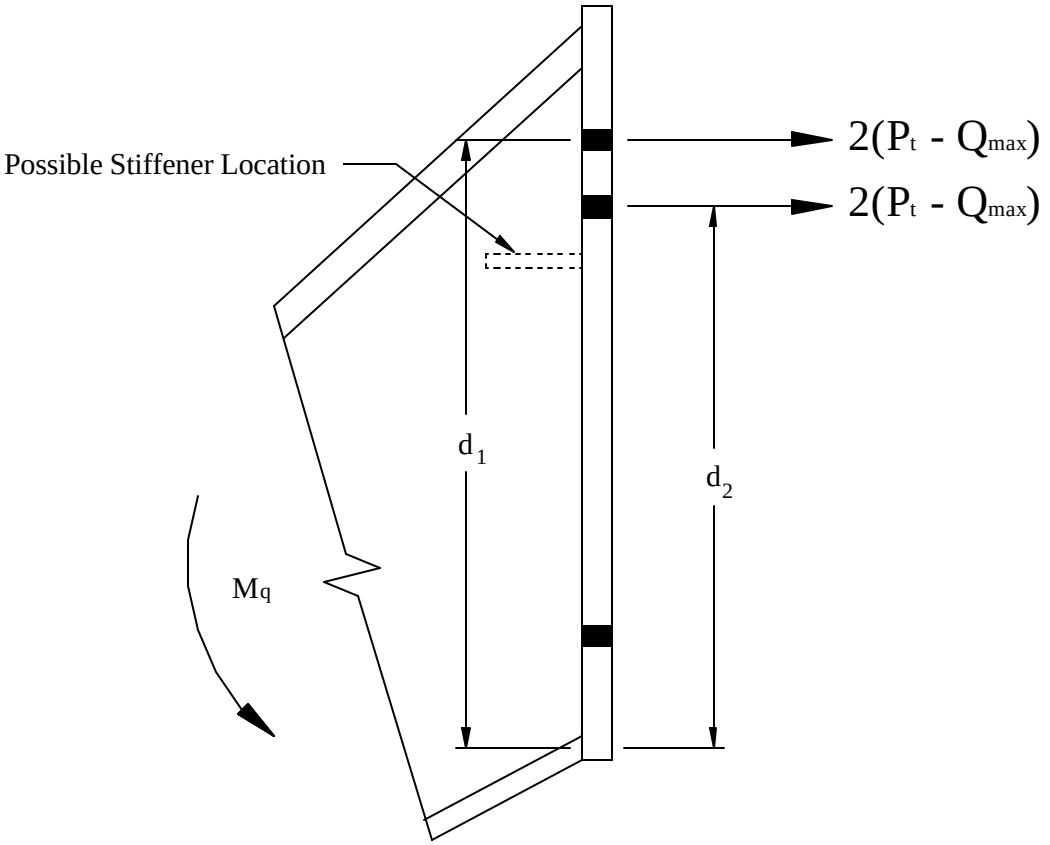

Figure 3.8 Simplified Bolt Force Model for Four-Bolt Flush Stiffened and Unstiffened Moment End-Plates

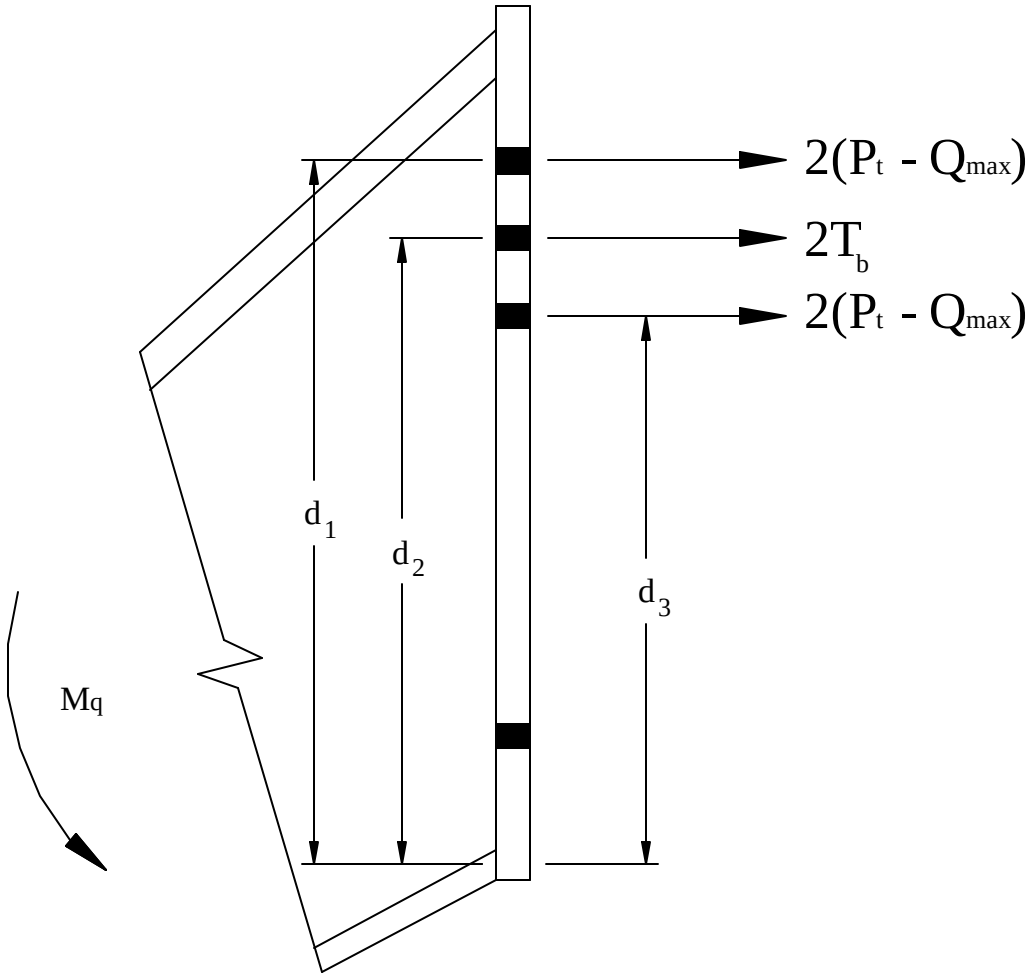

Figure 3.9 Simplified Bolt Force Model for a Six-Bolt Flush Unstiffened Moment End-Plate

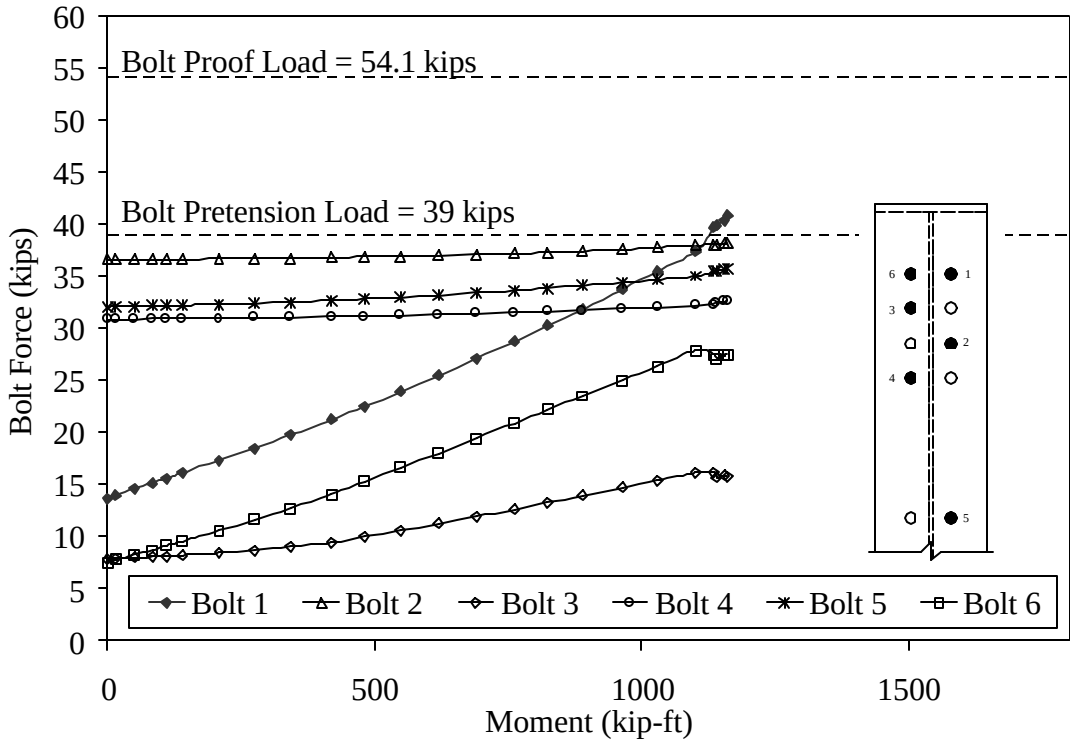

Figure 3.10 Bolt Force vs. Applied Moment for Test F4-$^{7}/_{8}$-$^{3}/_{4}$-67

force, but it is not as large or constant as the increase in bolt force in the outermost row of tension bolts. These results are typical of a moment end-plate connection where the end-plates are not completely flat. Moreover, the pretension load on the second outermost row of tension bolts was much lower than all other non-load-carrying bolts. This makes it difficult to determine whether or not the second outermost row of tension bolts are load-carrying or non-load-carrying at a higher pretension load. Therefore, two possibilities are formulated below. Since Option I is more conservative, it is used to determine the predicted strength based on bolt rupture with prying forces. However, the correct behavior can only be determined from further testing.

Option I:

The model used for this analysis is shown in Figure 3.11. The moment strength for the eight-bolt flush unstiffened connection based on bolt rupture with prying forces is calculated from

$$M_q = \max \begin{vmatrix} 2(P_t - Q_{max})(d_1) + 2(T_b)(d_2 + d_3 + d_4) \\ 2(T_b)(d_1 + d_2 + d_3 + d_4) \end{vmatrix} \quad (3.52)$$

Option II:

The model used for this analysis is shown in Figure 3.12. The moment strength for the eight-bolt flush unstiffened connection based on bolt rupture with prying forces is calculated from

$$M_q = \max \begin{vmatrix} 2(P_t - Q_{max})(d_1 + d_2) + 2(T_b)(d_3 + d_4) \\ 2(T_b)(d_1 + d_2 + d_3 + d_4) \end{vmatrix} \quad (3.53)$$

3.3.5 Four-Bolt Flush Moment End-Plate Stiffened Outside Tension Bolt Rows

The connection strength predictions presented here are taken from a study done by Borgsmiller and Murray (1995).

It was determined that the simplified method for the four-bolt flush stiffened connection is identical to the four-bolt flush unstiffened connection. Thus, all four bolts in the four-bolt stiffened moment end-plate connection are load-carrying bolts. The model used for this analysis is shown in Figure 3.8. The ultimate moment capacity of the four-bolt flush stiffened connection based on bolt rupture with prying forces is calculated from the same equation as the four-bolt flush unstiffened connection

$$M_q = \max \begin{vmatrix} 2(P_t - Q_{max})(d_1 + d_2) \\ 2(T_b)(d_1 + d_2) \end{vmatrix} \quad (3.54)$$

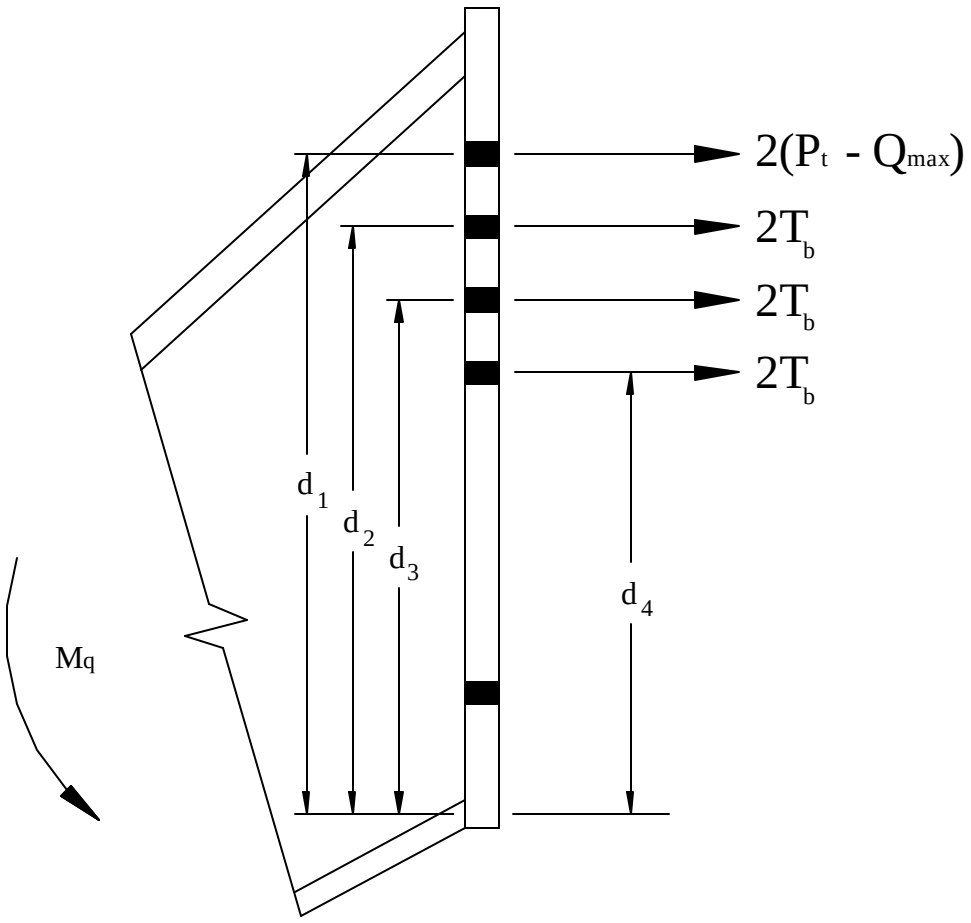

Figure 3.11 Simplified Bolt Force Model for an Eight-Bolt Flush Unstiffened Moment End-Plate – Option I

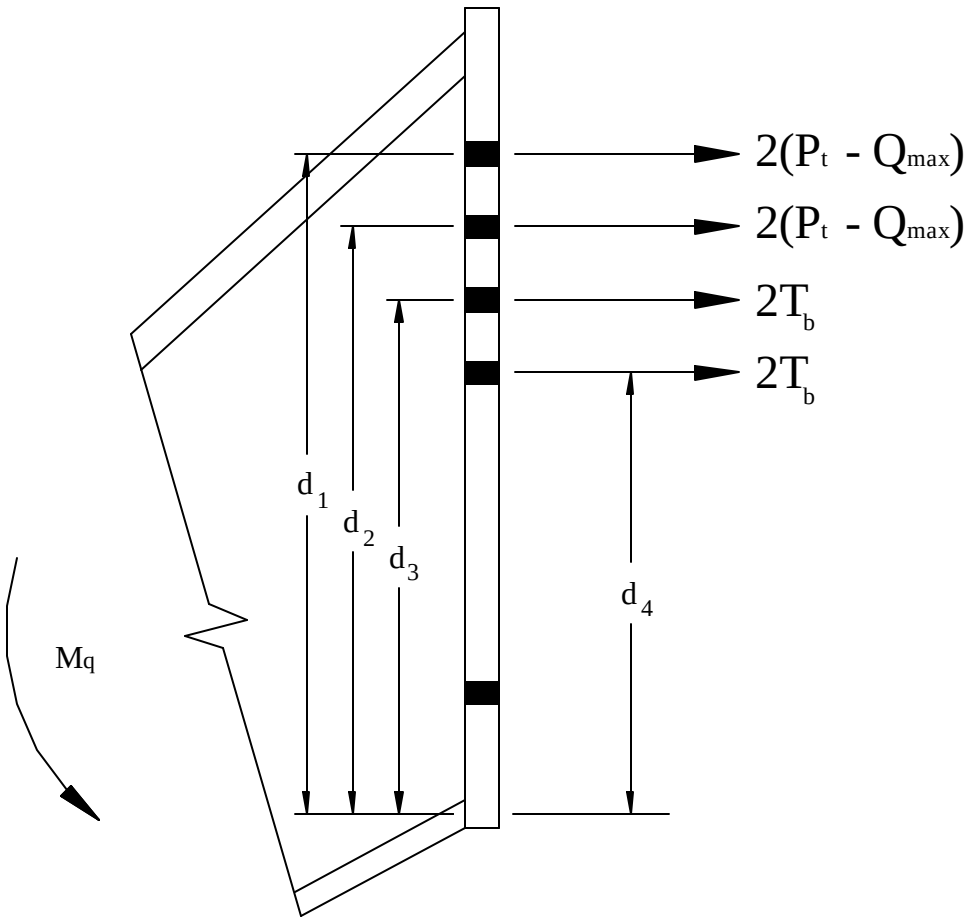

Figure 3.12 Simplified Bolt Force Model for an Eight-Bolt Flush Unstiffened Moment End-Plate – Option II

3.3.6 Multiple Row Extended ¼ Unstiffened Moment End-Plate

Based on testing performed for this study, the determination of load-carrying and non-load carrying bolts in the multiple row extended ¼ moment end-plate connection was inconclusive. From Figure 3.13, it is apparent that the outermost interior tension bolt row (bolt #23) and the exterior tension bolt row (bolt#22) consist of load-carrying bolts. It is also clear that the third outermost tension bolt row (bolt #25) consists of non-load-carrying bolts. The second and forth outermost tension bolt rows (bolt #24 and #26) are not as straightforward to analyze. These two bolt rows do not show an instantaneous increase in bolt force. Therefore, at lower loads, they would be analyzed as non-load carrying bolts. After the specimen has been substantially loaded, these two bolt rows begin to show a gradual increase in bolt force. These results are typical of a moment end-plate connection where the end-plates are not completely flat. Therefore, two

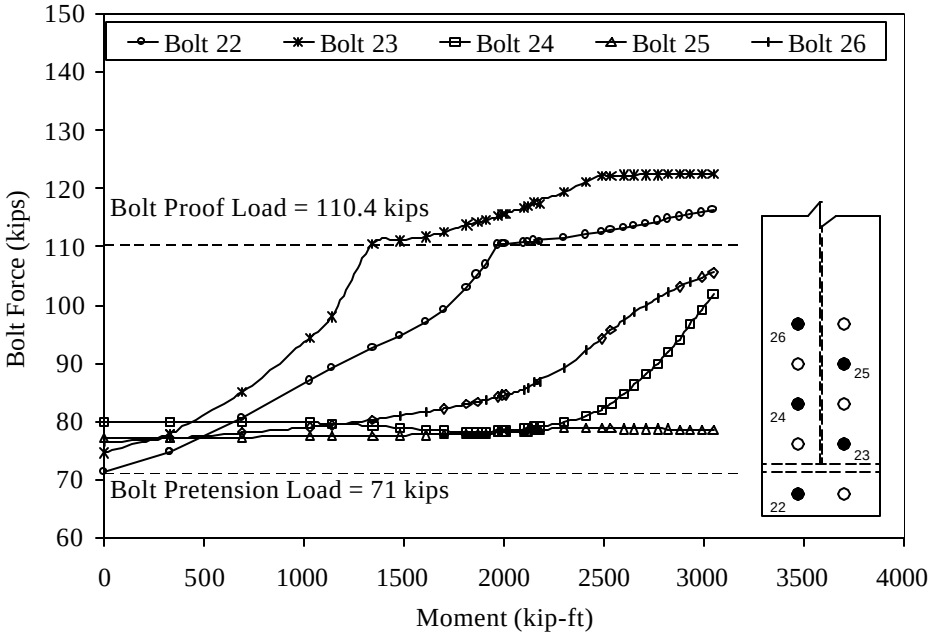

Figure 3.13 Bolt Force vs. Applied Moment for Test MRE$^{1}/_{4}$-1$^{1}/_{4}$-1-70$^{1}/_{2}$

possibilities are formulated below. Since Option I is more conservative, it is used to determine the predicted strength based on bolt rupture with prying forces. However, the correct behavior can only be determined from further testing.

Option I:

The model used for this analysis is shown in Figure 3.14. The moment strength for the multiple row ¼ extended connection based on bolt rupture with prying forces is calculated from

$$M_q = \max \begin{vmatrix} 2(P_t - Q_{max,o})d_0 + 2(P_t - Q_{max,i})d_1 + 2(T_b)(d_2 + d_3 + d_4) \\ 2(P_t - Q_{max,o})d_0 + 2(T_b)(d_1 + d_2 + d_3 + d_4) \\ 2(P_t - Q_{max,i})(d_1) + 2(T_b)(d_0 + d_2 + d_3 + d_4) \\ 2(T_b)(d_0 + d_1 + d_2 + d_3 + d_4) \end{vmatrix} \quad (3.55)$$

Option II:

The model used for this analysis is shown in Figure 3.15. The moment strength for the multiple row ¼ extended connection based on bolt rupture with prying forces is calculated from

$$M_q = \max \begin{vmatrix} 2(P_t - Q_{max,o})d_0 + 2(P_t - Q_{max,i})(d_1 + d_2 + d_4) + 2(T_b)(d_3) \\ 2(P_t - Q_{max,o})d_0 + 2(T_b)(d_1 + d_2 + d_3 + d_4) \\ 2(P_t - Q_{max,i})(d_1 + d_2 + d_4) + 2(T_b)(d_0 + d_3) \\ 2(T_b)(d_0 + d_1 + d_2 + d_3 + d_4) \end{vmatrix} \quad (3.56)$$

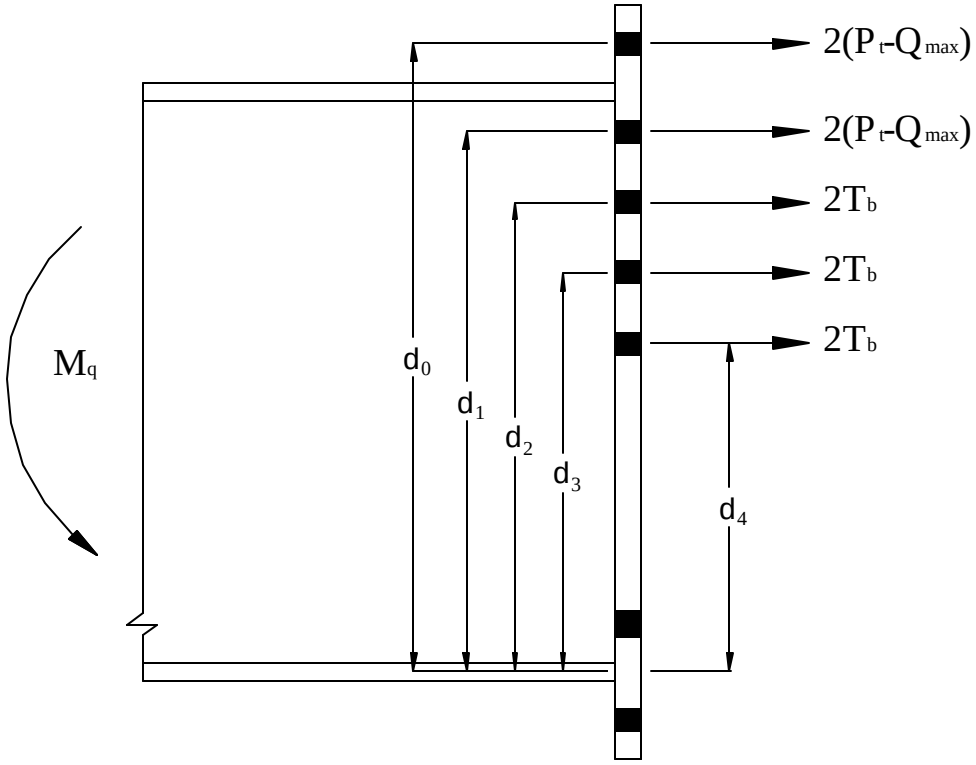

Figure 3.14 Simplified Bolt Force Model for a Multiple Row Extended Unstiffened ¼ Moment End-Plate – Option I

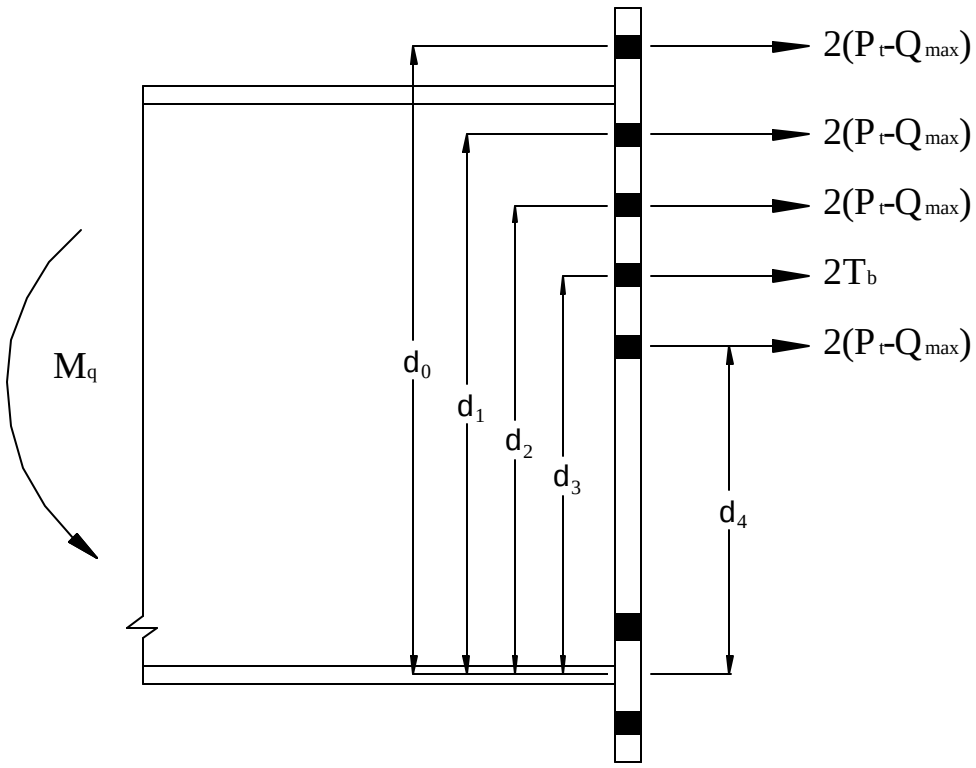

Figure 3.15 Simplified Bolt Force Model for a Multiple Row Extended Unstiffened ¼ Moment End-Plate – Option II

CHAPTER IV

COMPARISON OF EXPERIMENTAL AND ANALYTICAL RESULTS

4.1 OVERVIEW

The results from the experimental and analytical investigations are summarized in the following sections. The predicted connection moment strength, M_{pred}, is determined for each of the six specimens in this study based on the analytical methods presented in Chapter III and in the following section. The determination of the experimental moment strength is then presented. A ratio is used to compare the predicted strength to the experimental strength. This is followed by a discussion of the results.

4.2 DETERMINATION OF PREDICTED CONNECTION MOMENT STRENGTH

In Chapter III, an analytical method is presented to determine the connection strength of five different moment end-plate connections. Two limit states are used to predict the strength of the connection: end-plate yielding and bolt rupture including prying action. End-plate yielding is determined using yield-line theory while bolt rupture including prying action is determined using a simplified version of the Kennedy method (Borgsmiller and Murray 1995). From this analysis, the predicted connection moment strength, M_{pred}, is determined.

To determine the controlling connection moment strength, M_{pred}, one major assumption must be followed (Borgsmiller and Murray 1995); the end-plates must have sufficiently yielded for prying action to occur in the bolts. The moment at which sufficient yielding has occurred is termed the "prying action threshold". Before this point, it is assumed that the plate exhibits thick plate behavior and the prying forces are equal to zero. After the prying action threshold has been met, the plate behaves as a thin plate and the prying forces are set equal to Q_{max}, the maximum prying force. Note that intermediate plate behavior is eliminated in order to simplify the bolt analysis. Borgsmiller and Murray (1995) set the prying action threshold equal to $0.9M_{pl}$ and provide the following guidelines for determining the stage of plate behavior of an end-plate based on the applied moment:

- If applied moment $< 0.9M_{pl}$ thick plate behavior (4.1)
- If applied moment $> 0.9M_{pl}$ thin plate behavior (4.2)

If the end-plate displays thin-plate behavior, then prying forces are included in the predicted connection strength based on bolt rupture. If the end-plate shows thick-plate behavior, then prying forces are not included in the predicted connection strength based on bolt rupture.

In the case that prying forces are not included in the analysis, the predicted connection strength based on bolt rupture is calculated by assuming that all bolts are load-carrying and the prying force is equal to zero, resulting in the following general equation (Borgsmiller and Murray 1995):

$$M_{np} = \sum_{i=1}^{N} 2(P_t)_i d_i \qquad (4.3)$$

where N = the number of bolt rows, d_i = the distance from the respective bolt hole centerline to the centerline of the compression flange, P_t is defined in Equation 3.42, and the subscript "np" signifies that there are no prying forces included in the calculation.

The controlling predicted connection strength is determined by defining the controlling limit state of the end-plate connection. As discussed previously, there are two limit states for moment end-plate connections: end-plate yielding and bolt rupture. If the controlling limit state is bolt rupture, then it must be determined whether or not prying forces can be included in the analysis. The following provides a method to determine the controlling limit state. The limit states are defined based on the relationship between M_{pl}, M_q, and M_{np}:

1. If $M_{pl} < M_q$, the end-plate controls the strength of the connection and
   failure occurs by end-plate yielding.
2. If $M_{pl} > M_q$, the bolts control the strength of the connection and
   (a) If $0.9M_{pl} < M_{np}$, failure occurs by bolt rupture with prying action.
   (b) If $0.9M_{pl} > M_{np}$, failure occurs by bolt rupture with no prying action.

Using the analytical methods proposed in Chapter III and in this section, the predicted connection strengths based on end-plate yielding, M_{pl}, bolt rupture with prying action, M_q, and bolt rupture without prying action, M_{np}, were calculated for the five knee area specimens and the one plate girder specimen tested in this study. The average measured connection details given in Appendices B-G, and the measured yield strength of the end plate given in Table 2.3 were used in the calculations. Using the guidelines presented above, the controlling limit state was defined and thus, the controlling predicted connection strength, M_{pred}, was determined for each specimen. The results of

these calculations are presented in Table 4.1. The shaded regions in the table correspond to the controlling predicted connection strength for each specimen.

It is important to note that the predicted connection strengths were calculated for the number of tension bolt rows listed in the second column in Table 4.1 and not the number indicated in the test designations. The number of tension bolt rows is not in agreement with the test designations for tests F5-$1^1/_4$-$^3/_4$-84 and F5S-$1^1/_4$-$^3/_4$-84. These two knee area specimens were tested in a series of cycles. Prior to the commencement of each new cycle, bolts were removed from the connection. Thus, the number of bolt rows listed in column two of Table 4.1 for these two test specimens was the number of bolt rows during the last cycle of testing when failure occurred.

4.3 DETERMINATION OF EXPERIMENTAL CONNECTION MOMENT STRENGTH

The experimental connection moment strength presented in Table 4.1 is dependent on the failure mode of each specimen. For the test specimens that failed at the connection, the experimental moment strength is defined at the yield point of the connection. The yield point is determined by separating the moment vs. deflection plot into two linear segments. The yield point is defined as the intersection of these two segments, and the moment corresponding to this point is the yield moment, M_y. Figures 4.4 and 4.5 show the yield point and yield moment of the two knee area specimens that failed at the connection. For the test specimens that did not fail at the connection, the experimental moment strength is defined as the maximum moment applied to the specimen, M_{max}. Figures 4.1-4.3 and Figure 4.6 show the maximum applied moment of the test specimens that did not fail at the connection.

Table 4.1

Moment End-Plate Predicted and Experimental Results

Test Designation	No. of Tension Bolt Rows in Test	Predicted Strengths					Experimental Strength		M_{pred}/M_y kip-ft	M_{pred}/M_{max} kip-ft
		M_q kip-ft	M_{pl} kip-ft	$0.9M_{pl}$ kip-ft	M_{np} kip-ft	M_{pred} kip-ft	M_y kip-ft	M_{max} kip-ft		
F2-$^5/_8$-$^1/_2$-28	2	160	220	198	193	193		150		1.29*
F3-$^3/_4$-$^3/_4$-50	3	641	1353	1218	811	811		552		1.47*
F4-$^7/_8$-$^3/_4$-67	4	1465***	1878	1690	1969	1465		1160		1.26*
F5-1$^1/_4$-$^3/_4$-84	3	2538	2005	1805	3948	2005	2450		0.82	
F5S-1$^1/_4$-$^3/_4$-84	2	1742	1781	1603	2709	1742	2000		0.87	
MRE$^1/_4$-1$^1/_4$-1-70$^1/_2$	5	3399***	4056	3650	5030	3399		3044		1.12**

* Connection did not fail.
** Specimen did not reach failure.
***Calculated using Option I for bolt force distribution.

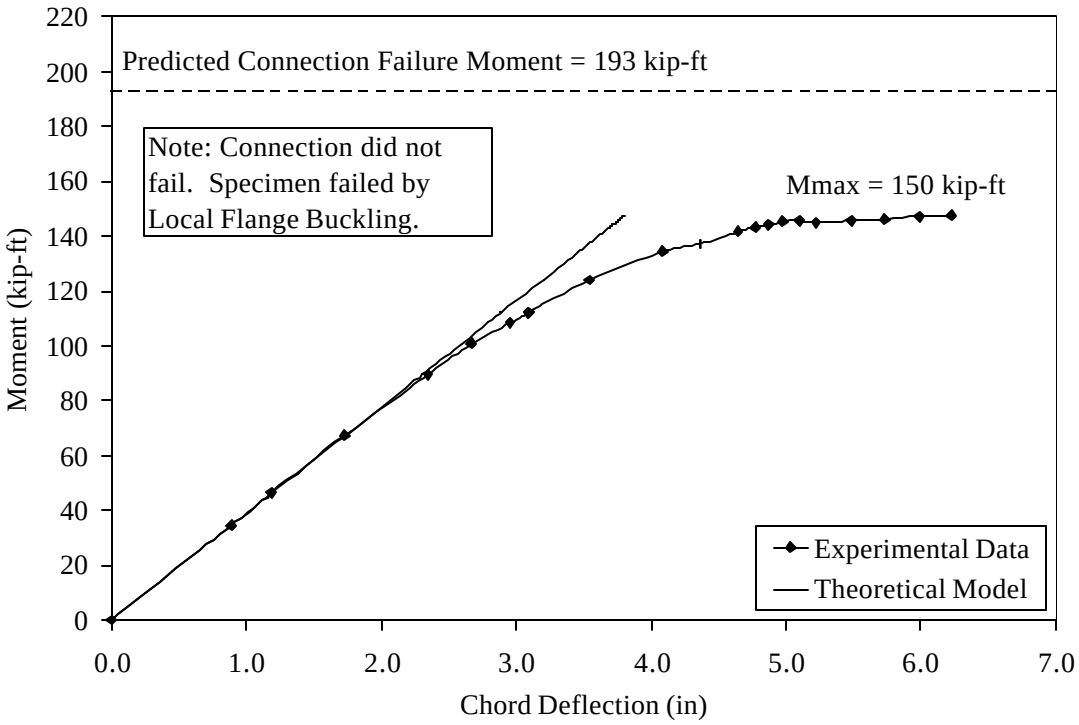

Figure 4.1 Applied Moment vs. Chord Deflection for Test F2-$^{5}/_{8}$-$^{1}/_{2}$-28

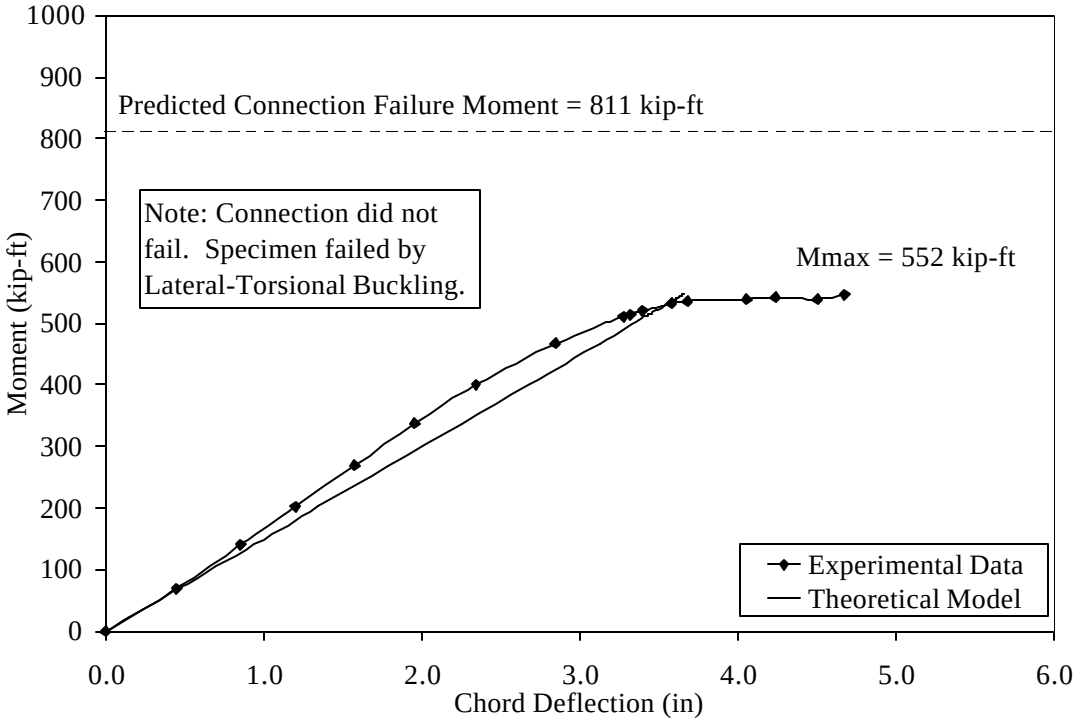

Figure 4.2 Applied Moment vs. Chord Deflection for Test F3-$^{3}/_{4}$-$^{3}/_{4}$-50

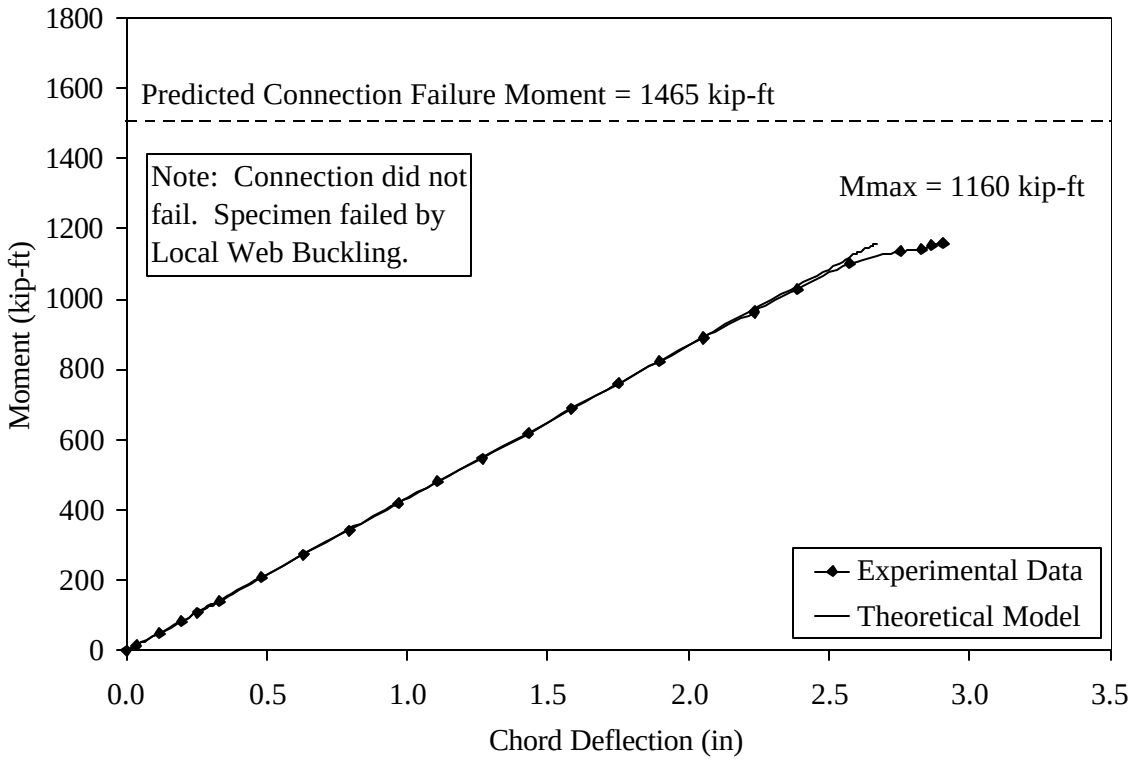

Figure 4.3 Applied Moment vs. Chord Deflection for Test F4-$^{7}/_{8}$-$^{3}/_{4}$-67

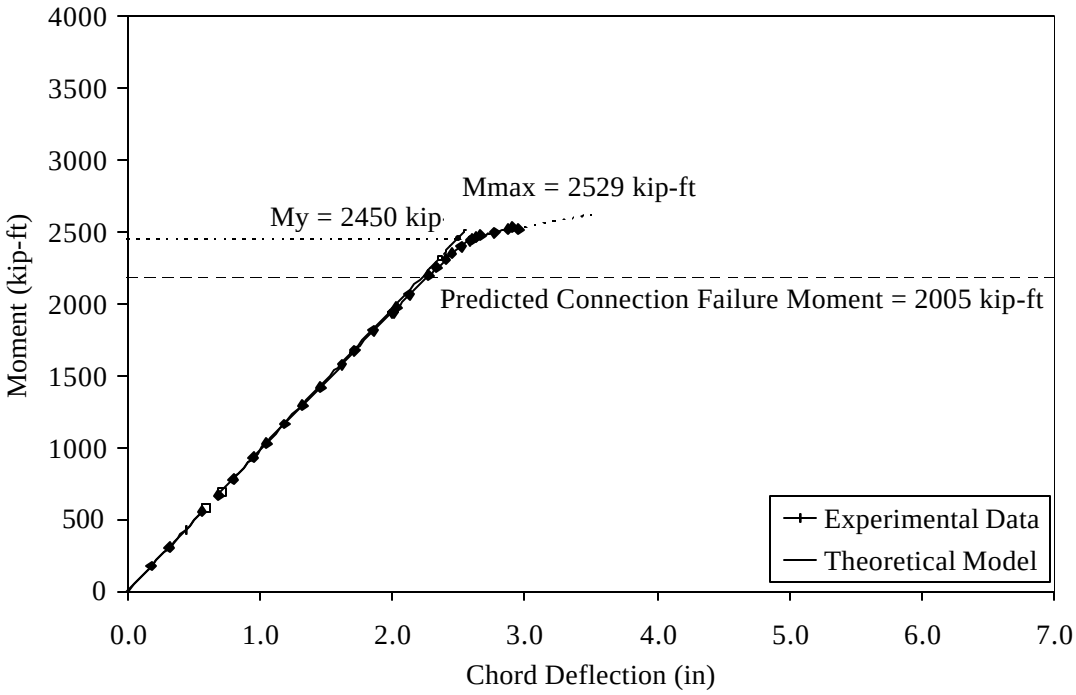

Figure 4.4 Applied Moment vs. Chord Deflection for Cycle 4 in Test F5-1$^{1}/_{4}$-$^{3}/_{4}$-84

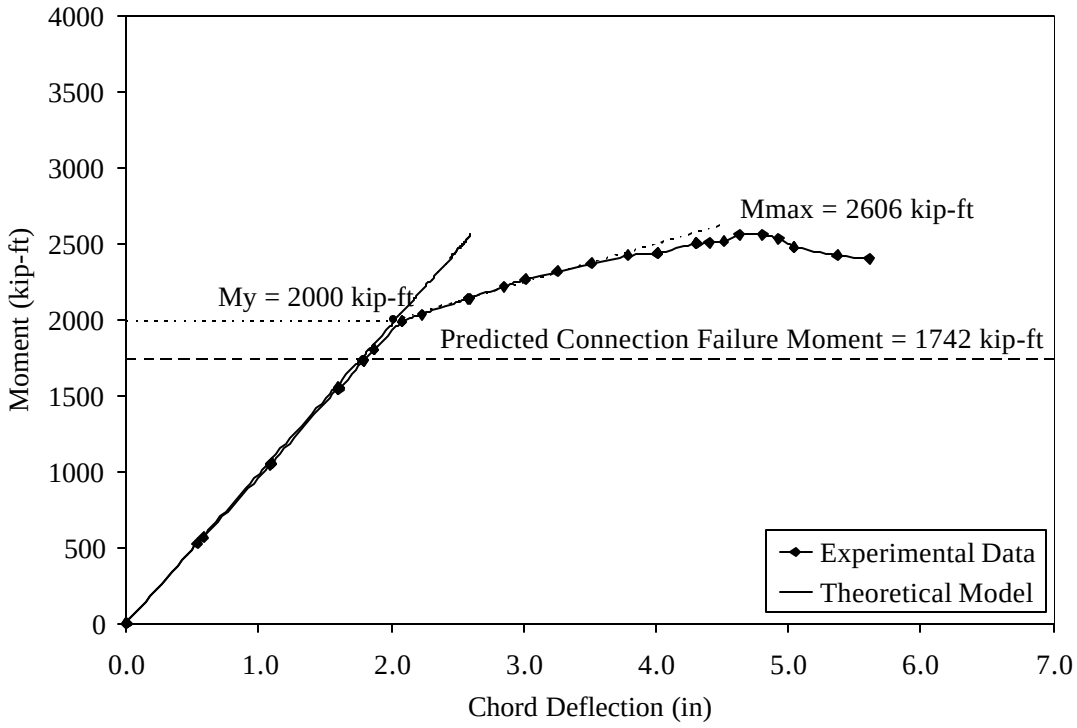

Figure 4.5 Applied Moment vs. Chord Deflection for Cycle 5 in Test F5S-$1^{1}/_{4}$-$^{3}/_{4}$-84

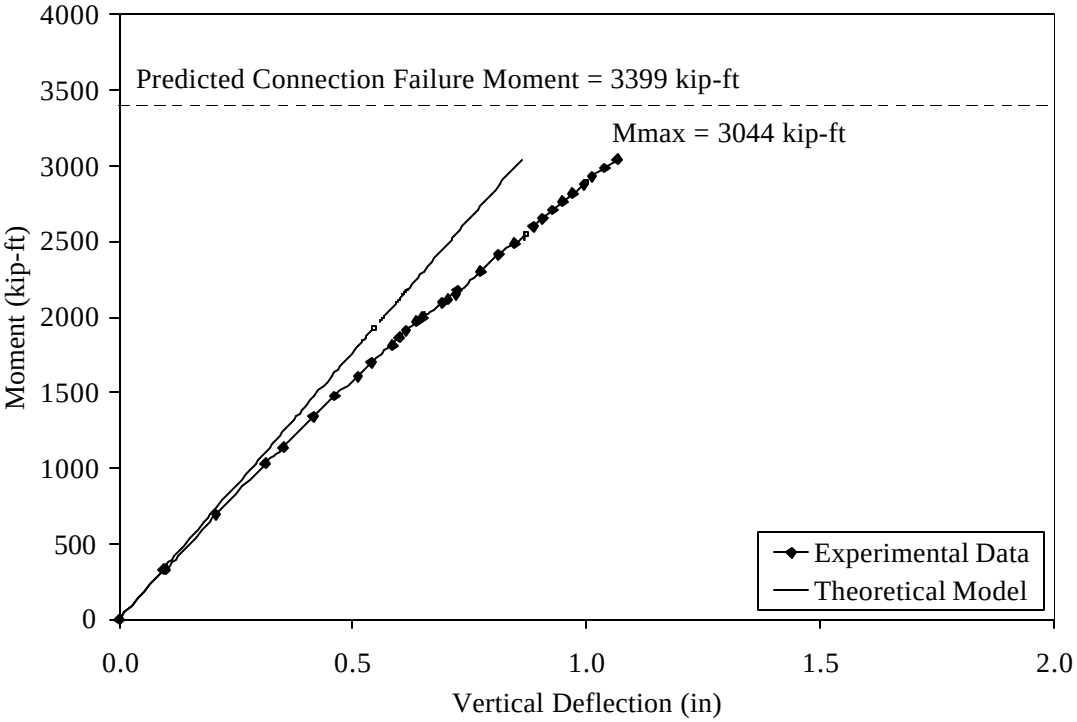

Figure 4.6 Applied Moment vs. Average Vertical Deflection at the Load Points for Test MRE$^{1}/_{4}$-$1^{1}/_{4}$-1-$70^{1}/_{2}$

4.4 COMPARISON OF EXPERIMENTAL AND PREDICTED CONNECTION STRENGTHS

A ratio of the predicted strength to the experimental strength is calculated for each specimen in Table 4.1. Moment strength ratio values less than one indicate that the predicted strength is conservative. Moment strength ratio values greater than one do not indicate whether or not the predicted strength is conservative because in each of these cases, the connection did not fail. Failure either occurred in the member or not at all.

Tests F2-$^{5}/_{8}$-$^{1}/_{2}$-28, F3-$^{3}/_{4}$-$^{3}/_{4}$-50, and F4-$^{7}/_{8}$-$^{3}/_{4}$-67 all reached their maximum moment by member failure, not connection failure. The ratios between the predicted moment strength and the experimental moment strength for each of these specimens are 1.29, 1.47, and 1.26, respectively. Although the predicted moment strength is substantially above the experimental moment strength, it does not necessarily indicate that the predicted values are unconservative. In each of the three specimens, it was apparent that the connection was capable of holding more load, had the member not failed. Since the predicted connection moment strength was above the experimental moment strength in each specimen, it is possible that the predicted connection moment strengths may correlate well with the experimental strengths had the connection been the controlling limit state. However, this can only be determined by further testing.

Tests F5-$1^{1}/_{4}$-$^{3}/_{4}$-84 and F5S-$1^{1}/_{4}$-$^{3}/_{4}$-84 both reached their maximum moment by connection failure. The ratios between the predicted connection moment strength and the experimental connection moment strength for the specimens are 0.82 and 0.87, respectively. Therefore, it can be concluded that the predicted moment strengths are conservative.

Test MRE$^{1}/_{4}$-$1^{1}/_{4}$-1-$70^{1}/_{2}$ did not reach failure. The strength of the specimen exceeded the strength of the test setup and the test was stopped before failure occurred. The ratio between the predicted moment strength and the experimental moment strength for this test specimen is 1.12. Since the predicted connection moment strength was above the experimental moment strength, it is possible that the predicted connection moment strength may correlate with the experimental strength, had the connection failed. As before, this can only be determined by further testing.

CHAPTER V

SUMMARY, CONCLUSIONS AND RECOMMENDATIONS

5.1 SUMMARY

An analytical investigation was conducted to study the behavior of diagonal knee moment end-plate connections and a multiple row extended moment end-plate connection. Due to the large pitch distances that are typically found in diagonal knee moment end-plate connections, provisions were added to accommodate these parameters. The analytical investigation was based on the limit states of end-plate yielding and bolt rupture. Yield-line theory was used to predict the end-plate yield strength of each configuration and a simplified method proposed by Borgsmiller and Murray (1995) was used to predict bolt forces including and excluding prying forces. The following five different end-plate connections were analyzed:

- Four-Bolt Flush Unstiffened Moment End-Plate
- Six-Bolt Flush Unstiffened Moment End-Plate
- Eight-Bolt Flush Unstiffened Moment End-Plate
- Four-Bolt Flush Moment End-Plate Stiffened Outside Tension Bolt Rows
- Multiple Row Extended Unstiffened ¼ Moment End-Plate

A summary of the analytical procedures is shown in Tables 5.1-5.6. Table 5.1 lists the equations needed to calculate the parameters in the bolt rupture equations. Tables 5.2-5.6 illustrate and summarize the equations used to calculate the moment strength of the five

end-plate connections in this study based on end-plate yielding, bolt rupture including prying action and bolt rupture excluding prying action. Note that m_p has been substituted into each equation and a variable "Y" is included to simplify the calculation of the connection strength based on the limit state of end-plate yielding.

An experimental investigation was used to verify the predicted results. Five knee area specimens and one plate girder specimen, each with a unique moment end-plate configuration, were tested to faliure. Three of the knee area specimens (F2-$^5/_8$-$^1/_2$-28, F3-$^3/_4$-$^3/_4$-50, and F4-$^7/_8$-$^3/_4$-67) failed in the rafter or column member. Two of the knee area specimens (F5-$1^1/_4$-$^3/_4$-84 and F5S-$1^1/_4$-$^3/_4$-84) failed in the connection. The plate girder specimen strength exceeded the strength of the test setup and thus, did not reach failure.

The experimental results were analyzed and compared with the predicted results. For the two knee area specimens that failed at the connection, the ratios of the predicted strengths to the experimental strengths were conservative (0.82 and 0.87). For the remaining test specimens, the ratio of the predicted strengths to the experimental strengths did not indicate whether or not the predicted strengths were conservative because the connection did not fail. However, since the predicted connection strength was above the experimental strength for the remaining specimens, it is possible that the predicted and experimental strengths may correlate well, had the connection failed. This can only be determined from further testing.

Table 5.1 Summary of Bolt Equations (after Borgsmiller and Murray 1995)

Bolt Proof Load	$P_t = A_b F_{yb} = \frac{\pi d_b^2}{4}(F_{yb})$ F_{yb} = 90 ksi, nominal tensile strength of A325 bolts, specified in Table J3.2 (AISC 1995)		
Bolt Pretension	T_b = specified force in Table J3.1 (AISC 1995)		
Maximum Prying Force	Flush Configurations	$Q_{max} = \frac{w' t_p^2}{4a}\sqrt{F_{py}^2 - 3\left(\frac{F'}{w' t_p}\right)^2}$ $F' = \frac{t_p^2 F_{py}(0.85 b_f/2 + 0.80 w') + \pi d_b^3 F_{yb}/8}{4 p_f}$ $a = 3.682\left(\frac{t_p}{d_b}\right)^3 - 0.085$	
	Extended Configurations	$Q_{max,i} = \frac{w' t_p^2}{4a_i}\sqrt{F_{py}^2 - 3\left(\frac{F_i'}{w' t_p}\right)^2}$ $a_i = 3.682\left(\frac{t_p}{d_b}\right)^3 - 0.085$ $F_i' = \frac{t_p^2 F_{py}(0.85 b_f/2 + 0.80 w') + \pi d_b^3 F_{yb}/8}{4 p_{f,i}}$	$Q_{max,o} = \frac{w' t_p^2}{4a_o}\sqrt{F_{py}^2 - 3\left(\frac{F_o'}{w' t_p}\right)^2}$ $a_o = \min\left\{\begin{array}{l} 3.682\left(\frac{t_p}{d_b}\right)^3 - 0.085 \\ p_{ext} - p_{f,o} \end{array}\right.$ $F_o' = \frac{t_p^2 F_{py}(0.85 b_f/2 + 0.80 w') + \pi d_b^3 F_{yb}/8}{4 p_{f,o}}$
		Inside Bolt Rows	Outside Bolt Rows

Table 5.2 Summary of Four-Bolt Flush Unstiffened Moment End-Plate Analysis

Geometry	Yield-Line Mechanism; Case I
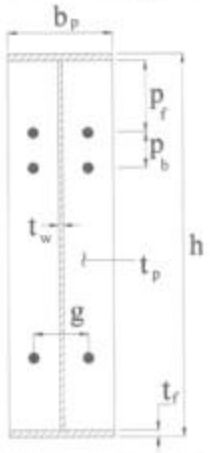	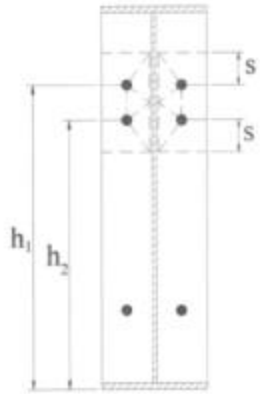
Bolt Force Model	**Yield-Line Mechanism; Case II**
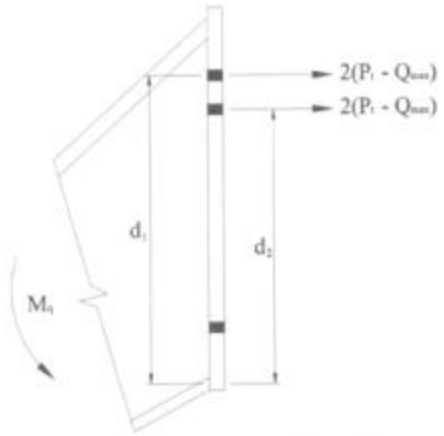	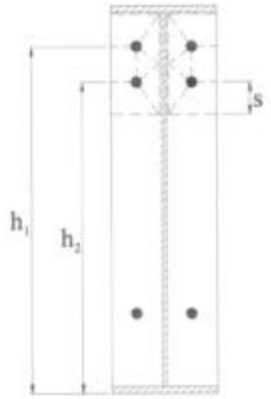

Table 5.2 Summary of Four-Bolt Flush Unstiffened Moment End-Plate Analysis (Con't)

End-Plate Yield	Case I: $p_f > s$	$M_{pl} = F_{py} t_p^2 Y$ $Y = \frac{b_p}{2}\left[h_1\left(\frac{1}{s}\right) + h_2\left(\frac{1}{s}\right)\right] + \frac{2}{g}\left[h_1(s + 0.75p_b) + h_2(s + 0.25p_b)\right] + \frac{g}{2}$ $s = \frac{1}{2}\sqrt{b_p g}$
	Case II: $p_f < s$	$M_{pl} = F_{py} t_p^2 Y$ $Y = \frac{b_p}{2}\left[h_1\left(\frac{1}{p_f}\right) + h_2\left(\frac{1}{s}\right)\right] + \frac{2}{g}\left[h_1(p_f + 0.75p_b) + h_2(s + 0.25p_b)\right] + \frac{g}{2}$ $s = \frac{1}{2}\sqrt{b_p g}$
Bolt Rupture w/Prying Action		$M_q = \max \begin{vmatrix} 2(P_t - Q_{max})(d_1 + d_2) \\ 2(T_b)(d_1 + d_2) \end{vmatrix}$
Bolt Rupture No Prying Action		$M_{np} = 2(P_t)(d_1 + d_2)$

Table 5.3 Summary of Six-Bolt Flush Unstiffened Moment End-Plate Analysis

Geometry	Yield-Line Mechanism; Case I
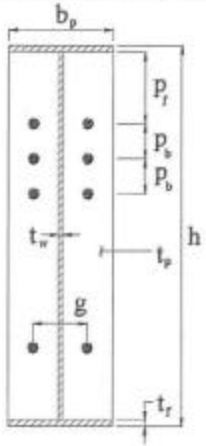	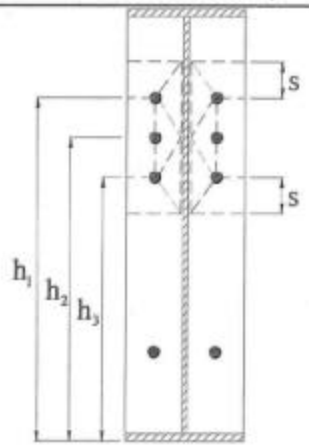
Bolt Force Model	**Yield-Line Mechanism; Case II**
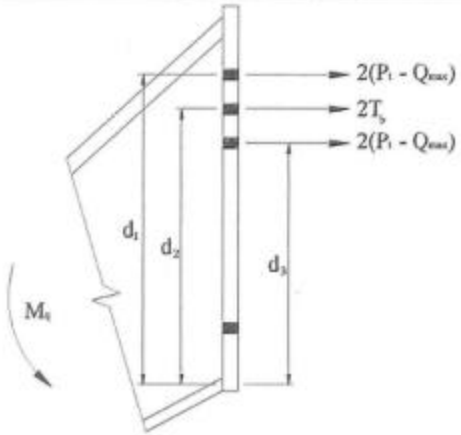	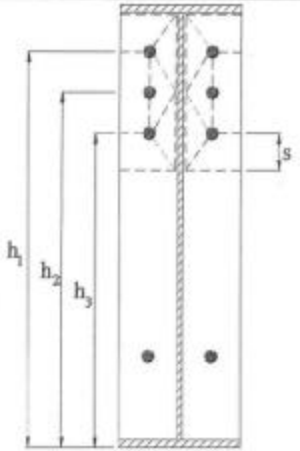

Table 5.3 Summary of Six-Bolt Flush Unstiffened Moment End-Plate Analysis (Con't)

End-Plate Yield	Case I: $p_f > s$	$M_{pl} = F_{py} t_p^2 Y$ $Y = \frac{b_p}{2}\left[h_1\left(\frac{1}{s}\right) + h_3\left(\frac{1}{s}\right)\right] + \frac{2}{g}\left[h_1(s + 1.5p_b) + h_3(s + 0.5p_b)\right] + \frac{g}{2}$ $s = \frac{1}{2}\sqrt{b_p g}$
	Case II: $p_f < s$	$M_{pl} = F_{py} t_p^2 Y$ $Y = \frac{b_p}{2}\left[h_1\left(\frac{1}{p_f}\right) + h_3\left(\frac{1}{s}\right)\right] + \frac{2}{g}\left[h_1(p_f + 1.5p_b) + h_3(s + 0.5p_b)\right] + \frac{g}{2}$ $s = \frac{1}{2}\sqrt{b_p g}$
Bolt Rupture w/Prying Action		$M_q = \max \begin{vmatrix} 2(P_t - Q_{max})(d_1 + d_3) + 2(T_b)d_2 \\ 2(T_b)(d_1 + d_2 + d_3) \end{vmatrix}$
Bolt Rupture No Prying Action		$M_{np} = 2(P_t)(d_1 + d_2 + d_3)$

Table 5.4 Summary of Eight-Bolt Flush Unstiffened Moment End-Plate Analysis

Geometry	Yield-Line Mechanism; Case I	Yield-Line Mechanism; Case II
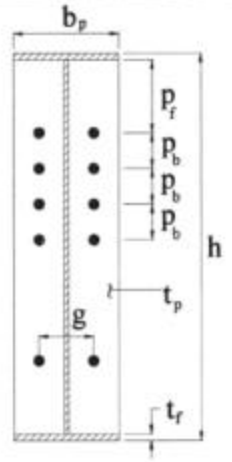	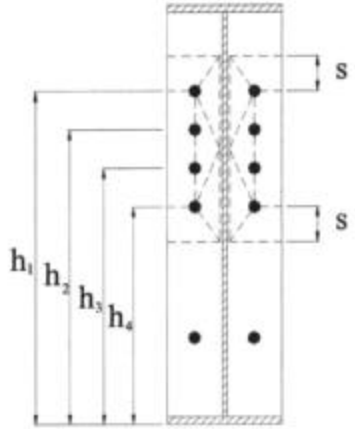	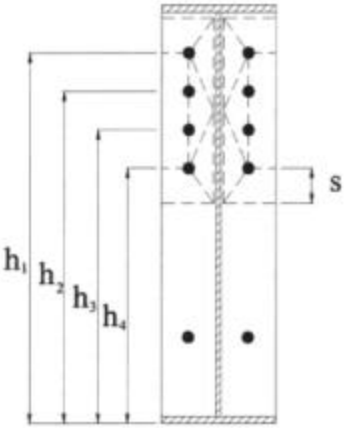
Bolt Force Model; Option I	**Bolt Force Model; Option II**	
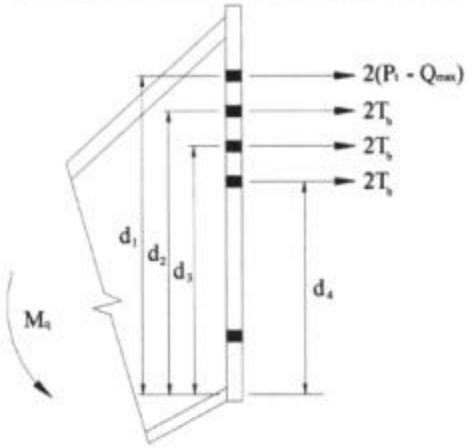	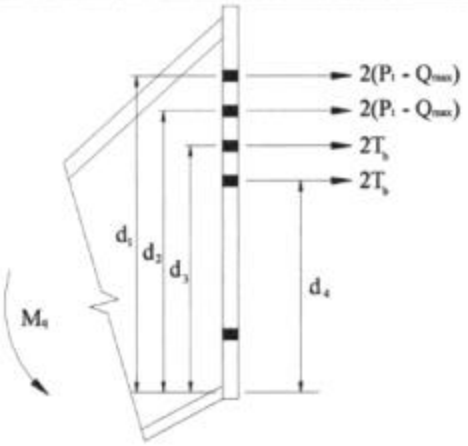	

Table 5.4 Summary of Eight-Bolt Flush Unstiffened Moment End-Plate Analysis (Con't)

End-Plate Yield	Case I: $p_f > s$	$M_{pl} = F_{py} t_p^2 Y$ $Y = \frac{b_p}{2}\left[h_1\left(\frac{1}{s}\right) + h_4\left(\frac{1}{s}\right)\right] + \frac{2}{g}\left[h_1(s + 2.25p_b) + h_4(s + 0.75p_b)\right] + \frac{g}{2}$ $s = \frac{1}{2}\sqrt{b_p g}$
	Case II: $p_f < s$	$M_{pl} = F_{py} t_p^2 Y$ $Y = \frac{b_p}{2}\left[h_1\left(\frac{1}{p_f}\right) + h_4\left(\frac{1}{s}\right)\right] + \frac{2}{g}\left[h_1(p_f + 2.25p_b) + h_4(s + 0.75p_b)\right] + \frac{g}{2}$ $s = \frac{1}{2}\sqrt{b_p g}$
Bolt Rupture w/Prying Action	Option I	$M_q = \max \begin{vmatrix} 2(P_t - Q_{max})(d_1) + 2(T_b)(d_2 + d_3 + d_4) \\ 2(T_b)(d_1 + d_2 + d_3 + d_4) \end{vmatrix}$
	Option II	$M_q = \max \begin{vmatrix} 2(P_t - Q_{max})(d_1 + d_2) + 2(T_b)(d_3 + d_4) \\ 2(T_b)(d_1 + d_2 + d_3 + d_4) \end{vmatrix}$
Bolt Rupture No Prying Action		$M_{np} = 2(P_t)(d_1 + d_2 + d_3 + d_4)$

Table 5.5 Summary of Four-Bolt Flush Stiffened Moment End-Plate Analysis (Stiffened Outside the Tension Bolt Rows)

Geometry	Yield-Line Mechanism; Case I
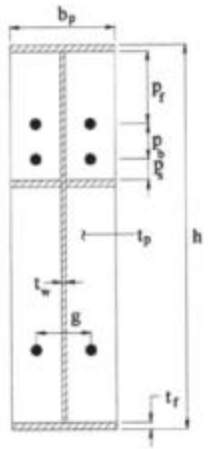	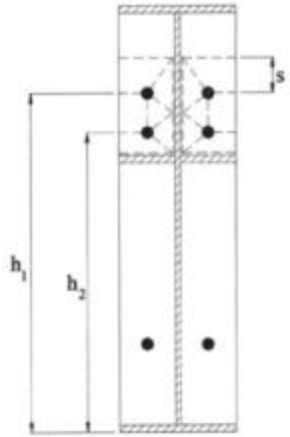
Bolt Force Model	**Yield-Line Mechanism; Case II**
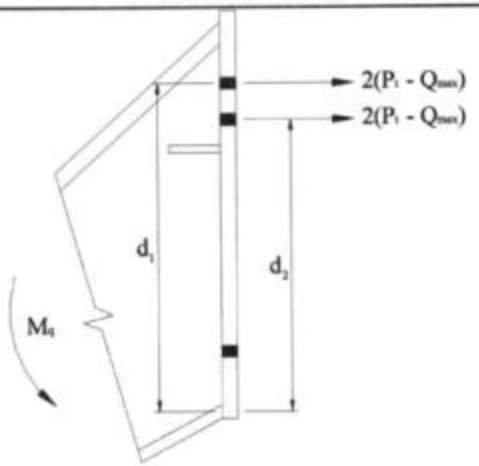	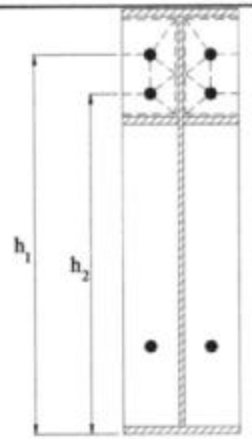

Table 5.5 Summary of Four-Bolt Flush Stiffened Moment End-Plate Analysis (Stiffened Outside the Tension Bolt Rows) (Con't)

End-Plate Yield ***NOTE:*** If $p_s > s$, use unstiffened case with $p_s = s$	Case I: $p_f > s$	$M_{pl} = F_{py} t_p^2 Y$ $Y = \frac{b_p}{2}\left[h_1\left(\frac{1}{s}\right) + h_2\left(\frac{1}{p_s}\right)\right] + \frac{2}{g}\left[h_1(s + 0.75p_b) + h_2(p_s + 0.25p_b)\right] + \frac{g}{2}$ $s = \frac{1}{2}\sqrt{b_p g}$
	Case II: $p_f < s$	$M_{pl} = F_{py} t_p^2 Y$ $Y = \frac{b_p}{2}\left[h_1\left(\frac{1}{p_f}\right) + h_2\left(\frac{1}{p_s}\right)\right] + \frac{2}{g}\left[h_1(p_f + 0.75p_b) + h_2(p_s + 0.25p_b)\right] + \frac{g}{2}$ $s = \frac{1}{2}\sqrt{b_p g}$
Bolt Rupture w/Prying Action		$M_q = \max \begin{vmatrix} 2(P_t - Q_{max})(d_1 + d_2) \\ 2(T_b)(d_1 + d_2) \end{vmatrix}$
Bolt Rupture No Prying Action		$M_{np} = 2(P_t)(d_1 + d_2)$

Table 5.6 Summary of Multiple Row Extended Unstiffened ¼ Moment End-Plate Analysis

Geometry	Yield-Line Mechanism
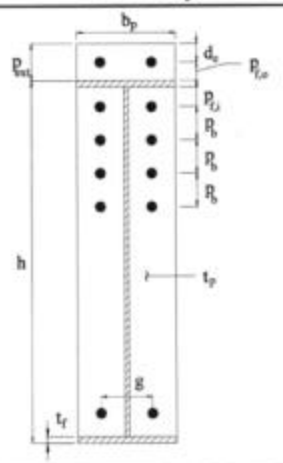	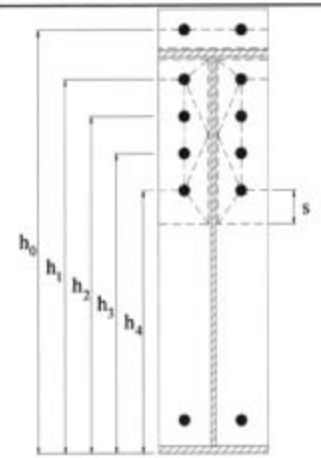
Bolt Force Model; Option I	**Bolt Force Model; Option II**
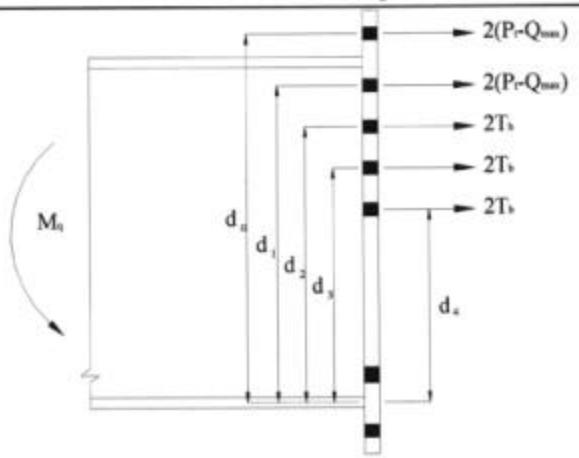	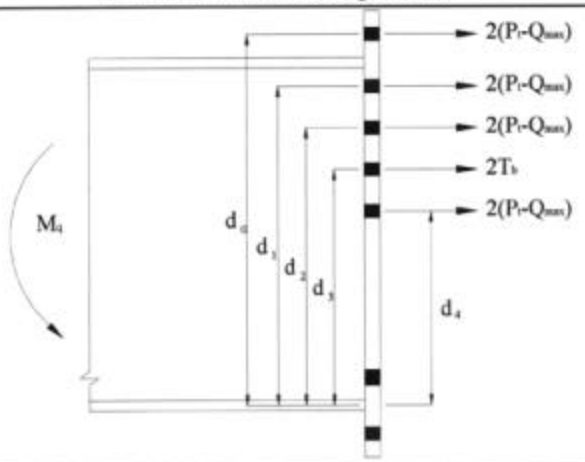

Table 5.6 Summary of Multiple Row Extended Unstiffened ¼ Moment End-Plate Analysis

End-Plate Yield		$M_{pl} = F_{py} t_p^2 Y$ $Y = \frac{b_p}{2}\left[h_1\left(\frac{1}{p_{f,i}}\right) + h_4\left(\frac{1}{s}\right) + h_0\left(\frac{1}{p_{f,o}}\right) - \frac{1}{2}\right] + \frac{2}{g}\left[h_1\left(p_{f,i} + 2.25p_b\right) + h_4\left(s + 0.75p_b\right)\right] + \frac{g}{2}$ $s = \frac{1}{2}\sqrt{b_p g}$
Bolt Rupture w/Prying Action	Option I	$M_q = \max \begin{vmatrix} 2(P_t - Q_{max,o})d_0 + 2(P_t - Q_{max,i})d_1 + 2(T_b)(d_2 + d_3 + d_4) \\ 2(P_t - Q_{max,o})d_0 + 2(T_b)(d_1 + d_2 + d_3 + d_4) \\ 2(P_t - Q_{max,i})(d_1) + 2(T_b)(d_0 + d_2 + d_3 + d_4) \\ 2(T_b)(d_0 + d_1 + d_2 + d_3 + d_4) \end{vmatrix}$
	Option II	$M_q = \max \begin{vmatrix} 2(P_t - Q_{max,o})d_0 + 2(P_t - Q_{max,i})(d_1 + d_2 + d_4) + 2(T_b)(d_3) \\ 2(P_t - Q_{max,o})d_0 + 2(T_b)(d_1 + d_2 + d_3 + d_4) \\ 2(P_t - Q_{max,i})(d_1 + d_2 + d_4) + 2(T_b)(d_0 + d_3) \\ 2(T_b)(d_0 + d_1 + d_2 + d_3 + d_4) \end{vmatrix}$
Bolt Rupture No Prying Action		$M_{np} = 2(P_t)(d_o + d_1 + d_2 + d_3 + d_4)$

5.2 CONCLUSIONS

From this study, the following conclusions can be drawn:

1. Design solutions were developed for five moment end-plate configurations: one extended end-plate and four flush end-plates. Provisions were added to the flush end-plate configurations to account for the large pitch distances found in diagonal knee moment end-plate connections.

2. In support of the design solutions presented in this study and based on Test F5-$1^1/_4$-$^3/_4$-84, the yield-line mechanism for the six-bolt flush unstiffened moment end-plate with $p_f > s$ adequately predicts the yield strength of this connection. The ratio of the predicted strength to the experimental strength for Test F5-$1^1/_4$-$^3/_4$-84 was 0.82.

3. In support of the design solutions presented in this study and based on Test F5S-$1^1/_4$-$^3/_4$-84, the simplified version of the Kennedy method (Borgsmiller and Murray 1995) adequately predicts the moment strength of this connection for the limit state of bolt rupture including prying action. The ratio of the predicted strength to the experimental strength for Test F5S-$1^1/_4$-$^3/_4$-84 was 0.87.

5.3 RECOMMENDATIONS FOR FURTHER TESTING

Several analytical methods have been presented that were not verified from the experimental investigation conducted. Therefore, it is recommended that further testing be conducted to

1. Verify the yield-line mechanisms presented for the analysis of the four-bolt flush stiffened and unstiffened moment end-plate connections with $p_f > s$.

2. Verify all yield-line mechanisms presented for the analysis of the eight-bolt flush unstiffened moment end-plate connection and the multiple row extended ¼ unstiffened moment end-plate connection.
3. Verify the correct model for the determination of the connection strength based on the limit state of bolt rupture including prying action for the eight-bolt flush unstiffened moment end-plate connection and the multiple row extended ¼ unstiffened moment end-plate connection.

5.2 SAMPLE CALCULATIONS

A design solution is demonstrated in the following sample calculations. For a description of design procedures and design examples, refer to Borgsmiller and Murray (1995).

5.2.1 Four-Bolt Flush Moment End-Plate Connection Stiffened Outside Tension Bolt Rows

Determine the predicted connection moment strength for the four bolt flush stiffened moment end-plate shown in Figure 5.1. The yield strength of the end-plate material is 50 ksi and the bolts are A325.

Part I: Determine End-Plate Yield Strength, M_{pl}

1. Calculate geometric parameters:

$$h_1 = h - t_f - p_f = 84 - 0.5 - 7.5 = 76 \text{ in.}$$

$$h_2 = h - t_f - p_f - p_b = 84 - 0.5 - 7.5 - 4 = 72 \text{ in.}$$

$$s = \frac{1}{2}\sqrt{b_p g} = \frac{1}{2}\sqrt{12(4.5)} = 3.674 \text{ in.}$$

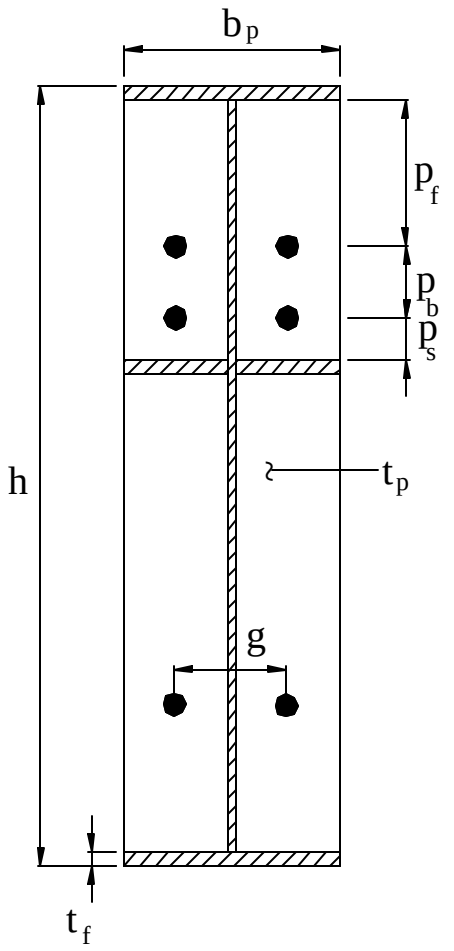

Parameter	Value (in)
h	84
b_p	12
t_p	¾
t_f	½
p_f	7 ½
p_b	4
p_s	2 ¼
g	4 ½
d_b	1 ¼

Figure 5.1 Geometric Parameters for the Four-Bolt Stiffened Moment End-Plate Connection Sample Calculation

$p_s < s$, Use Four-Bolt Flush Stiffened End-Plate Analysis (Table 5.5)

$p_f > s$, Use Case I.

2. Calculate Y:

$$Y = \frac{b_p}{2}\left[h_1\left(\frac{1}{s}\right) + h_2\left(\frac{1}{p_s}\right)\right] + \frac{2}{g}\left[h_1\left(s + 0.75p_b\right) + h_2\left(p_s + 0.25p_b\right)\right] + \frac{g}{2}$$

$$Y = \frac{12}{2}\left[76\left(\frac{1}{3.674}\right) + 72\left(\frac{1}{2.25}\right)\right] +$$

$$\frac{2}{4.5}\left[76\left(3.674 + 0.75(4)\right) + 72\left(2.25 + 0.25(4)\right)\right] + \frac{4.5}{2} = 647.8 \text{ in.}$$

3. Calculate M_{pl}:

$$M_{pl} = F_{py} t_p^2 Y = 50(0.75)^2 (647.8) = 18{,}219 \text{ k} - \text{in.} = 1518 \text{ k} - \text{ft.}$$

Part II: Determine Bolt Rupture Strength including Prying Action, M_q

1. Calculate geometric parameters:

$$d_1 = h - t_f - p_f - \frac{t_f}{2} = 84 - 0.5 - 7.5 - 0.5/2 = 75.75 \text{ in.}$$

$$d_2 = h - t_f - p_f - p_b - \frac{t_f}{2} = 84 - 0.5 - 7.5 - 4 - 0.5/2 = 71.75 \text{ in.}$$

2. Calculate P_t:

$F_{yb} = 90$ ksi [nominal tensile strength of A325 bolts specified in Table J3.2 (AISC 1995)]

$$P_t = A_b F_{yb} = \frac{\pi d_b^2}{4}\left(F_{yb}\right) = \frac{\pi(1.25)^2}{4}(90) = 110.4 \text{ k}$$

3. Calculate Q_{max}:

$$a = 3.682\left(\frac{t_p}{d_b}\right)^3 - 0.085 = 3.682\left(\frac{0.75}{1.25}\right)^3 - 0.085 = 0.710 \text{ in.}$$

$$w' = \frac{b_p}{2} - \phi - \frac{12}{2} - \left(1.25 + \frac{1}{16}\right) = 4.688 \text{ in.}$$

$$F' = \frac{t_p^2 F_{py}\left(0.85 b_f/2 + 0.80 w'\right) + \eth d_b^3 F_{yb}/8}{4 p_f}$$

$$= \frac{(0.75)^2 (50)\left(0.85(12/2) + 0.80(4.688)\right) + \eth(1.25)^3 (90)/8}{4(7.5)} = 10.60 \text{ k}$$

$$Q_{max} = \frac{w' t_p^{\,2}}{4a}\sqrt{F_{py}^2 - 3\left(\frac{F'}{w' t_p}\right)^2} = \frac{4.688(0.75)^2}{4(0.710)}\sqrt{(50)^2 - 3\left(\frac{10.60}{4.688(0.75)}\right)^2}$$

$$= 46.17 \text{ k}$$

4. Calculate M_q:

$T_b = 71$ k [minimum bolt tension of A325 1 ¼ diameter bolts as specified in Table J3.1 (AISC 1995)]

$$M_q = \max \begin{vmatrix} 2(P_t - Q_{max})(d_1 + d_2) = 2(110.4 - 46.17)(75.75 + 71.75) \\ 2(T_b)(d_1 + d_2) = 2(71)(75.75 + 71.75) \end{vmatrix}$$

$$= \max \begin{vmatrix} 18960 \text{ k} - \text{in.} \\ 20945 \text{ k} - \text{in.} \end{vmatrix} = 20{,}945 \text{ k} - \text{in.} = 1745 \text{ k} - \text{ft.}$$

Part III: Determine Bolt Rupture Strength without Prying Action, M_{np}

1. Calculate M_{np}:

$$M_{np} = 2(P_t)(d_1 + d_2) = 2(110.4)(75.75 + 71.75) = 32{,}581 \text{ k} - \text{in.}$$

$$= 2715 \text{ k} - \text{ft.}$$

Part IV: Determine the Predicted Connection Strength, M_{pred}

1. Determine the controlling limit state:

$M_{pl} = 1518 \text{ k} - \text{ft.}$

$M_q = 1745 \text{ k} - \text{ft.}$

$M_{pl} < M_q \therefore$ Connection fails by End-Plate Yielding.

$M_{pred} = M_{pl} = 1518$ k-ft.

5.2.2 Multiple Row Extended ¼ Unstiffened Moment End-Plate Connection

Determine the predicted connection moment strength for the multiple row extended ¼ unstiffened moment end-plate shown in Figure 5.2. The yield strength of the end-plate material is 50 ksi and the bolts are A325.

Part I: Determine End-Plate Yield Strength, M_{pl}

1. Calculate geometric parameters:

$$h_0 = h + p_{f,o} = 61.5 + 2.25 = 63.75 \text{ in.}$$

$$h_1 = h - t_f - p_f = 61.5 - 0.75 - 2 = 58.75 \text{ in.}$$

$$h_4 = h - t_f - p_f - 3p_b = 61.5 - 0.75 - 2 - 3(4) = 46.75 \text{ in.}$$

$$s = \frac{1}{2}\sqrt{b_p g} = \frac{1}{2}\sqrt{12(4.5)} = 3.674 \text{ in.}$$

2. Calculate Y:

$$Y = \frac{b_p}{2}\left[h_1\left(\frac{1}{p_{f,i}}\right) + h_4\left(\frac{1}{s}\right) + h_0\left(\frac{1}{p_{f,o}}\right) - \frac{1}{2}\right] + \frac{2}{g}\left[h_1\left(p_{f,i} + 2.25p_b\right) + h_4\left(s + 0.75p_b\right)\right] + \frac{g}{2}$$

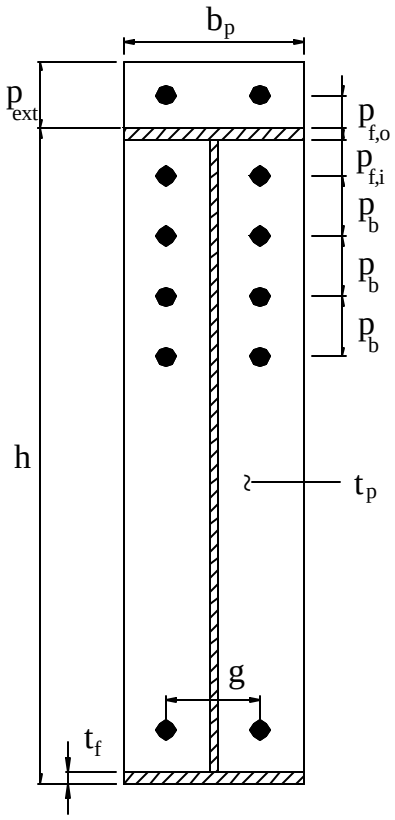

Parameter	Value (in)
h	61 ½
b_p	12
t_p	1
t_f	¾
p_{ext}	4 ½
$p_{f,o}$	2 ¼
$p_{f,i}$	2
p_b	4
g	4 ½
d_b	1 ¼

Figure 5.2 Geometric Parameters for the Multiple Row Extended ¼ Unstiffened Moment End-Plate Connection Sample Calculation

$$Y = \frac{12}{2}\left[58.75\left(\frac{1}{2}\right) + 46.75\left(\frac{1}{3.674}\right) + 63.75\left(\frac{1}{2.25}\right) - \frac{1}{2}\right] +$$
$$\frac{2}{4.5}\left[58.75\left(2 + 2.25(4)\right) + 46.75\left(3.674 + 0.75(4)\right)\right] + \frac{4.5}{2} = 847.7 \text{ in.}$$

3. Calculate M_{pl}:

$$M_{pl} = F_{py} t_p^2 Y = 50(1)^2 (847.7) = 42{,}385 \text{ k} - \text{in.} = 3532 \text{ k} - \text{ft.}$$

Part II: Determine Bolt Rupture Strength including Prying Action, M_g

1. Calculate geometric parameters:

$$d_0 = h + p_{fo} - \frac{t_f}{2} = 61.5 + 2.25 - 0.75/2 = 63.375 \text{ in.}$$

$$d_1 = h - t_f - p_f - \frac{t_f}{2} = 61.5 - 0.75 - 2 - 0.75/2 = 58.375 \text{ in.}$$

$$d_2 = h - t_f - p_f - p_b - \frac{t_f}{2} = 61.5 - 0.75 - 2 - 4 - 0.75/2 = 54.375 \text{ in.}$$

$$d_3 = h - t_f - p_f - 2p_b - \frac{t_f}{2} = 61.5 - 0.75 - 2 - 2(4) - 0.75/2 = 50.375 \text{ in.}$$

$$d_4 = h - t_f - p_f - 3p_b - \frac{t_f}{2} = 61.5 - 0.75 - 2 - 3(4) - 0.75/2 = 46.375 \text{ in.}$$

2. Calculate P_t:

$F_{yb} = 90$ ksi [nominal tensile strength of A325 bolts specified in Table J3.2 (AISC 1995)]

$$P_t = A_b F_{yb} = \frac{\eth d_b^2}{4}\left(F_{yb}\right) = \frac{\eth(1.25)^2}{4}(90) = 110.4 \text{ k}$$

3. Calculate Q_{max}:

$$w' = \frac{b_p}{2} - \ddot{o} - \frac{12}{2} - \left(1.25 + \frac{1}{16}\right) = 4.688 \text{ in.}$$

$$a_i = 3.682\left(\frac{t_p}{d_b}\right)^3 - 0.085 = 3.682\left(\frac{1}{1.25}\right)^3 - 0.085 = 1.800 \text{ in.}$$

$$F_i' = \frac{t_p^2 F_{py}\left(0.85 b_f/2 + 0.80 w'\right) + \eth d_b^3 F_{yb}/8}{4 p_{f,i}}$$

$$= \frac{(1)^2(50)\left(0.85(12/2) + 0.80(4.688)\right) + \eth(1.25)^3(90)/8}{4(2)} = 63.94 \text{ k}$$

$$Q_{max,\,i} = \frac{w' t_p^{\,2}}{4a_i}\sqrt{F_{py}^2 - 3\left(\frac{F_i'}{w' t_p}\right)^2} = \frac{4.688(1)^2}{4(1.800)}\sqrt{(50)^2 - 3\left(\frac{63.94}{4.688(1)}\right)^2}$$

$$= 28.69 \text{ k}$$

$$a_o = \min \begin{vmatrix} 3.682\left(\frac{t_p}{d_b}\right)^3 - 0.085 = 3.682\left(\frac{1}{1.25}\right)^3 - 0.085 = 1.800 \text{ in.} \\ p_{ext} - p_{f,o} = 4.5 - 2.25 = 2.25 \text{ in.} \end{vmatrix}$$

$$F_o' = \frac{t_p^2 F_{py}\left(0.85 b_f/2 + 0.80 w'\right) + \eth d_b^3 F_{yb}/8}{4 p_{f,o}}$$

$$= \frac{(1)^2(50)\left(0.85(12/2) + 0.80(4.688)\right) + \eth(1.25)^3(90)/8}{4(2.25)} = 56.84 \text{ k}$$

$$Q_{max,\,o} = \frac{w' t_p^{\,2}}{4a_o}\sqrt{F_{py}^2 - 3\left(\frac{F_o'}{w' t_p}\right)^2} = \frac{4.688(1)^2}{4(1.800)}\sqrt{(50)^2 - 3\left(\frac{56.84}{4.688(1)}\right)^2}$$

$$= 29.55 \text{ k}$$

4. Calculate M_q:

$T_b = 71$ k [minimum bolt tension of A325 1 ¼ diameter bolts as specified in Table J3.1 (AISC 1995)]

Option I:

$$M_q = \max \begin{vmatrix} 2\left(P_t - Q_{max,\,o}\right)d_0 + 2\left(P_t - Q_{max,\,i}\right)d_1 + 2\left(T_b\right)\left(d_2 + d_3 + d_4\right) \\ 2\left(P_t - Q_{max,\,o}\right)d_0 + 2\left(T_b\right)\left(d_1 + d_2 + d_3 + d_4\right) \\ 2\left(P_t - Q_{max,\,i}\right)\left(d_1\right) + 2\left(T_b\right)\left(d_0 + d_2 + d_3 + d_4\right) \\ 2\left(T_b\right)\left(d_0 + d_1 + d_2 + d_3 + d_4\right) \end{vmatrix}$$

$$= \begin{vmatrix} 2(110.4-29.55)63.375+2(110.4-28.69)58.375+ \\ 2(71)(54.375+50.375+46.375)=41258\ \text{k}-\text{in}. \\ \\ 2(110.4-29.55)63.375+ \\ 2(71)(58.375+54.375+50.375+46.375)=40003\ \text{k}-\text{in}. \\ \\ 2(110.4-28.69)(58.375)+ \\ 2(71)(63.375+54.375+50.375+46.375)=40003\ \text{k}-\text{in} \\ \\ 2(71)(63.375+58.375+54.375+50.375+46.375)=38748\ \text{k}-\text{in}. \end{vmatrix}_{\max}$$

$$= 41258\ \text{k}-\text{in}. = 3438\ \text{k}-\text{ft}.$$

Option II:

$$M_q = \begin{vmatrix} 2(P_t - Q_{max,o})d_0 + 2(P_t - Q_{max,i})(d_1+d_2+d_4) + 2(T_b)(d_3) \\ 2(P_t - Q_{max,o})d_0 + 2(T_b)(d_1+d_2+d_3+d_4) \\ 2(P_t - Q_{max,i})(d_1+d_2+d_4) + 2(T_b)(d_0+d_3) \\ 2(T_b)(d_0+d_1+d_2+d_3+d_4) \end{vmatrix}_{\max}$$

$$= \begin{vmatrix} 2(110.4-29.55)63.375+ \\ 2(110.4-28.69)(58.375+54.375+46.375) \\ +2(71)(50.375)=43425\ \text{k}-\text{in}. \\ \\ 2(110.4-29.55)63.375+ \\ 2(71)(58.375+54.375+50.375+46.375)=40003\ \text{k}-\text{in}. \\ \\ 2(110.4-28.69)(58.375+54.375+46.375)+ \\ 2(71)(63.375+50.375)=42170\ \text{k}-\text{in}. \\ \\ 2(71)(63.375+58.375+54.375+50.375+46.375)=38748\ \text{k}-\text{in}. \end{vmatrix}_{\max}$$

$$= 43425\ \text{k}-\text{in}. = 3619\ \text{k}-\text{ft}.$$

$$M_q = \min \begin{vmatrix} \text{Option I} = 3438 \text{ k - ft.} \\ \text{Option II} = 3619 \text{ k - ft.} \end{vmatrix}$$

$$M_q = 3438 \text{ k} - \text{ft.}$$

Part III: Determine Bolt Rupture Strength without Prying Action, M_{np}

1. Calculate M_{np}:

$$M_{np} = 2(P_t)(d_0 + d_1 + d_2 + d_3 + d_4)$$
$$= 2(110.4)(63.375 + 58.375 + 54.375 + 50.375 + 46.375) = 60275 \text{ k} - \text{in.}$$
$$= 5023 \text{ k} - \text{ft.}$$

Part IV: Determine the Predicted Connection Strength, M_{pred}

1. Determine the controlling limit state:

$$M_{pl} = 3532 \text{ k} - \text{ft.}$$
$$M_q = 3438 \text{ k} - \text{ft.}$$

$M_{pl} > M_q \therefore$ Connection fails by Bolt Rupture.

2. Determine if prying forces are included:

$0.9M_{pl} = 0.9(3532) = 3179$ k-ft

$0.9M_{pl} < M_{np} \therefore$ Prying forces are included

$M_{pred} = M_q = 3438$ k-ft.

REFERENCES

Abel, M. (1993). "Four-Bolt Extended Unstiffened Moment End-Plate Connections," Master of Science Thesis, Virginia Polytechnic Institute and State University, Blacksburg, Virginia.

American Institute of Steel Construction, (1995) "Load and Resistance Factor Design," *Manual of Steel Construction* 2nd Edition, Vol. I and II, Chicago, Illinois.

American Society for Testing and Materials, (1998) "Standard Test Methods for Tension Testing of Metallic Materials," *Annual Book of ASTM Standards*, Vol. 03.01, Designation: E 8, pp. 57-65.

Bond, D.E., (1989) *Analytical and Experimental Investigation of a Flush Moment End-Plate Connection with Six Bolts at the Tension Flange*, Master of Science Thesis, Virginia Polytechnic Institute and State University, Blacksburg, Virginia.

Borgsmiller, J.T., and Murray, T.M., (1995) "Simplified Method for Design of Moment End-Plate Connections" Report No. CE/VPI-ST 95/19, Virginia Polytechnic Institute and State University, Blacksburg, Virginia.

Hendrick, D., Kukreti, A.R., and Murray, T.M. (1985) "Unification of Flush End-Plate Design Procedures" Report No. FSEL/MBMA 8305, University of Oklahoma, Norman, Oklahoma.

Hibbeler, R.C., (1995) *Structural Analysis*, 3rd Edition, Prentice Hall, Upper Saddle River, New Jersey.

Johansen, K.W., (1962) *Yield-line Theory,* Cement and Concrete Association, London.

Kennedy, N.A., Vinnakota, S., and Sherbourne, A.N. (1981), "The Split-Tee Analogy in Bolted Splices and Beam-Column Connections", *Joints in Structural Steelwork*, John Wiley & Sons, London-Toronto, pp. 2-138-2.157.

Krishnamurthy, N., (1978), "Fresh Look at Bolted End-Plate Behavior and Design", *Engineering Journal*, American Institute of Steel Construction, Vol. 15, No. 2, pp.39-49.

Mays, T.W. (2000a), *Application of the Finite Element Method to the Seismic Design and Analysis of Large Moment End-Plate Connections*. Ph.D. Dissertation, Virginia Polytechnic Institute and State University, Blacksburg, Virginia..

Mays, T.W. (2000b), "Personal Correspondence", April 2000.

Morrison, S.J., Astaneh-Asl, A., and Murray, T.M., (1985) "Analytical and Experimental Investigation of the Extended Stiffened Moment End-Plate Connection with Four Bolts at the Beam Tension Flange" Report No. FSEL/MBMA 85-05, University of Oklahoma, Norman, Oklahoma.

Morrison, S.J., Astaneh-Asl, A., and Murray, T.M., (1986) "Analytical and Experimental Investigation of the Multiple Row Extended $^1/_3$ Moment End-Plate Connection with Eight Bolts at the Beam Tension Flange" Report No. FSEL/MBMA 86-01, University of Oklahoma, Norman, Oklahoma.

Murray, T.M. (1988), "Recent Developments for the Design of Moment End-Plate Connections", *Journal of Constructional Steel Research*, Vol. 10, pp.133-162.

Murray, T.M, and Borgsmiller, J.T. (1995), "Strength of Moment End-Plate Connections with Multiple Bolt Rows at the Beam Tension Flange", *Proceedings of the Third International Workshop, Connections in Steel Structures III, Behaviour, Strength and Design*, Trento, Italy, May 1995.

Srouji, R., Murray, T.M., and Kukreti, A.R., (1983) "Yield-Line Analysis of End-Plate Connections with Bolt Force Predictions" Report No. FSEL/MBMA 8305, University of Oklahoma, Norman, Oklahoma.

Sumner, E.A. (1995), *Experimental and Analytical Investigation of the LRFD Strength of Tapered Members*, Master of Science Thesis, Virginia Polytechnic Institute and State University, Blacksburg, Virginia.

APPENDIX A

NOMENCLATURE

NOMENCLATURE

A_b	=	nomimal bolt cross-sectional area
a	=	distance from bolt centerline to the prying force
a	=	horizontal distance from support to the nearest load point for plate girder test
a_i	=	distance from interior bolt centerline to interior prying force
a_o	=	distance from exterior bolt centerline to exterior prying force
B	=	bolt force per bolt
$BF_{plastic}$	=	bolt force in plastic region
b	=	distance from theface of the beam flange to the nearest bolt centerline
b_p	=	end-plate width
b_f	=	beam width
d	=	distance from the center of the beam compression flange to a bolt row
d_b	=	bolt diameter
d_e	=	distance from end of extended end plate to bolt centerline of end-plate extension
d_i	=	distance from the center of the beam compression flange to a bolt row
d_0	=	distance from the center of the beam compression flange to the bolt centerline of end-plate extension
d_1	=	distance from the center of the beam compression flange to the farthest bolt-line
d_2	=	distance from the center of the beam compression flange to the second farthest bolt-line

d_3 = distance from the center of the beam compression flange to the third farthest bolt-line

d_4 = distance from the center of the beam compression flange to the forth farthest bolt-line

E = modulus of elasticity

F = beam flange force per bolt

F_{py} = yield stress of end-plate material

F_{yb} = design strength of bolt (Table J3.2, AISC)

F' = flange force per bolt at the thin plate limit

g = end-plate bolt gage

h = beam depth

h_0 = distance from outside face of beam compression flange to the bolt centerline of end-plate extension

h_1 = distance from the outside face of the beam compression flange to the farthest bolt-line

h_2 = distance from the outside face of the beam compression flange to the second farthest bolt-line

h_3 = distance from the outside face of the beam compression flange to the third farthest bolt-line

h_4 = distance from the outside face of the beam compression flange to the fourth farthest bolt-line

I = beam moment of inertia

L_n = length of yield line n

L_x = x-component of length of yield line n

L_y = y-component of length of yield line n

l = distance between test specimen supports

M_{max} = maximum applied moment in experimental test

M_{np} = moment capacity of end-plate for the limit state of bolt-rupture without prying action

M_{pl} = moment capacity of end-plate for the limit state of end-plate yielding

M_{pred} = predicted connection moment strength

M_q = moment capacity of end-plate for the limit state of bolt-rupture with prying action

M_u = ultimate moment capacity at end-plate

M_y = yield moment of specimen in experimental test

$m_{elastic}$ = slope of load vs. strain in elastic region for bolt

= $\frac{P_y}{\varepsilon_y}$

m_p = plastic moment capacity of plate per unit length

= $\frac{F_{py} t_p^2}{4}$

m_{px} = x-component of the normal plastic moment capacity of end-plate per unit length

m_{py} = y-component of the normal plastic moment capacity of end-plate per unit length

N = total number of yield lines in a mechanism

= total number of bolt rows on tension side of end-plate connection

N_i = total number of load-carrying bolt rows on tension side of end-plate connection

N_j = total number of non-load-carrying bolt rows on tension side of end-plate connection

P = load applied to test specimen by hydraulic ram

P_y = bolt proof load

= $A_b F_{yb}$

P_t = bolt proof load

= $A_b F_{yb}$

p_b = pitch distance from bolt centerline to bolt centerline

p_{ext} = pitch distance from outside face of beam flange to end of extended end-plate

p_f = pitch distance from inside face of beam flange to nearest bolt centerline

$p_{f,i}$ = pitch distance from inside face of beam flange to nearest bolt centerline

$p_{f,o}$ = pitch distance from outside face of beam flange to bolt centerline of end-plate extension

p_s = pitch distance from nearest bolt centerline to near face of stiffener in four-bolt flush stiffened configuration

Q = prying force per bolt

Q_{max} = maximum prying force

$Q_{max,i}$ = maximum prying force for interior bolts

$Q_{max,o}$ = maximum prying force for exterior bolts

R = bolt relationship

s = distance from outermost yield line to nearest bolt centerline

T_b = minimum bolt tension (Table J3.1, AISC)

t_f = flange thickness

t_{f1} = top flange thickness

t_{f2} = bottom flange thickness

t_p = end-plate thickness

t_s = stiffener thickness

t_l = thick plate limit

t_{l1} = thin plate limit

W_e = total external wok

W_{in} = internal work stored in the n-th yield line

W_i = total internal energy stored in a yield line mechanism

w = width of the end-plate per bolt pair

w' = width of end plate per bolt minus the bolt hole diameter

$\varepsilon_{plastic}$ = bolt strain in the plastic region

ε_y = bolt yield strain

Δ = theoretical deflection at load points for plate girder test

ϕ = hole diameter

θ = virtual rotation of end-plate connection

θ_n = relative plate rotation of yield line n

θ_{nx} = x-component of relative plate rotation of yield line n

θ_{ny} = y-component of relative plate rotation of yield line n

APPENDIX B

F2-$^{5}/_{8}$-$^{1}/_{2}$-28 KNEE TEST RESULTS

TEST NAME: F2-$^{5}/_{8}$-$^{1}/_{2}$-28
TEST DATE: February 2, 2000

CONNECTION DESCRIPTION

NOMINAL YIELD STRESS	50 ksi
NUMBER OF TENSION BOLTS	4
NUMBER OF COMPRESSION BOLTS	4
NOMINAL GAGE	3 in.
NOMINAL PITCH	4 in.
NOMINAL END PLATE WIDTH	6 in.
NOMINAL END PLATE LENGTH	28 in.
NOMINAL END PLATE THICKNESS	0.5 in.

BOLT DATA

BOLT DIAMETER	5/8 in.
BOLT TYPE	A325
BOLT PRETENSION	19 kips

COLUMN DATA

NOMINAL FLANGE WIDTH	6 in.
NOMINAL TOP FLANGE THICKNESS	0.1875 in.
NOMINAL BOTTOM FLANGE THICKNESS	0.25 in.
NOMINAL WEB THICKNESS	0.1345 in.

RAFTER DATA

NOMINAL FLANGE WIDTH	6 in.
NOMINAL TOP FLANGE THICKNESS	0.1875 in.
NOMINAL BOTTOM FLANGE THICKNESS	0.25 in.
NOMINAL WEB THICKNESS	0.1345 in.

EXPERIMENTAL

FAILURE LOAD	13.4 kips
MAXIMUM APPLIED END-PLATE MOMENT	150 kip-ft
FAILURE LOCATION	Column Flange
FAILURE MODE	Local Flange Buckling
PREDICTED CONNECTION FAILURE MOMENT	193 kip-ft

TEST NAME: F2-$^{5}/_{8}$-$^{1}/_{2}$-28
TEST DATE: February 2, 2000

DISCUSSION

The data acquisition system was zeroed, except for the bolt channels, and the test was started. The specimen was loaded at one kip intervals. At approximately 13 kips, there was visible plate separation and yielding around the top tension bolts. Yielding was also apparent on the tension side of the column web and the compression side of the rafter web. As soon as load was applied, it gradually dropped off. The specimen was loaded up to a maximum load of 13.4 kips. A lateral brace began to twist the bottom flange of the column. The specimen had reached its maximum load. The test was ended and the specimen was unloaded. The gaged bolts increased in strain with the outermost tension bolts experiencing the highest strains. The theoretical and chord deflections correlated for this test.

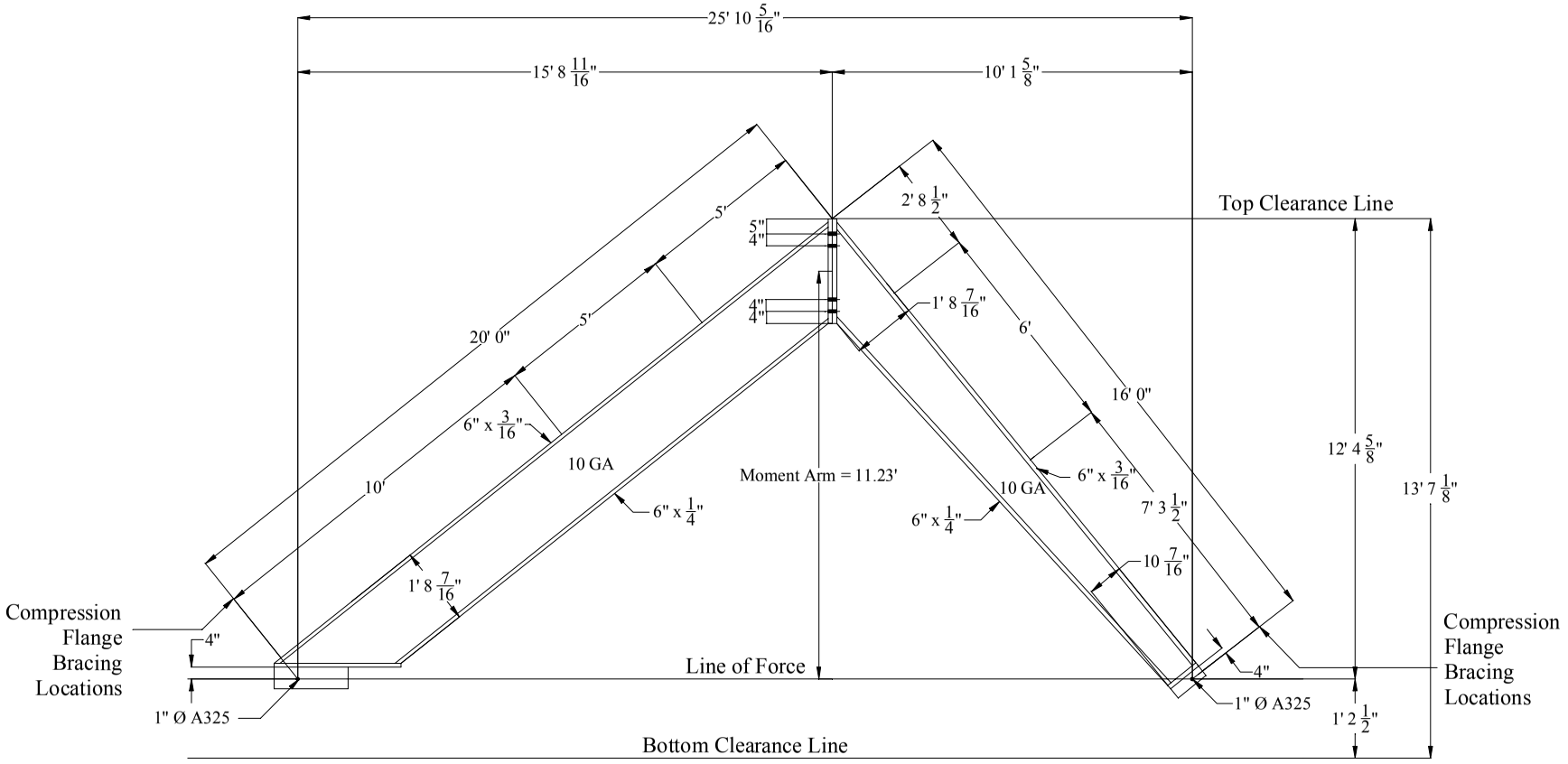

Figure B.1 Specimen Nominal Dimensions for Test F2-$^{5}/_{8}$-$^{1}/_{2}$-28

Table B.1 Geometric Dimensions and Material Properties for Test F2-$^{5}/_{8}$-$^{1}/_{2}$-28

	Nominal Specimen Dimensions	Measured Specimen Dimensions	Measured Yield Stress *	Measured Ultimate Stress	% Elongation
Rafter					
Top Flange	$^{3}/_{16}$" x 6" x 20' 4 $^{7}/_{16}$"	0.190" x 6" x 20' 3 $^{7}/_{8}$"	70.0 ksi	83.1 ksi	19.0 %
Web	0.1345"	0.137"	60.8 ksi	71.6 ksi	21.0 %
Bottom Flange	$^{1}/_{4}$" x 6" x 16' 4 $^{3}/_{4}$"	0.262" x 6 $^{1}/_{16}$" x 16' 4 $^{5}/_{8}$"	64.4 ksi	75.0 ksi	22.0 %
End Plate	$^{1}/_{2}$" x 6" x 2' 4"	0.501" x 6 $^{1}/_{16}$" x 2' 4$^{1}/_{16}$"	58.1 ksi	88.2 ksi	32.3 %
Column					
Top Flange	$^{3}/_{16}$" x 6" x 15' 6 $^{3}/_{8}$"	0.186" x 6" x 15' 6 $^{5}/_{16}$"	70.0 ksi	82.7 ksi	17.0 %
Web	0.1345"	0.137"	59.0 ksi	69.5 ksi	23.0 %
Bottom Flange	$^{1}/_{4}$" x 6" x 14'	0.256" x 6 $^{1}/_{16}$" x 13' 11 $^{13}/_{16}$"	62.2 ksi	74.8 ksi	24.0 %
End Plate	$^{1}/_{2}$" x 6" x 2' 4"	0.503" x 6 $^{1}/_{16}$" x 2' 4$^{1}/_{8}$"	58.1 ksi	88.2 ksi	32.3 %

* Nominal Yield Stress = 50 ksi

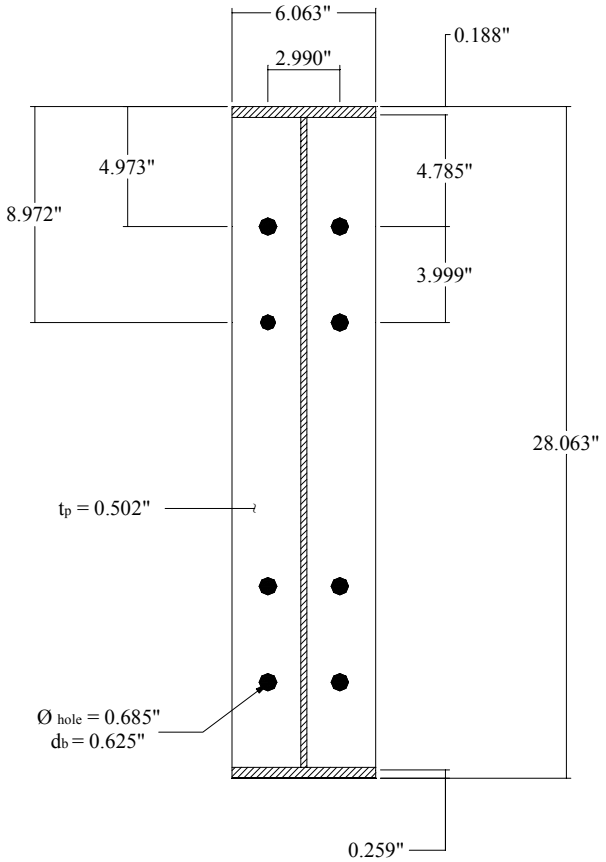

Figure B.2 Average Measured Connection Details for Test F2-$^{5}/_{8}$-$^{1}/_{2}$-28

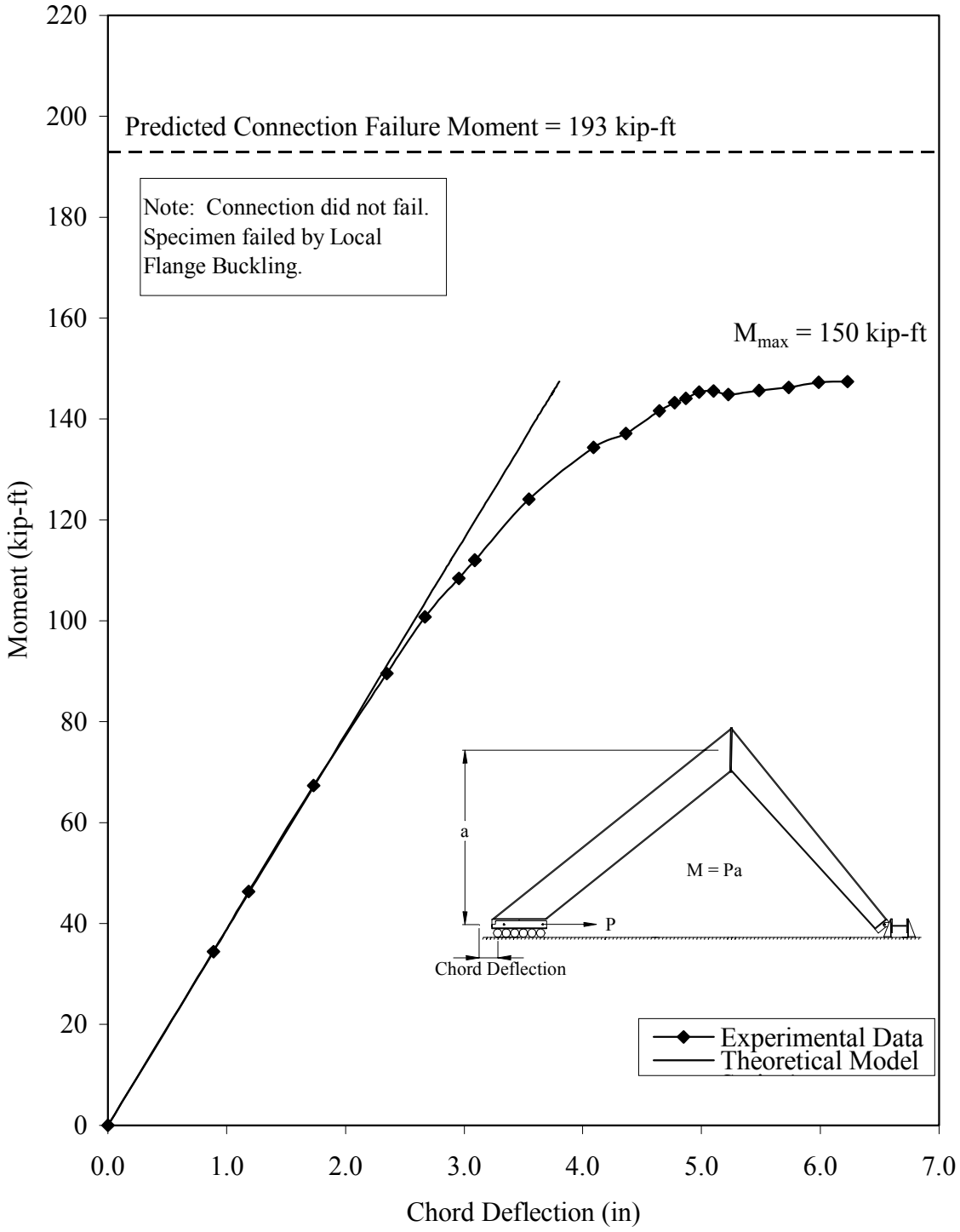

Figure B.3 Applied Moment vs. Chord Deflection for Test F2-$^{5}/_{8}$-$^{1}/_{2}$-28

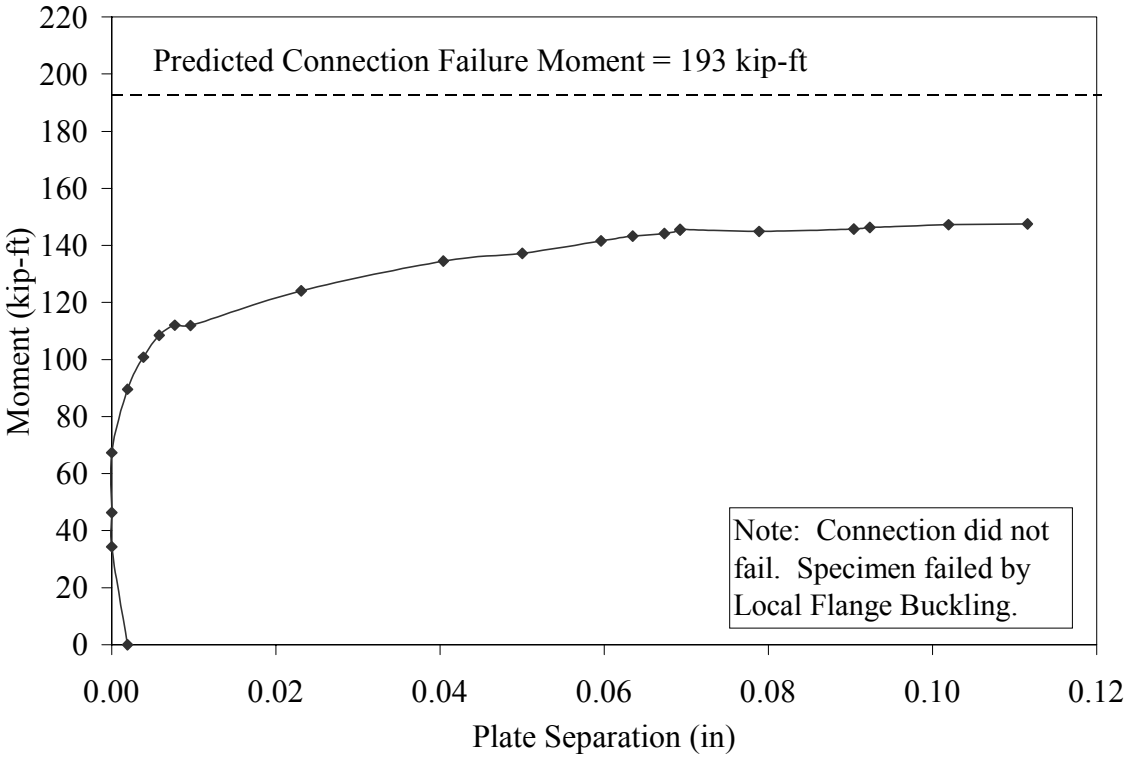

Figure B.4 Applied Moment vs. Plate Separation for Test F2-$^{5}/_{8}$-$^{1}/_{2}$-28

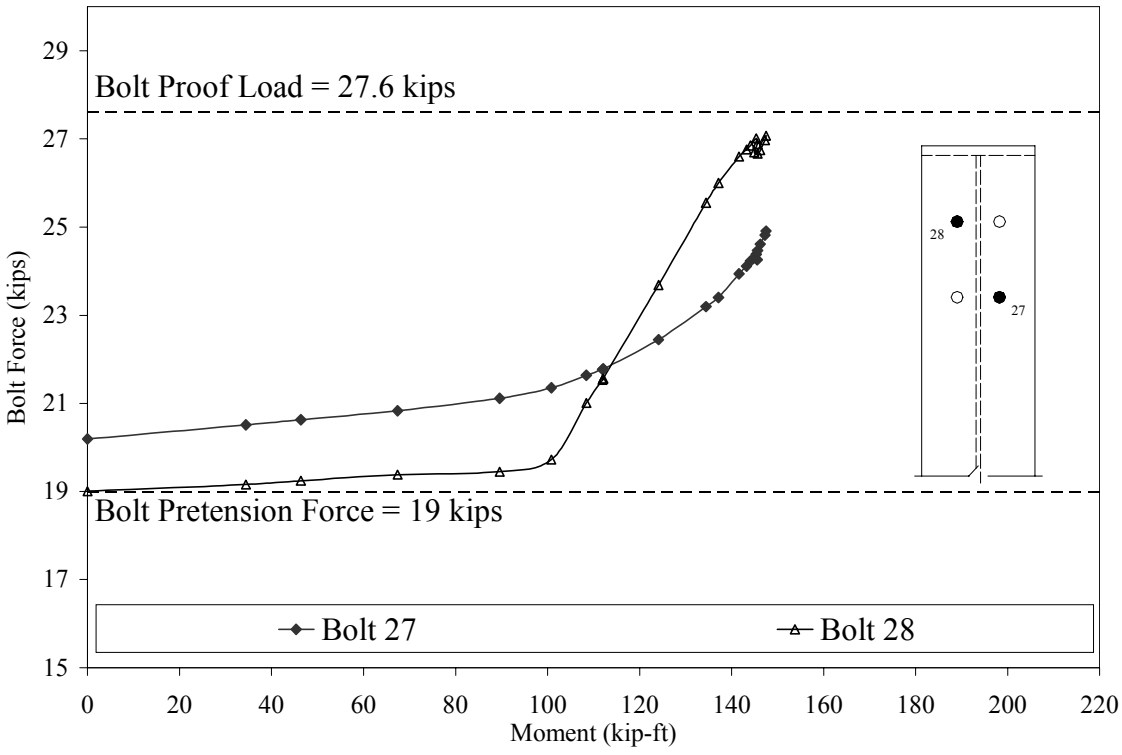

Figure B.5 Bolt Force vs. Applied Moment for Test F2-$^{5}/_{8}$-$^{1}/_{2}$-28

a) Yielding of Column Web

b) Local Flange Buckling of Column Flange

Figure B.6 F2-$^{5}/_{8}$-$^{1}/_{2}$-28 at end of Test

APPENDIX C

F3-$^{3}/_{4}$-$^{3}/_{4}$-50 KNEE TEST RESULTS

TEST NAME: F3-$^{3}/_{4}$-$^{3}/_{4}$-50
TEST DATE: February 9, 2000

CONNECTION DESCRIPTION

NOMINAL YIELD STRESS	50 ksi
NUMBER OF TENSION BOLTS	6
NUMBER OF STITCH BOLTS	2
NUMBER OF COMPRESSION BOLTS	4
NOMINAL GAGE	3 in
NOMINAL PITCH	4 in
NOMINAL END PLATE WIDTH	8 in
NOMINAL END PLATE LENGTH	50 in
NOMINAL END PLATE THICKNESS	0.75 in

BOLT DATA

BOLT DIAMETER	3/4 in
BOLT TYPE	A325
BOLT PRETENSION	28 kips

COLUMN DATA

NOMINAL FLANGE WIDTH	8 in
NOMINAL TOP FLANGE THICKNESS	0.25 in
NOMINAL BOTTOM FLANGE THICKNESS	0.375 in
NOMINAL WEB THICKNESS	0.25 in

RAFTER DATA

NOMINAL FLANGE WIDTH	8 in
NOMINAL TOP FLANGE THICKNESS	0.25 in
NOMINAL BOTTOM FLANGE THICKNESS	0.375 in
NOMINAL WEB THICKNESS	0.25 in

EXPERIMENTAL

FAILURE LOAD	41.25 kips
MAXIMUM APPLIED END-PLATE MOMENT	552 kip-ft
FAILURE LOCATION	Column and Rafter Sections
FAILURE MODE	Lateral-Torsional Buckling
PREDICTED CONNECTION FAILURE MOMENT	811 kip-ft

TEST NAME: F3-$^{3}/_{4}$-$^{3}/_{4}$-50
TEST DATE: February 9, 2000

DISCUSSION

The data acquisition system was zeroed, except for the bolt channels, and the test was started. The specimen was loaded at 5 kip intervals. At 25 kips, the bottom flange of the rafter began to torque and the web buckled. The test was stopped, and a lateral brace was added to the bottom flange of the rafter. Once again, the data acquisition system was zeroed, except for the bolt channels, and the test was started. At 38 kips, the specimen began to yield. The deflection increased with very little increase in load. As deflection increased, the web of both the rafter and the column began to move laterally, with the column having larger displacements. The compression flange of the rafter and the column was twisted to the side. The specimen reached a maximum load of 41.25 kips. It was determined that the specimen failed by lateral-torsional buckling and the specimen was unloaded. During testing, the bolt strains increased, but not enough to cause failure. The specimen was stiffer than the theoretical deflection predicted. .

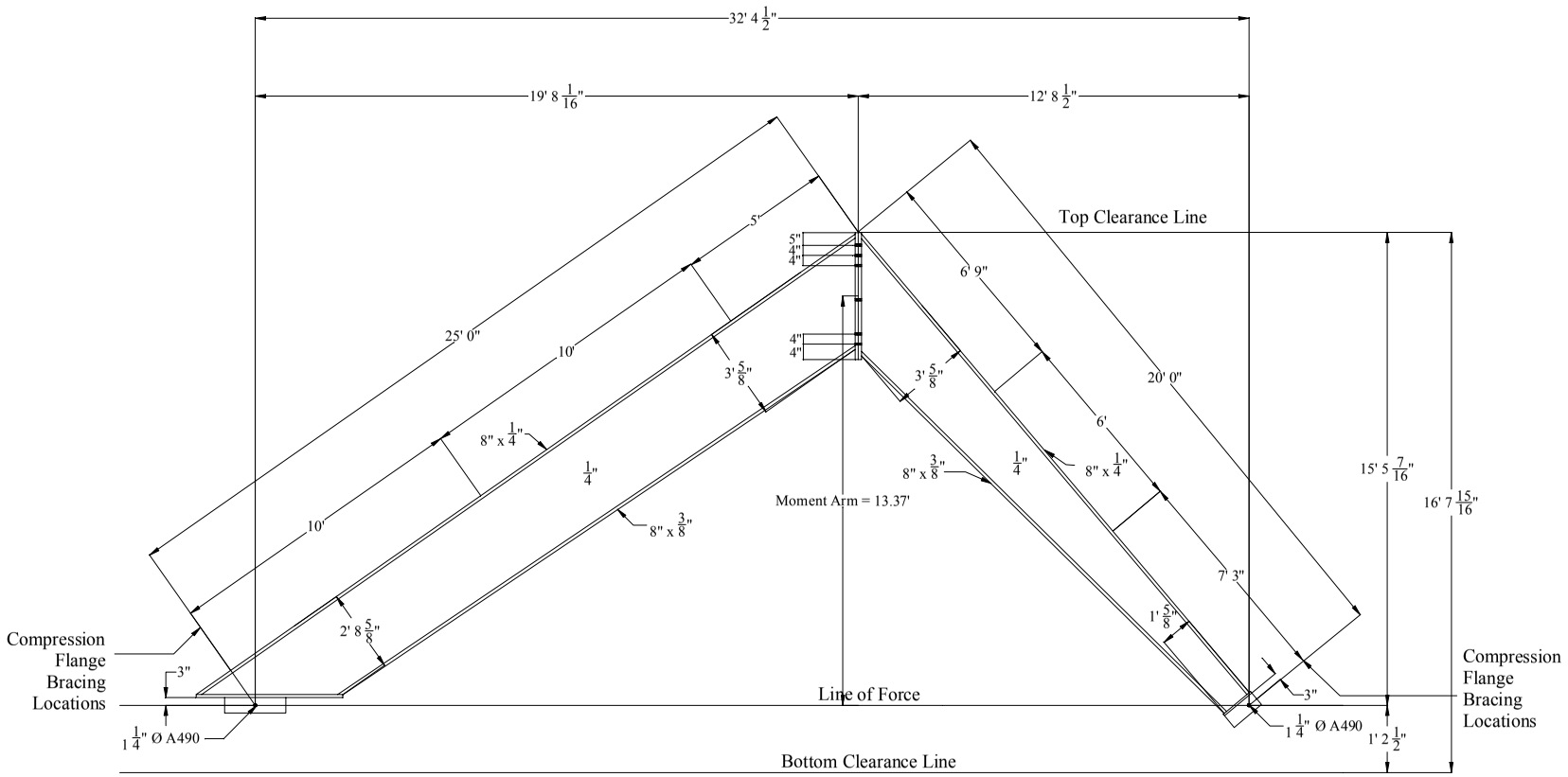

Figure C.1 Specimen Nominal Dimensions for Test F3-$^{3}/_{4}$-$^{3}/_{4}$-50

Table C.1 Geometric Dimensions and Material Properties for Test F3-$^3/_4$-$^3/_4$-50

	Nominal Specimen Dimensions	Measured Specimen Dimensions	Measured Yield Stress *	Measured Ultimate Stress	% Elongation
Rafter					
Top Flange	$^1/_4$" x 8" x 26' 3 $^1/_4$"	0.245" x 8" x 26' 2"	56.1 ksi	68.4 ksi	24.0 %
Web	$^1/_4$"	0.251"	67.6 ksi	77.8 ksi	21.5 %
Bottom Flange	$^3/_8$" x 8" x 19' 6 $^7/_8$"	0.363" x 8" x 19' 7$^1/_4$"	59.2 ksi	77.6 ksi	22.0 %
End Plate	$^3/_4$" x 8" x 4' 2"	0.765" x 8" x 50"	55.7 ksi	84.7 ksi	24.5 %
Column					
Top Flange	$^1/_4$" x 8" x 19' 7 $^1/_8$"	0.245" x 8" x 19' 6 $^3/_4$"	55.0 ksi	68.1 ksi	24.0 %
Web	$^1/_4$"	0.250"	67.0 ksi	78.6 ksi	21.5 %
Bottom Flange	$^3/_8$" x 8" x 16' 10"	0.362" x 8" x 16' 11"	59.3 ksi	78.8 ksi	22.0 %
End Plate	$^3/_4$" x 8" x 4' 2"	0.764" x 8" x 50"	55.7 ksi	84.7 ksi	24.5 %

* Nominal Yield Stress = 50 ksi

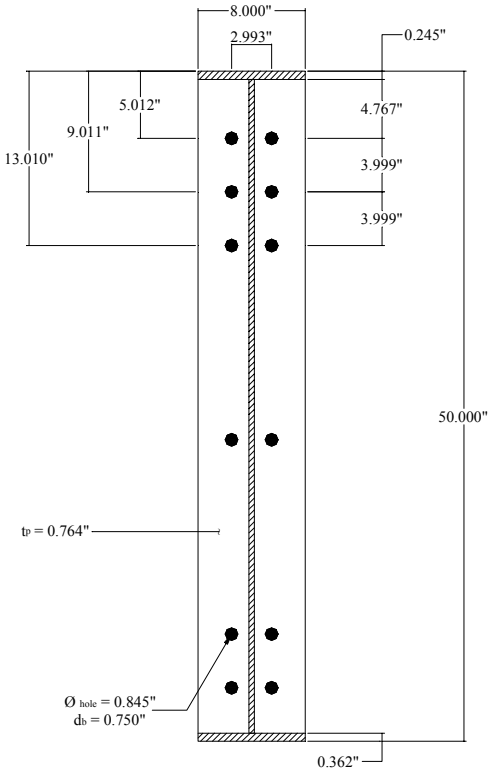

Figure C.2 Average Measured Connection Details for Test F3-$^3/_4$-$^3/_4$-50

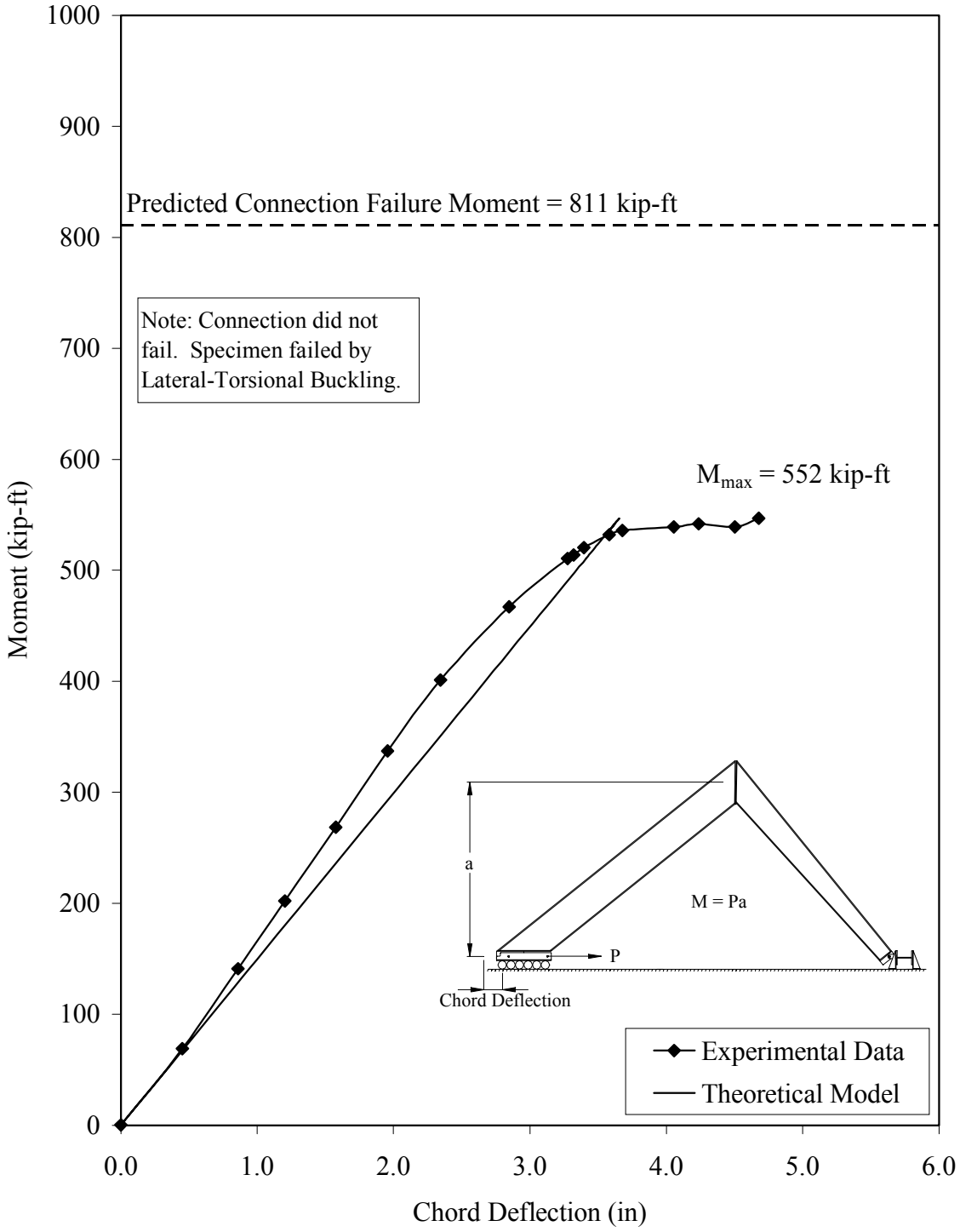

Figure C.3 Applied Moment vs. Chord Deflection for Test F3-$^3/_4$-$^3/_4$-50

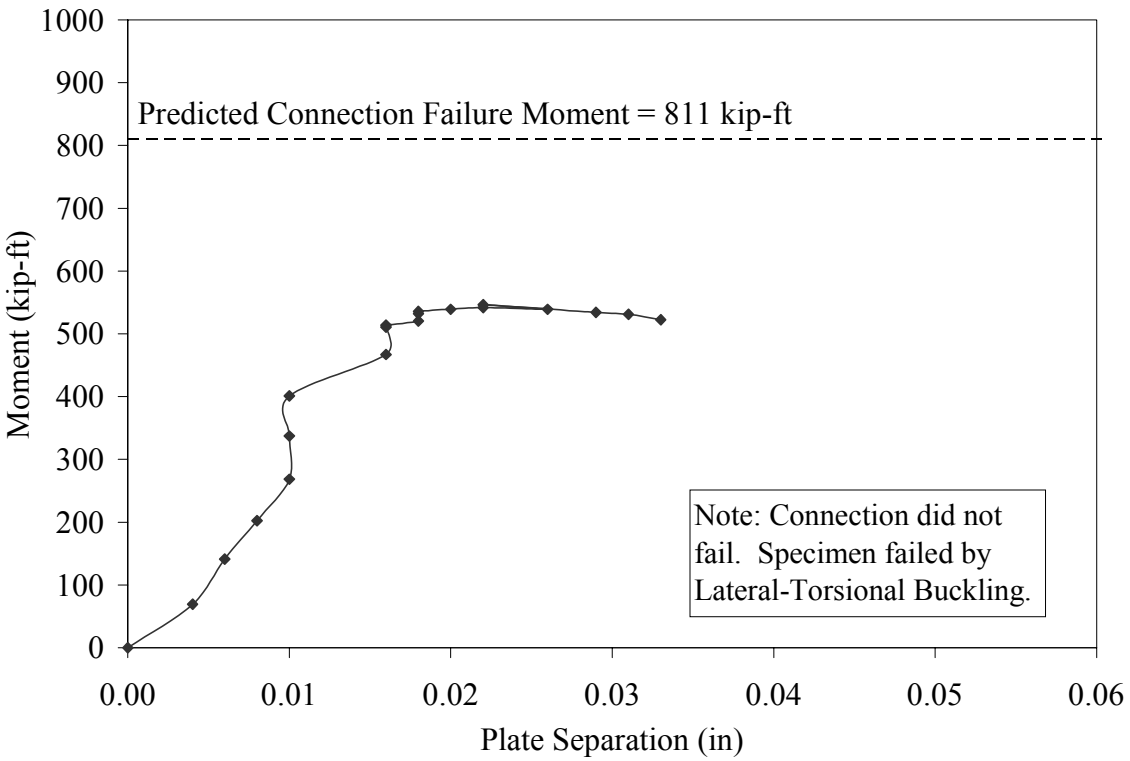

Figure C.4 Applied Moment vs. Plate Separation for Test F3-$^{3}/_{4}$-$^{3}/_{4}$-50

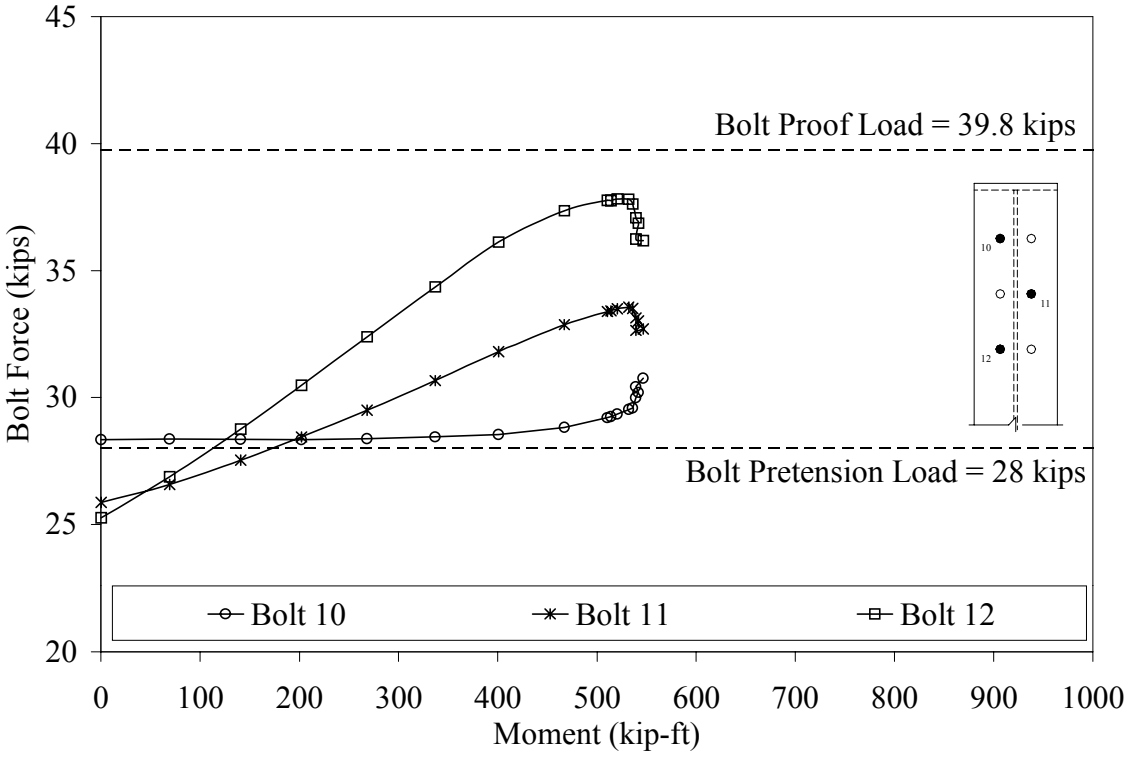

Figure C.5 Bolt Force vs. Applied Moment for Test F3-$^{3}/_{4}$-$^{3}/_{4}$-50

a) Web Buckling of Column (near connection)

b) Connection Subsequent to Testing
(Note: No significant yielding or plate separation is visible.)

Figure C.6 F3-$^{3}/_{4}$-$^{3}/_{4}$-50 at end of Test

APPENDIX D

F4-$^{7}/_{8}$-$^{3}/_{4}$-67 KNEE TEST RESULTS

TEST NAME: F4-$^{7}/_{8}$-$^{3}/_{4}$-67
TEST DATE: November 30, 1999

CONNECTION DESCRIPTION

NOMINAL YIELD STRESS	50 ksi
NUMBER OF TENSION BOLTS	8
NUMBER OF STITCH BOLTS	2
NUMBER OF COMPRESSION BOLTS	4
NOMINAL GAGE	3.5 in.
NOMINAL PITCH	4 in.
NOMINAL END PLATE WIDTH	8 in.
NOMINAL END PLATE LENGTH	67 in.
NOMINAL END PLATE THICKNESS	0.75 in.

BOLT DATA

BOLT DIAMETER	7/8 in.
BOLT TYPE	A325
BOLT PRETENSION	39 kips

COLUMN DATA

NOMINAL FLANGE WIDTH	8 in.
NOMINAL TOP FLANGE THICKNESS	0.375 in.
NOMINAL BOTTOM FLANGE THICKNESS	0.750 in.
NOMINAL WEB THICKNESS	0.3125 in.

RAFTER DATA

NOMINAL FLANGE WIDTH	8 in.
NOMINAL TOP FLANGE THICKNESS	0.375 in.
NOMINAL BOTTOM FLANGE THICKNESS	0.750 in.
NOMINAL WEB THICKNESS	0.250 in.

EXPERIMENTAL

FAILURE LOAD	84.6 kips
MAXIMUM APPLIED END-PLATE MOMENT	1160 kip-ft
FAILURE LOCATION	Rafter Web
FAILURE MODE	Local web buckling
PREDICTED CONNECTION FAILURE MOMENT	1465 kip-ft

TEST NAME: F4-$^{7}/_{8}$-$^{3}/_{4}$-67
TEST DATE: November 30, 1999

DISCUSSION

The bolts in the two outermost tension rows were not fully tightened to the minimum bolt tension, but to an amount that could be safely attained with the equipment available.

The data acquisition system was zeroed, except for the bolt channels, and the test was started. The specimen was loaded at 5 kip intervals. At 70 kips, yielding was visible on the inner tension flange of the column and the rafter. At 80 kips, there was a general increase in yielding along the tension flange as well as initial yielding along the outer compression flange of the rafter. At 83 kips, yielding was visible adjacent to the web stiffener on the compression side of the rafter web. The specimen resisted a maximum load of 85 kips. Load continued to be applied. At a deflection of 4.7 in, a lateral brace failed and the specimen failed. Failure occurred by local web buckling. During testing, there was an increase in bolt strains in the three outermost bolts. Upon unloading, the three innermost tension bolts returned to their initial readings. Two of the outermost tension bolts decreased in strain upon unloading, while the outermost tension bolt showed some slight permanent strain. The theoretical and measured deflections correlated for this test.

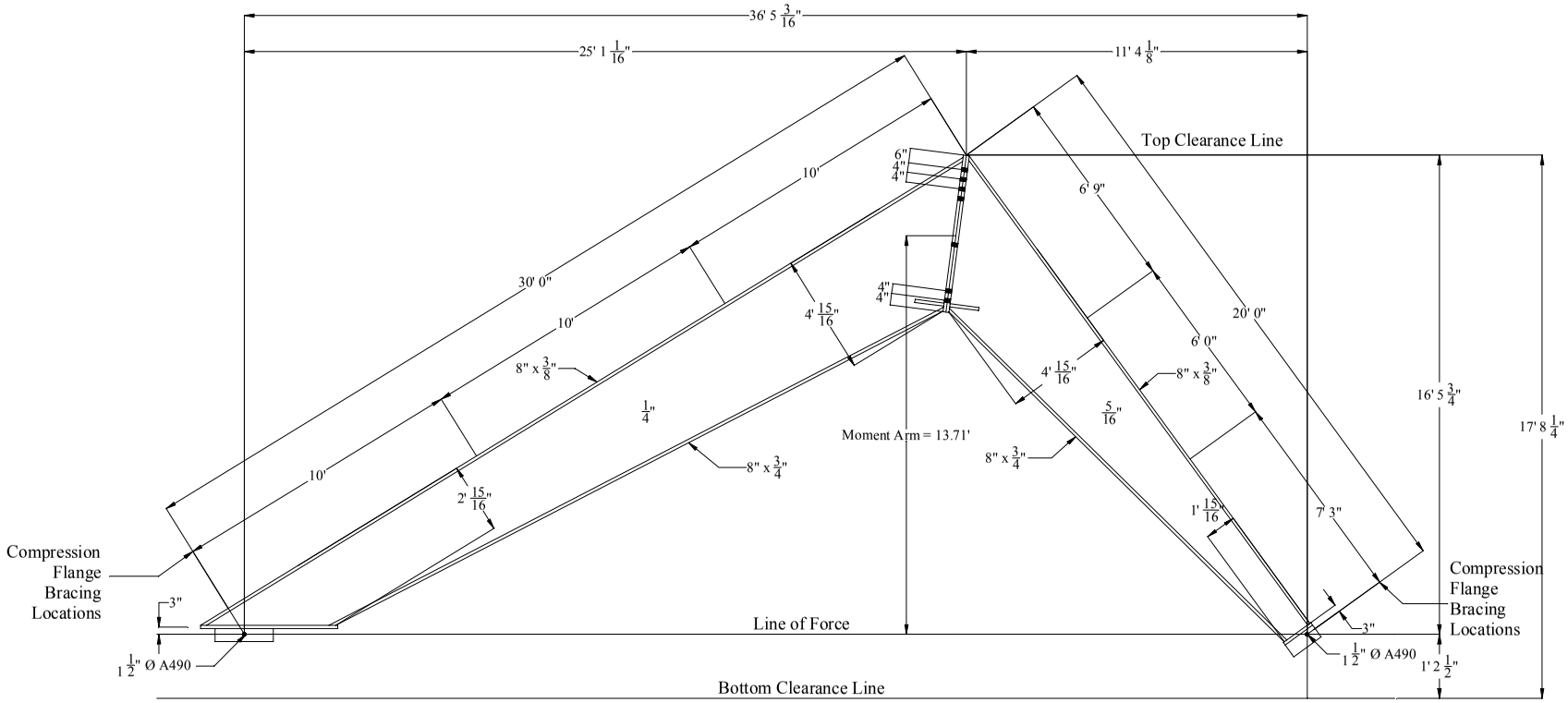

Figure D.1 Specimen Nominal Dimensions for Test F4-$^{7}/_{8}$-$^{3}/_{4}$-67

Table D.1 Geometric Dimensions and Material Properties for Test F4-$^{7}/_{8}$-$^{3}/_{4}$-67

	Nominal Specimen Dimensions	Measured Specimen Dimensions	Measured Yield Stress *	Measured Ultimate Stress	% Elongation
Rafter					
Top Flange	$^{3}/_{8}$" x 8" x 30' 10 $^{1}/_{8}$"	0.381" x 8" x 30' 9 $^{3}/_{4}$"	61.0 ksi	91.3 ksi	23.0 %
Web	0.250"	0.245"	52.0 ksi	68.7 ksi	23.0 %
Bottom Flange	$^{3}/_{4}$" x 8" x 23' 3 $^{1}/_{8}$"	0.746" x 8" x 23' 1 $^{1}/_{4}$"	55.0 ksi	82.0 ksi	28.0 %
End Plate	$^{3}/_{4}$" x 8" x 5' 7"	0.747" x 8" x 5' 7"	55.0 ksi	84.8 ksi	25.5 %
Column					
Top Flange	$^{3}/_{8}$" x 8" x 19' 6 $^{5}/_{8}$"	0.384" x 8" x 19' 6 $^{1}/_{4}$"	61.0 ksi	91.3 ksi	23.0 %
Web	0.3125"	0.325"	52.0 ksi **	68.7 ksi **	23.0 % **
Bottom Flange	$^{3}/_{4}$" x 8" x 16' 0 $^{5}/_{8}$"	0.746" x 8" x 16' $^{1}/_{2}$"	56.2 ksi	85.5 ksi	24.0 %
End Plate	$^{3}/_{4}$" x 8" x 5' 7"	0.748" x 8" x 5' 6 $^{7}/_{8}$"	55.0 ksi	84.8 ksi	25.5 %

* Nominal Yield Stress = 50 ksi

** Assummed to be the same as those for the rafter web. No coupons were pulled from the column web.

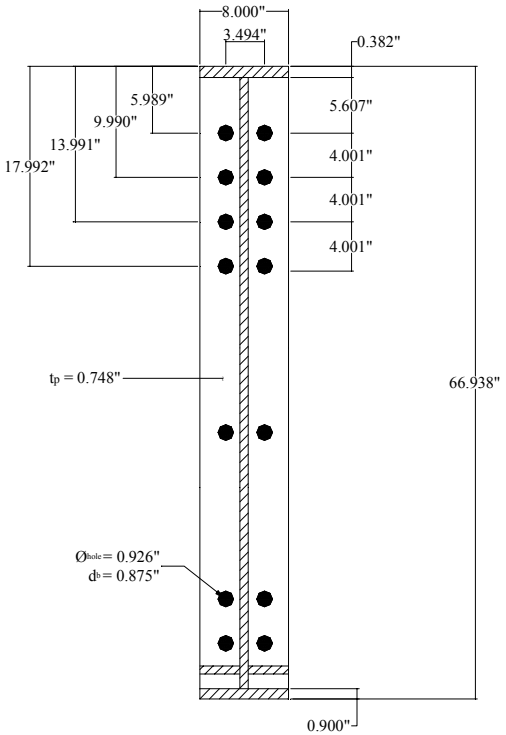

Figure D.2 Average Measured Connection Details for Test F4-$^{7}/_{8}$-$^{3}/_{4}$-67

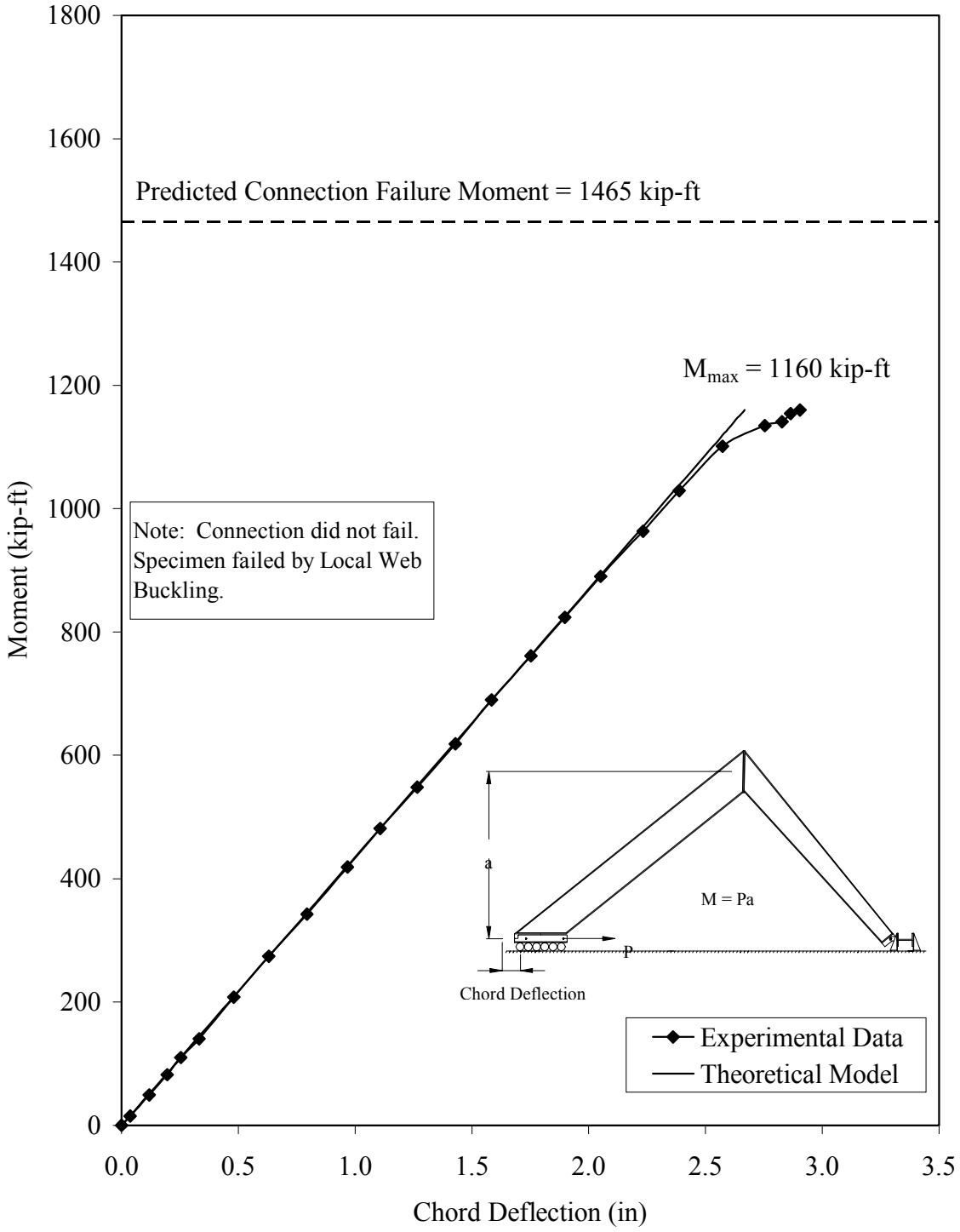

Figure D.3 Applied Moment vs. Chord Deflection for Test F4-$^{7}/_{8}$-$^{3}/_{4}$-67

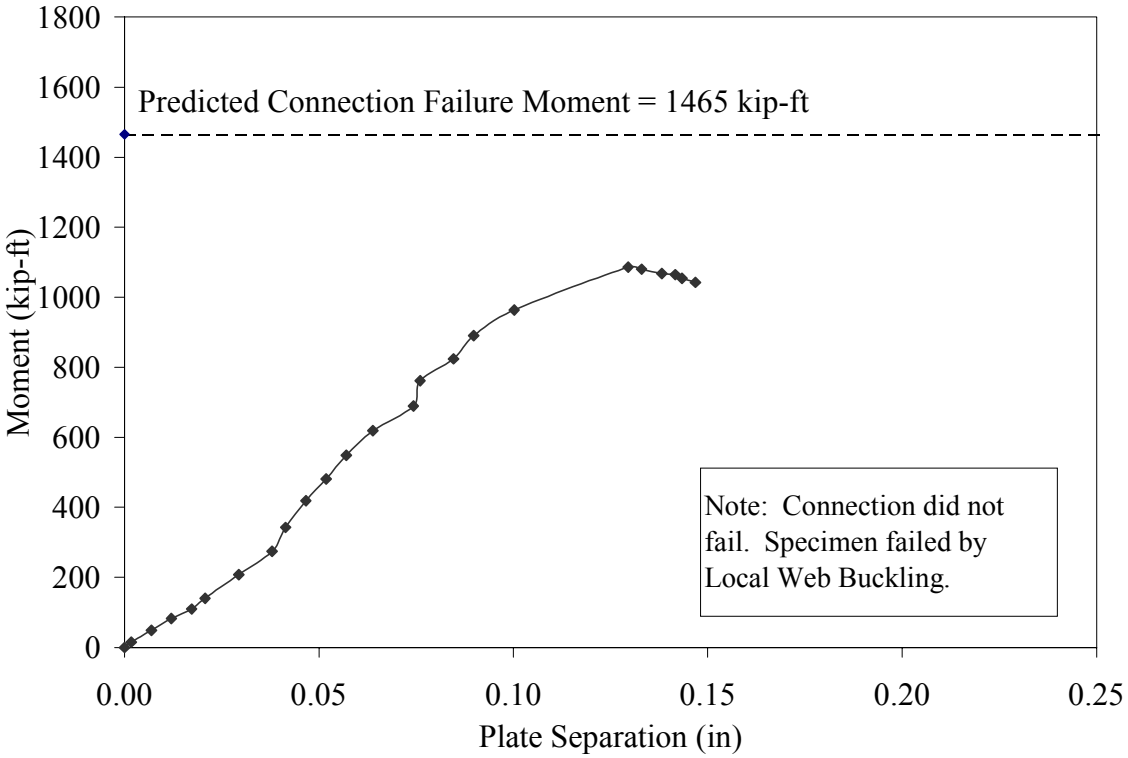

Figure D.4 Applied Moment vs. Plate Separation for Test F4-$^{7}/_{8}$-$^{3}/_{4}$-67

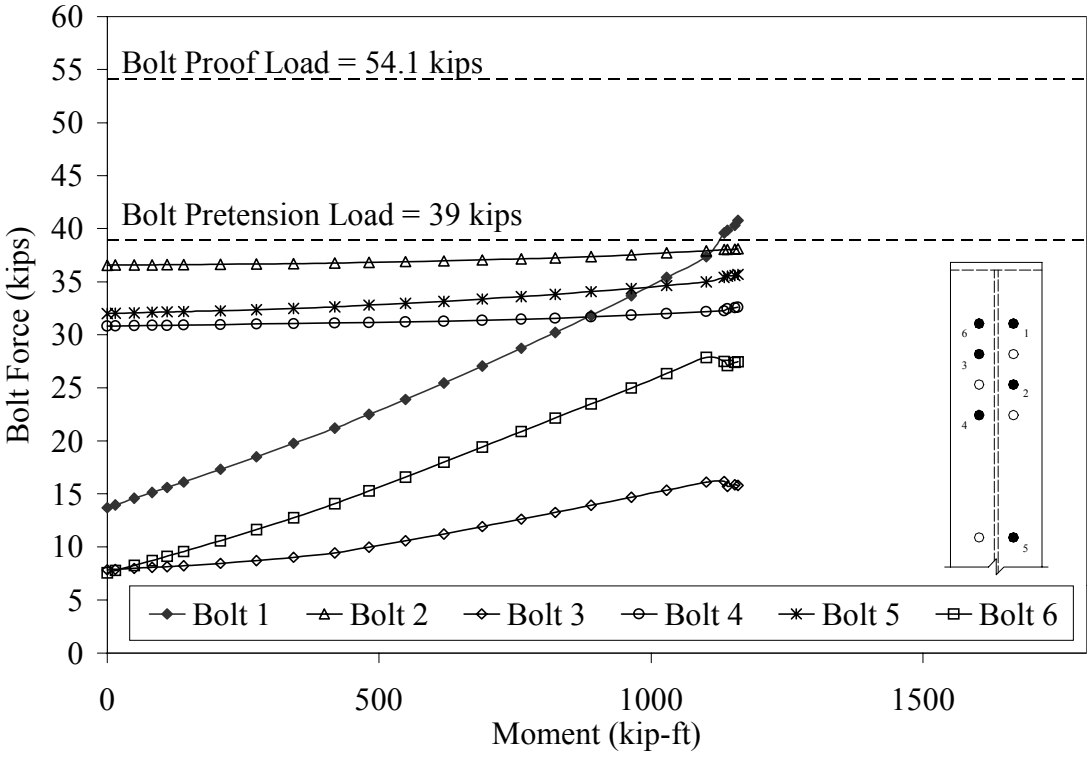

Figure D.5 Bolt Force vs. Applied Moment for Test F4-$^{7}/_{8}$-$^{3}/_{4}$-67

a) Web Buckling of Rafter

c) Yielding of Rafter Flange

Figure D.6 F4-$^{7}/_{8}$-$^{3}/_{4}$-67 at end of Test

APPENDIX E

F5-1$^{1}/_{4}$-$^{3}/_{4}$-84 KNEE TEST RESULTS

TEST NAME: F5-$1^{1}/_{4}$-$^{3}/_{4}$-84
TEST DATE: March 22, 2000

CONNECTION DESCRIPTION

NOMINAL YIELD STRESS	50 ksi
NUMBER OF TENSION BOLTS	10
NUMBER OF STITCH BOLTS	2
NUMBER OF COMPRESSION BOLTS	6
NOMINAL GAGE	4.5 in
NOMINAL PITCH	4 in
NOMINAL END PLATE WIDTH	12 in
NOMINAL END PLATE LENGTH	84 in
NOMINAL END PLATE THICKNESS	0.75 in

BOLT DATA

BOLT DIAMETER	1 1/4 in
BOLT TYPE	A325
BOLT PRETENSION	71 kips

COLUMN DATA

NOMINAL FLANGE WIDTH	12 in
NOMINAL TOP FLANGE THICKNESS	0.5 in
NOMINAL BOTTOM FLANGE THICKNESS	1 in
NOMINAL WEB THICKNESS	0.375 in

RAFTER DATA

NOMINAL FLANGE WIDTH	12 in
NOMINAL TOP FLANGE THICKNESS	0.5 in
NOMINAL BOTTOM FLANGE THICKNESS	1 in
NOMINAL WEB THICKNESS	0.3125 in

EXPERIMENTAL (All values are for an end-plate connection with three rows of tension bolts. See Cycle 4 in attached discussion.)

FAILURE LOAD	196.5 kips
MAXIMUM APPLIED END-PLATE MOMENT	2529 kip-ft
FAILURE LOCATION	End Plates
FAILURE MODE	End plate yielding with high bolt strains
PREDICTED CONNECTION FAILURE MOMENT	2005 kip-ft

TEST NAME: F5-$1^{1}/_{4}$-$^{3}/_{4}$-84
TEST DATE: March 22, 2000

DISCUSSION

The test was divided into four cycles, each one using a different bolt pattern. The bolts in the outermost tension row were not fully tightened to the minimum bolt tension, but to an amount that could be safely attained with the equipment available.

CYCLE 1 (18 BOLTS)

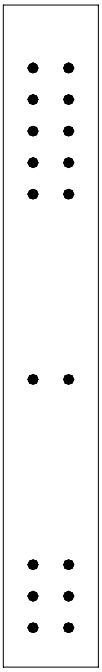

The first cycle was run using all 18 bolts. The data acquisition system was zeroed, except for the bolt and the web strain gage channels, and the test was started. At approximately 170 kips, some yielding was visible on the rafter web in the tension area. The specimen was loaded to 200 kips and then unloaded. The two outermost tension bolts experienced an increase in bolt strains. Upon unloading, the strains returned to their original values. All of the strain gages on the rafter web exceeded the yield strain. The specimen was slightly more flexible than the theoretical deflection predicted.

TEST NAME: F5-$1^{1}/_{4}$-$^{3}/_{4}$-84
TEST DATE: March 22, 2000

DISCUSSION CON'T

CYCLE 2 (14 BOLTS)

The four innermost tension bolts were removed prior to beginning Cycle #2, leaving six bolts on the tension side of the end plate, six bolts on the compression side, and two stitch bolts. The load cell and the displacement transducers were zeroed and the test was started. Readings were taken at 10 kip intervals. At 170 kips, there were signs of yielding on both the rafter and the column webs adjacent to the stitch bolts. There was also an increase in yielding on the rafter web near the tension bolts. The specimen was again loaded to 200 kips without failure and then unloaded. There was a significant increase in the two outermost tension bolts. Upon unloading, these bolts returned to their initial strain readings (no permanent deformation). The remaining bolts experienced a smaller increase in bolt strain. However, upon unloading, the two center tension bolts returned to their original strains while the two innermost tension bolts decreased in strain. As before, the web strain gages indicated that the web strain had well exceeded the yield strain. The theoretical and measured deflections correlated for this cycle.

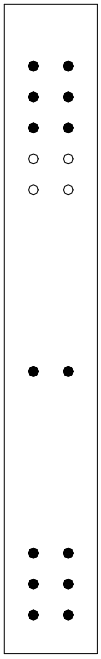

TEST NAME: F5-1$^{1}/_{4}$-$^{3}/_{4}$-84
TEST DATE: March 22, 2000

DISCUSSION CON'T

CYCLE 3 (12 BOLTS))

The two stitch bolts were removed prior to beginning Cycle #3. The load cell and the displacement transducers were zeroed and the test was started. At 190 kips, yielding was visible on the outside face of the compression flange of the rafter. There was also significant plate separation (approximately $1^{1}/_{2}$ in) between the tension side of the end plates. The specimen was loaded to 200 kips without failure and then unloaded. There were increased bolt strains in all bolts, with permanent strain resulting in four of the six tension bolts (Bolt #34, Bolt #35, Bolt #38, Bolt #39). As before, the web strain gages indicated that the web strain had well exceeded the yield strain. The theoretical and measured deflections correlated for this cycle.

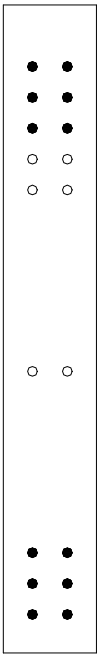

TEST NAME: F5-1$^{1}/_{4}$-$^{3}/_{4}$-84
TEST DATE: March 22, 2000

DISCUSSION CON'T

CYCLE 4 (8 BOLTS)

For Cycle #4, four bolts were removed from the compression side, leaving six bolts in tension and two bolts in compression. The load cell and the displacement transducers were zeroed, and the test was started. At 170 kips, the tension flange of the rafter was warped (buckled) a few inches away from the end plate connection. There were very large plate separations and very high bolt strains in the two outermost tension bolts. It appeared as if the two top bolts were taking all of the load applied. The test was stopped at 196.5 kips. All of the bolt gages indicated high bolt strains and some permanent deformation. The two outermost tension bolts developed the highest strains, with the two innermost tension bolts producing the next highest strains. Strain increase in the two center tension bolts was significantly lower than the other four. As before, the web strain gages indicated that the web strain had well exceeded the yield strain. The theoretical and measured deflections correlated for this cycle.

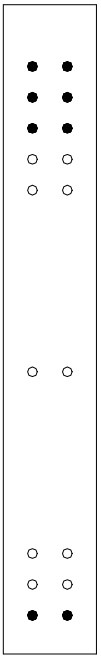

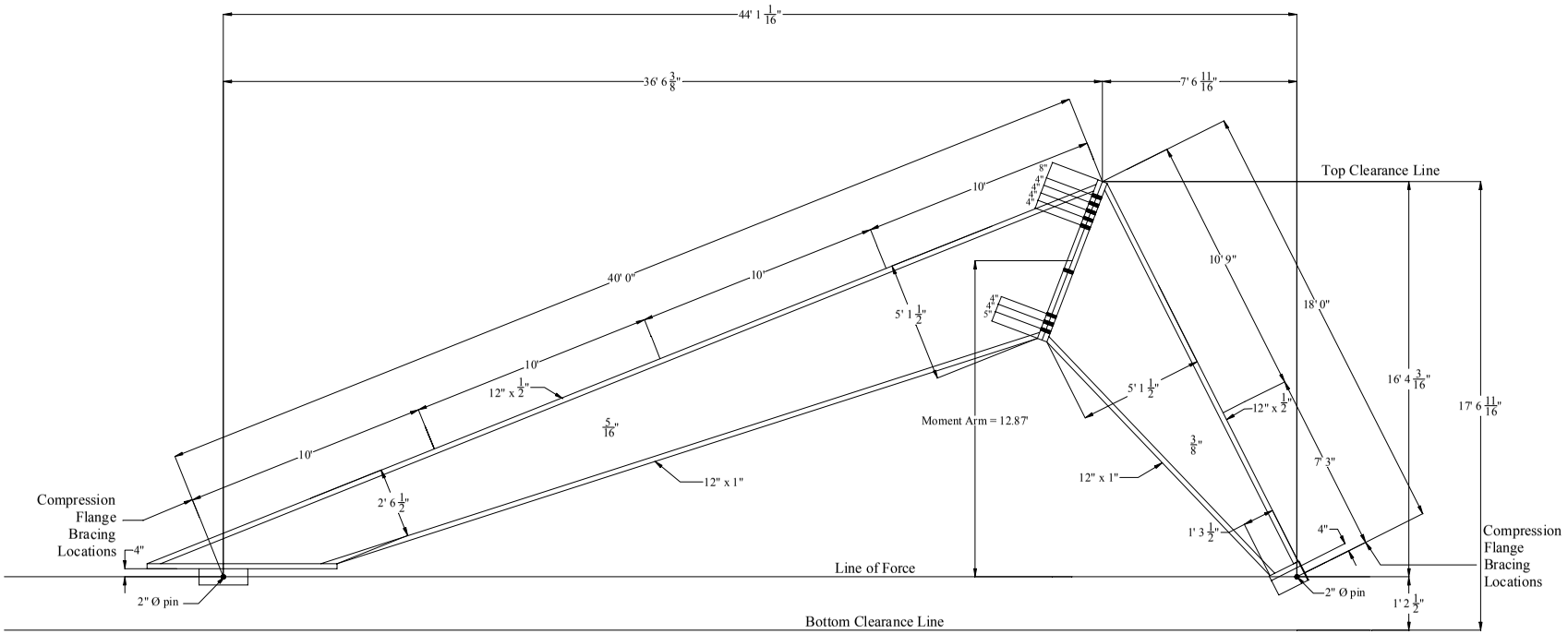

Figure E.1 Specimen Nominal Dimensions for Test F5-$1^{1}/_{4}$-$^{3}/_{4}$-84

Table E.1 Geometric Dimensions and Material Properties for Test F5-1 1/4-3/4-84

	Nominal Specimen Dimensions	Measured Specimen Dimensions	Measured Yield Stress *	Measured Ultimate Stress	% Elongation
Rafter					
Top Flange	1/2" x 12" x 42' 3 15/16"	0.507" x 12" x 42' 6"	57.1 ksi	81.4 ksi	25.0 %
Web	5/16"	0.305"	47.1 ksi	67.0 ksi	29.5 %
Bottom Flange	1" x 12" x 30' 10 3/4"	1.014" x 12" x 30' 11"	56.1 ksi	84.1 ksi	27.0 %
End Plate	3/4" x 12" x 7'	0.767" x 12 1/16" x 7'	55.6 ksi	84.3 ksi	25.0 %
Column					
Top Flange	1/2" x 12" x 17' 5 9/16"	0.506" x 12" x 17' 6"	57.9 ksi	81.4 ksi	25.0 %
Web	3/8"	0.368"	50.4 ksi	69 ksi	24.0 %
Bottom Flange	1" x 12" x 13' 3 3/4"	1.013" x 12" x 13' 6"	55.4 ksi	84.0 ksi	27.0 %
End Plate	3/4" x 12" x 7'	0.769" x 12" x 7'	55.6 ksi	84.3 ksi	25.0 %

* Nominal Yield Stress = 50 ksi

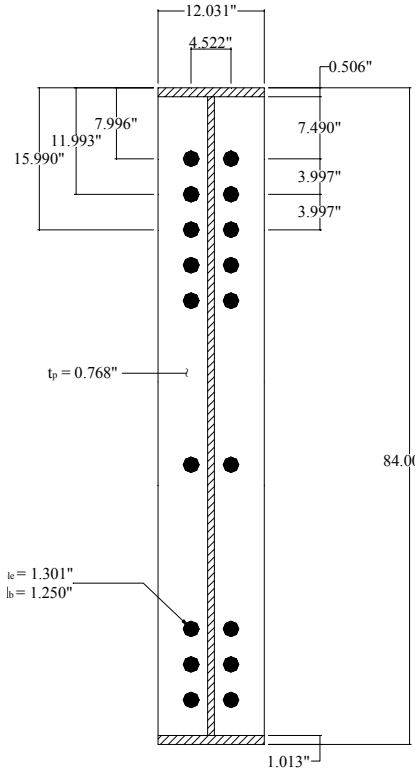

Figure E.2 Average Measured Connection Details for Test F5-1 1/4-3/4-84

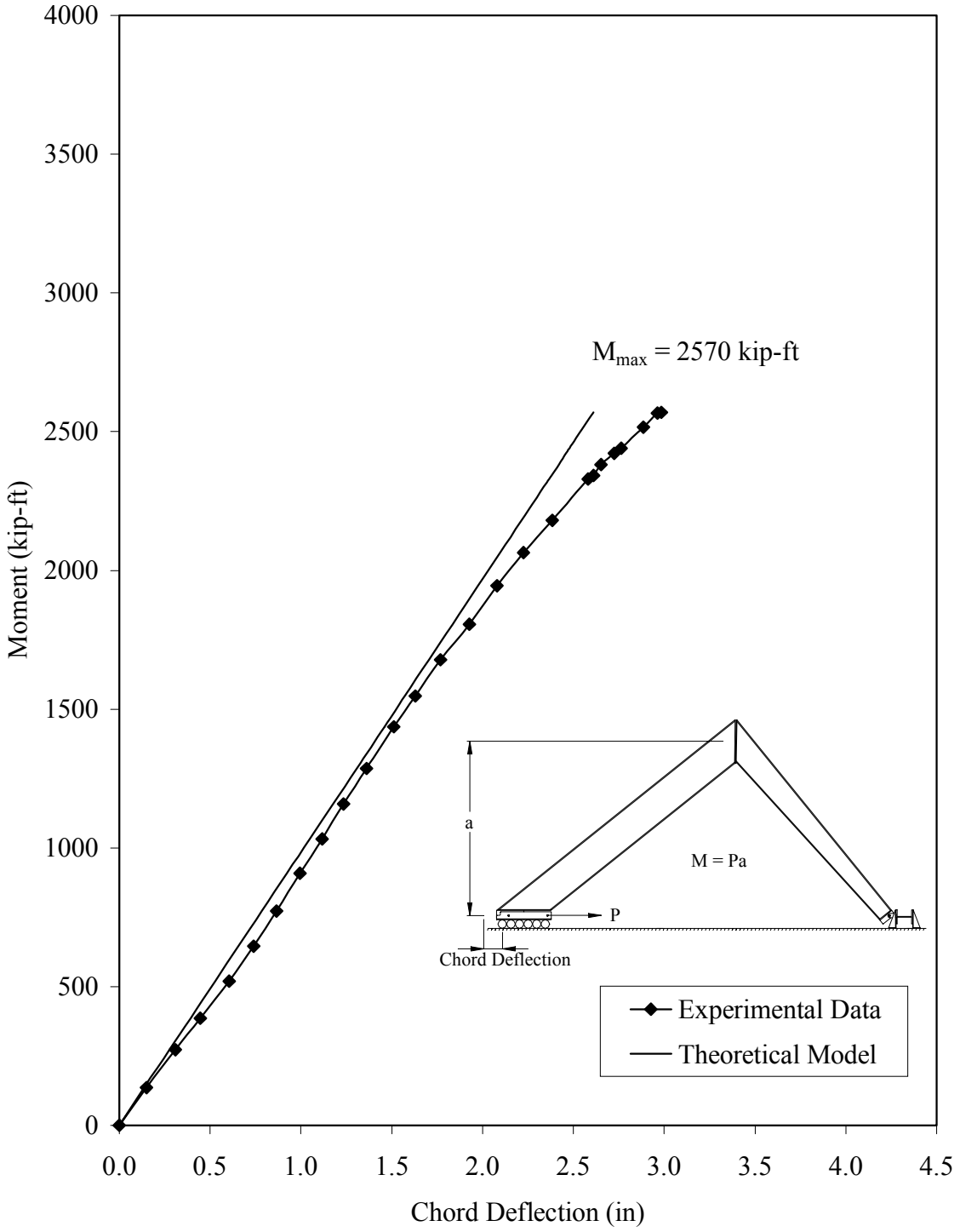

Figure E.3 Applied Moment vs. Chord Deflection for Cycle 1 in Test F5-$1^{1}/_{4}$-$^{3}/_{4}$-84

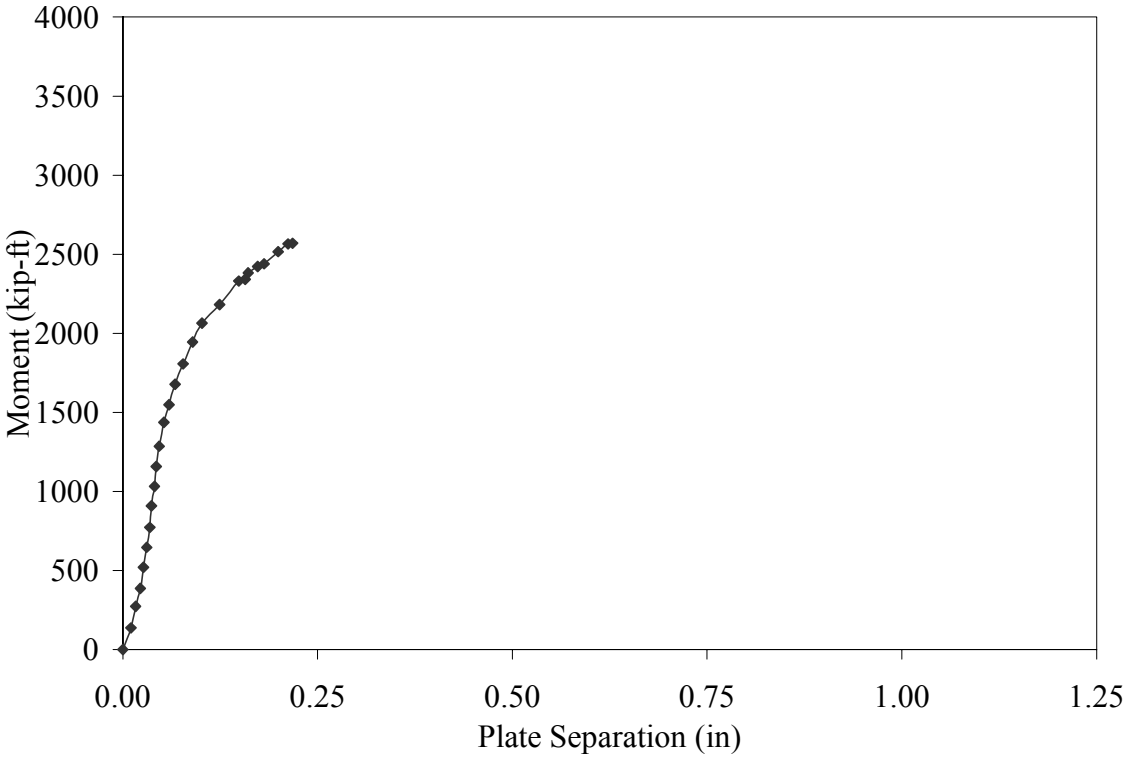

Figure E.4 Applied Moment vs. Plate Separation for Cycle 1 in Test F5-1$^{1}/_{4}$-$^{3}/_{4}$-84

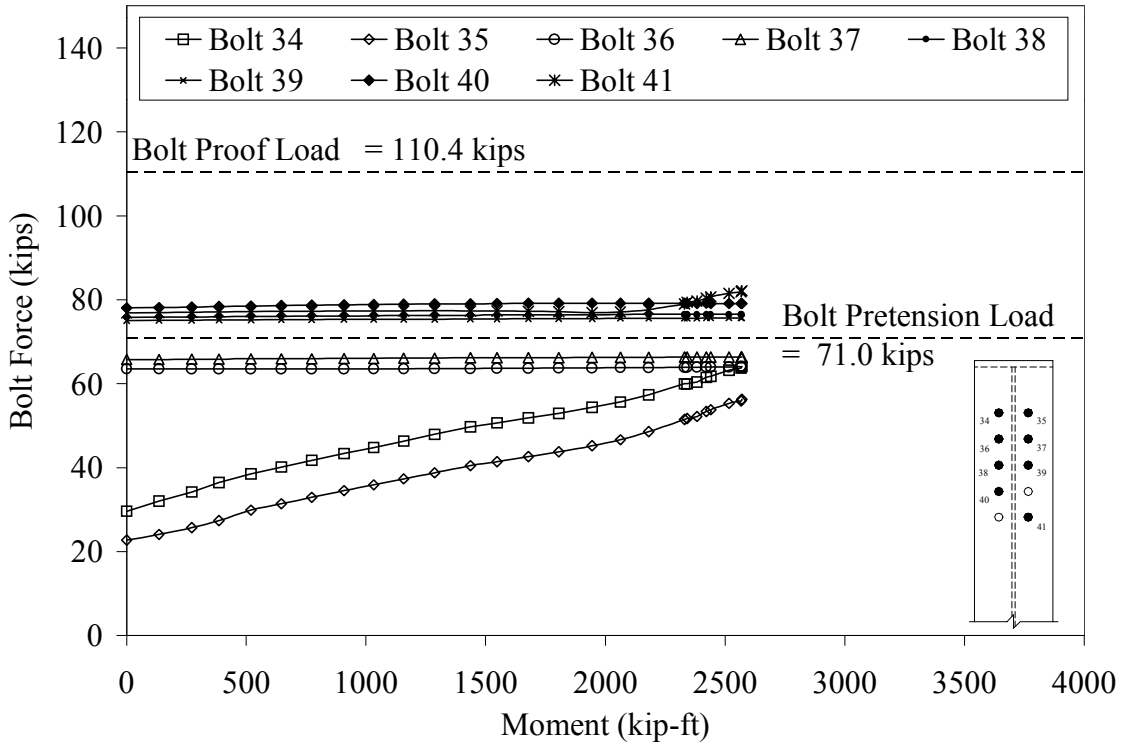

Figure E.5 Bolt Force vs. Applied Moment for Cycle 1 in Test F5-1$^{1}/_{4}$-$^{3}/_{4}$-84

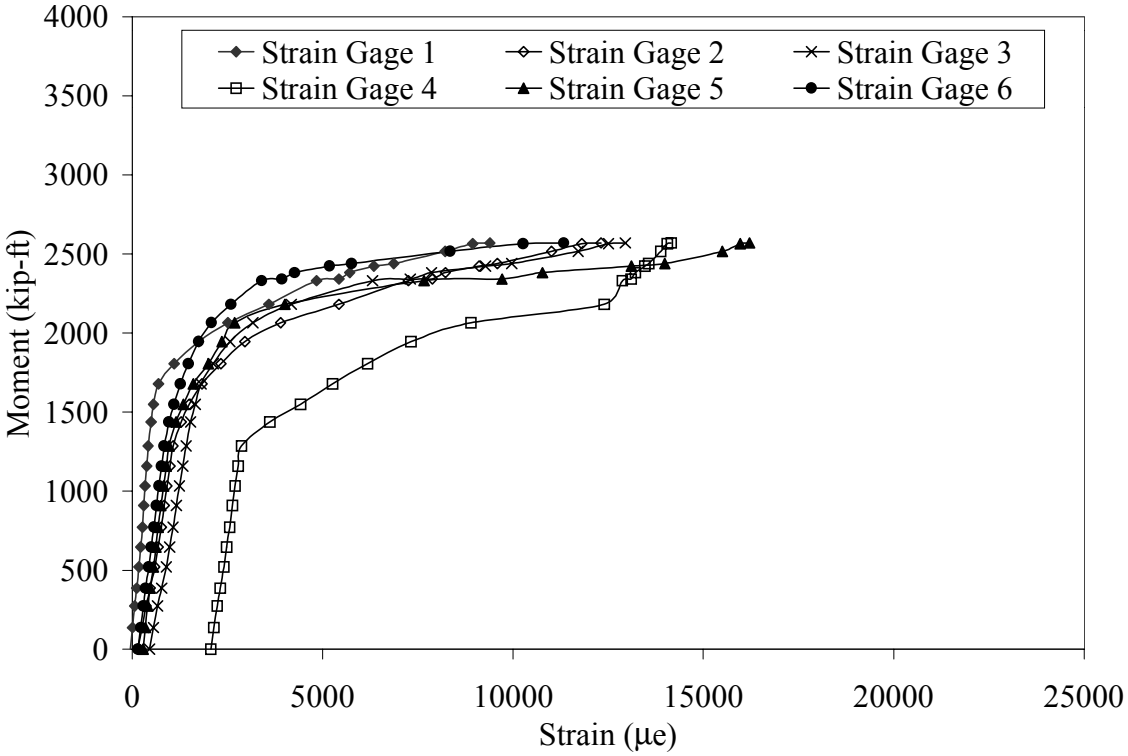

Figure E.6 Applied Moment vs. Web Strain for Cycle 1 in Test F5-$1^{1}/_{4}$-$^{3}/_{4}$-84

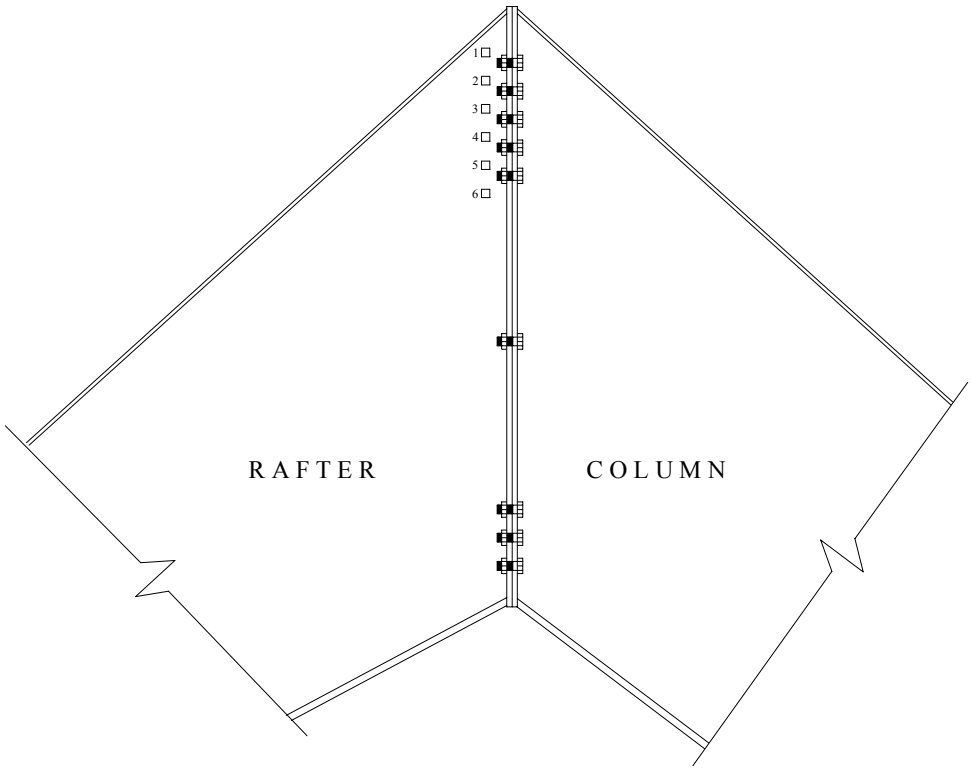

Figure E.7 Strain Gage Locations for Test F5-$1^{1}/_{4}$-$^{3}/_{4}$-84

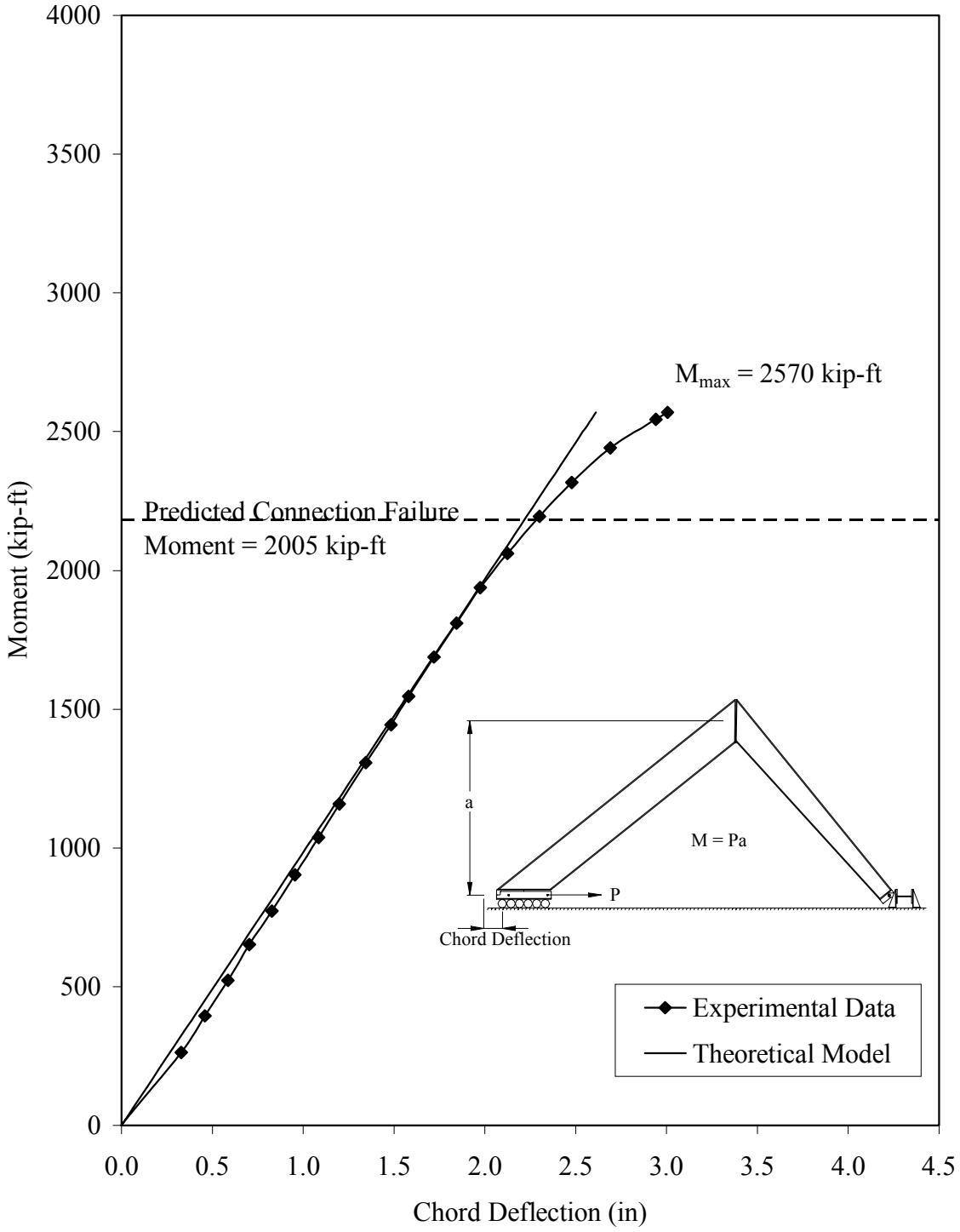

Figure E.8 Applied Moment vs. Chord Deflection for Cycle 2 in Test F5-$1^{1}/_{4}$-$^{3}/_{4}$-84

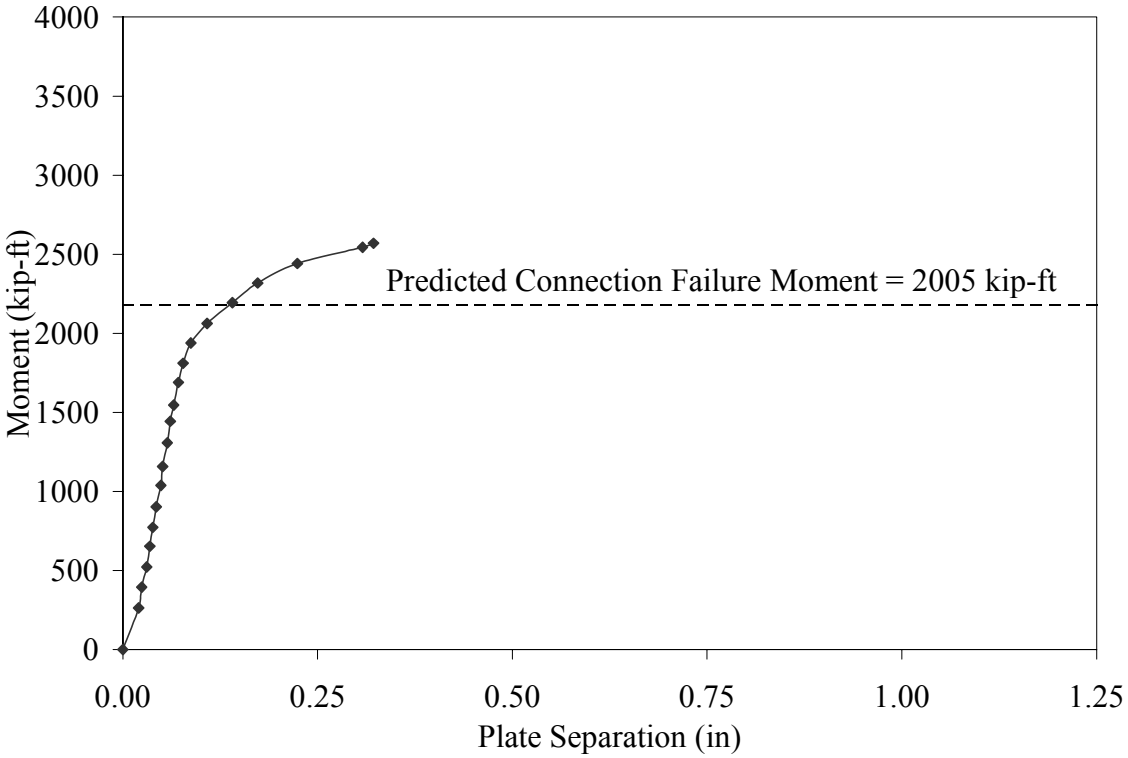

Figure E.9 Applied Moment vs. Plate Separation for Cycle 2 in Test F5-1$^{1}/_{4}$-$^{3}/_{4}$-84

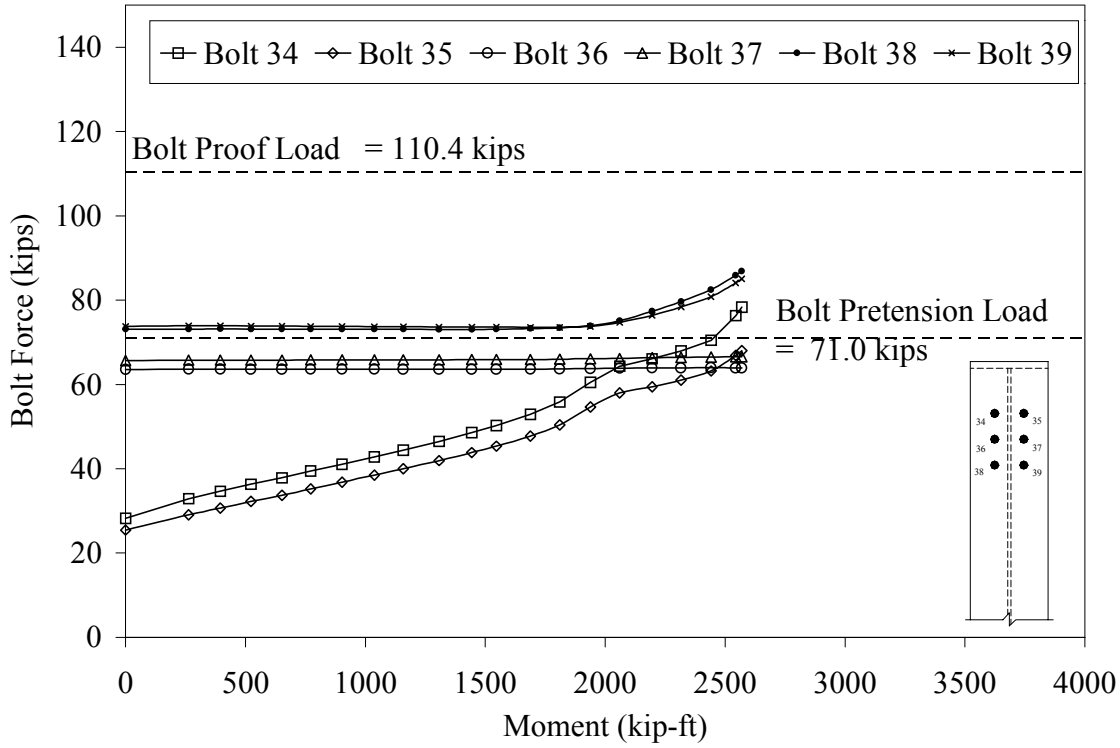

Figure E.10 Bolt Force vs. Applied Moment for Cycle 2 in Test F5-1$^{1}/_{4}$-$^{3}/_{4}$-84

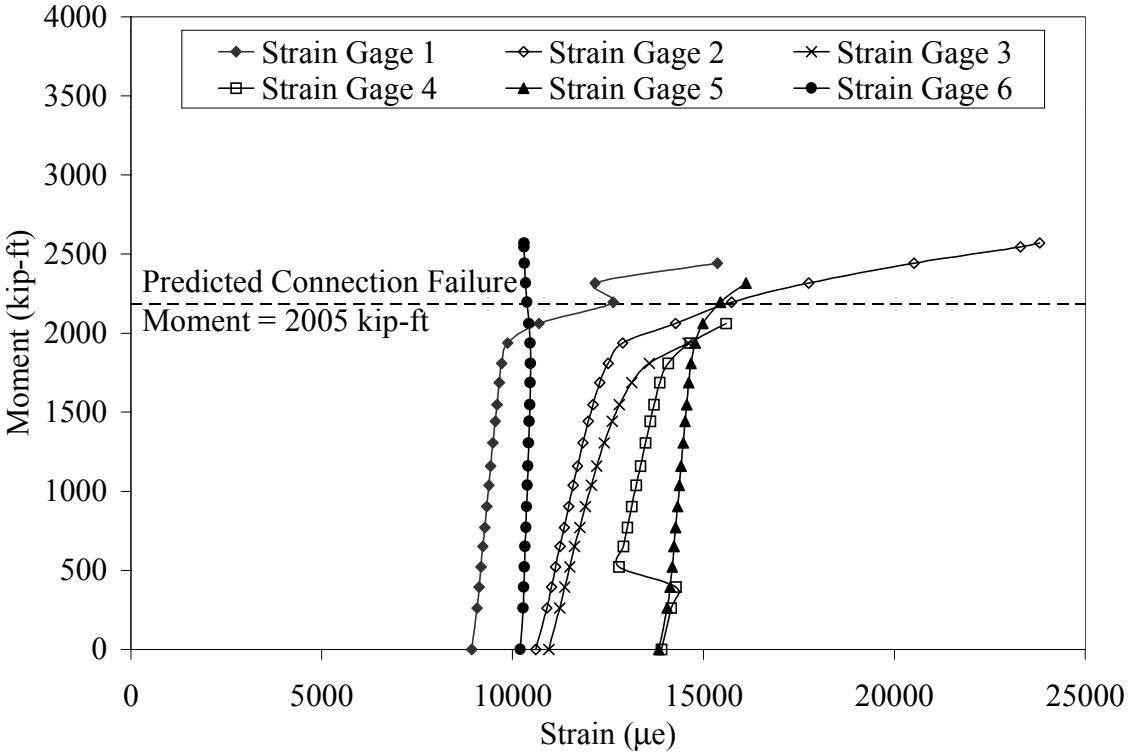

Figure E.11 Applied Moment vs. Web Strain for Cycle 2 in Test F5-$1^{1}/_{4}$-$^{3}/_{4}$-84

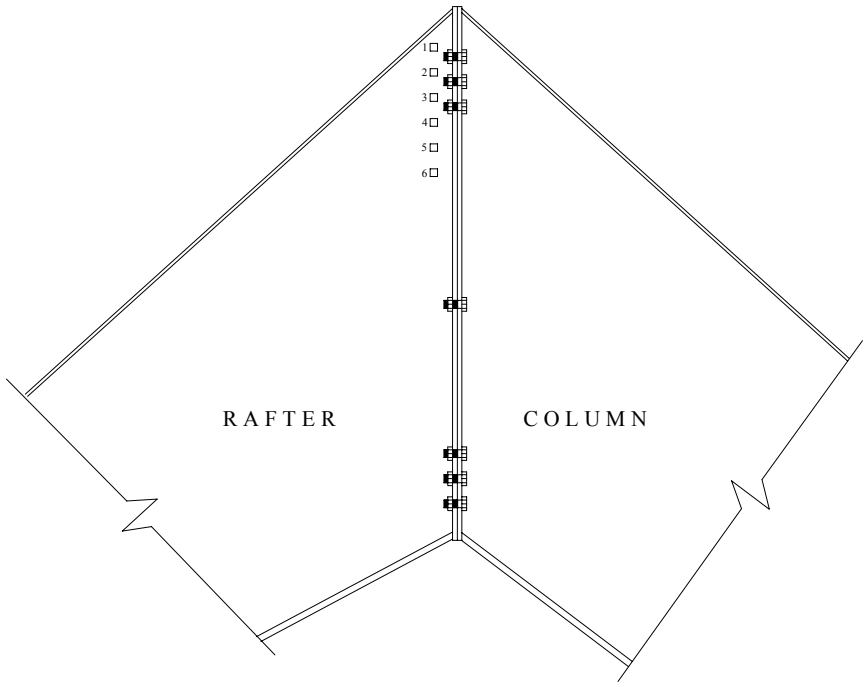

Figure E.12 Strain Gage Locations for Cycle 2 in Test F5-$1^{1}/_{4}$-$^{3}/_{4}$-84

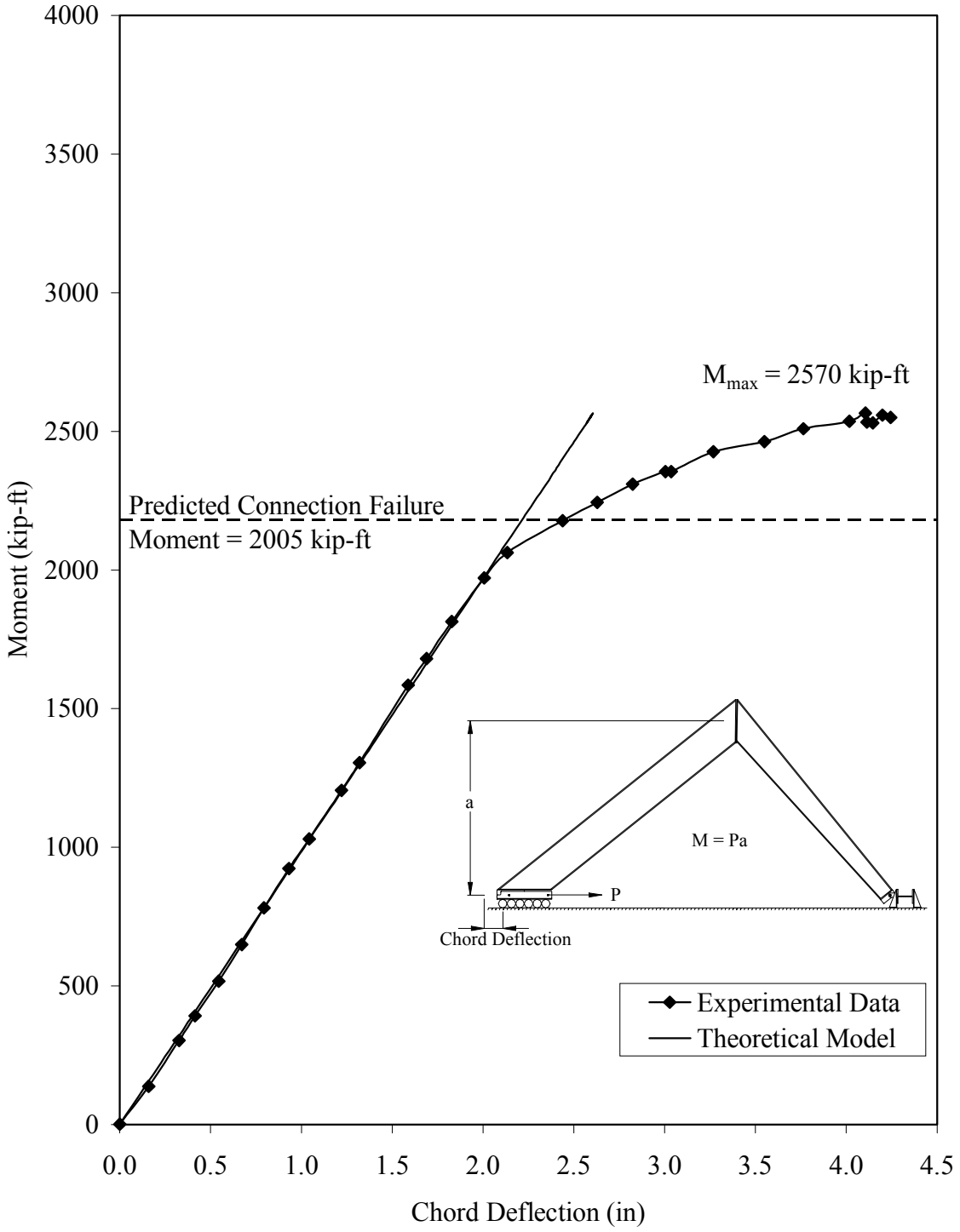

Figure E.13 Applied Moment vs. Chord Deflection for Cycle 3 in Test F5-$1^{1}/_{4}$-$^{3}/_{4}$-84

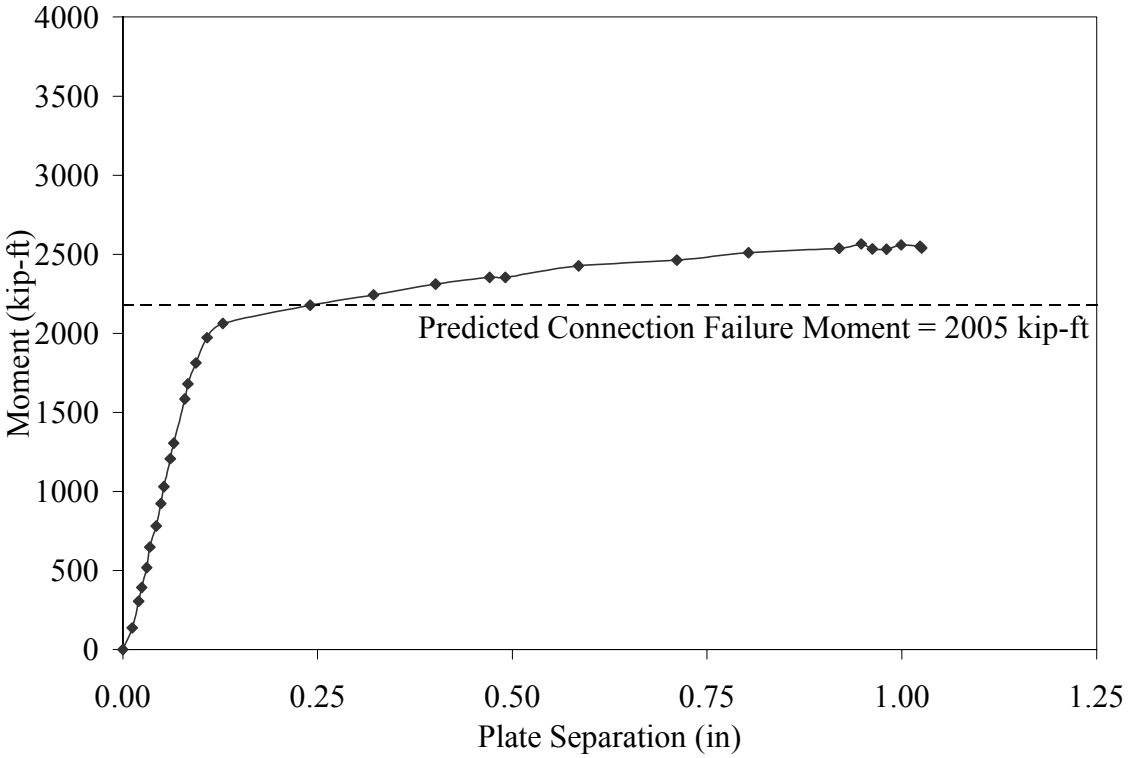

Figure E.14 Applied Moment vs. Plate Separation for Cycle 3 in Test F5-$1^{1}/_{4}$-$^{3}/_{4}$-84

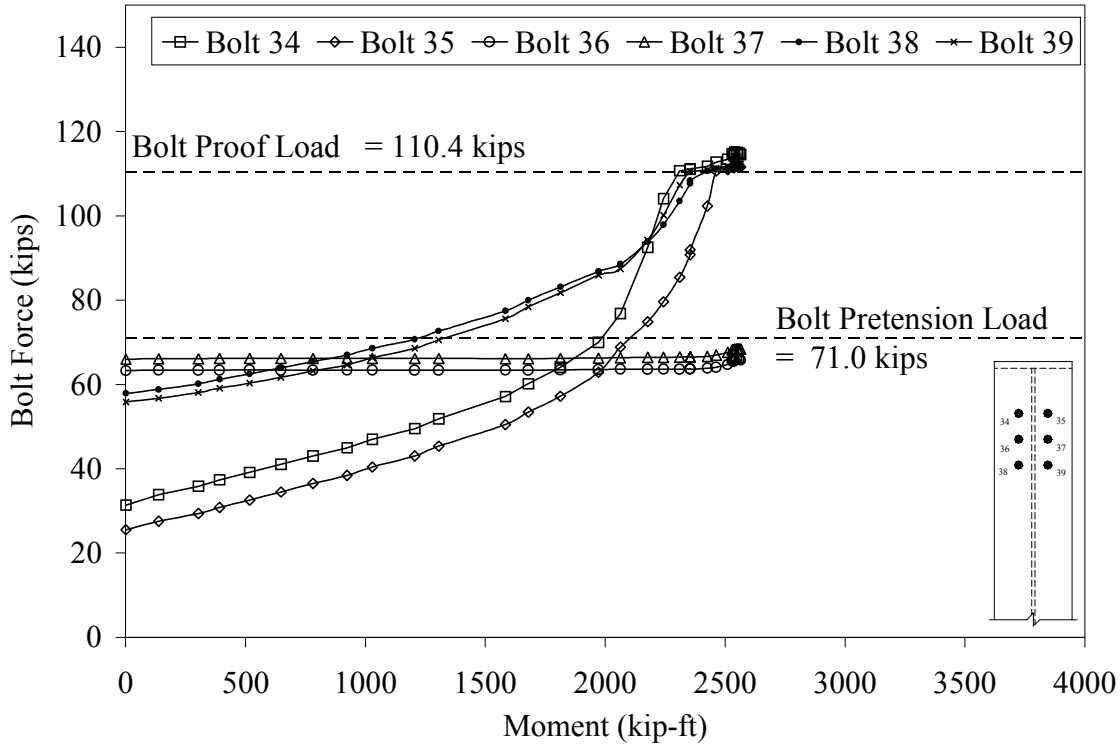

Figure E.15 Bolt Force vs. Applied Moment for Cycle 3 in Test F5-$1^{1}/_{4}$-$^{3}/_{4}$-84

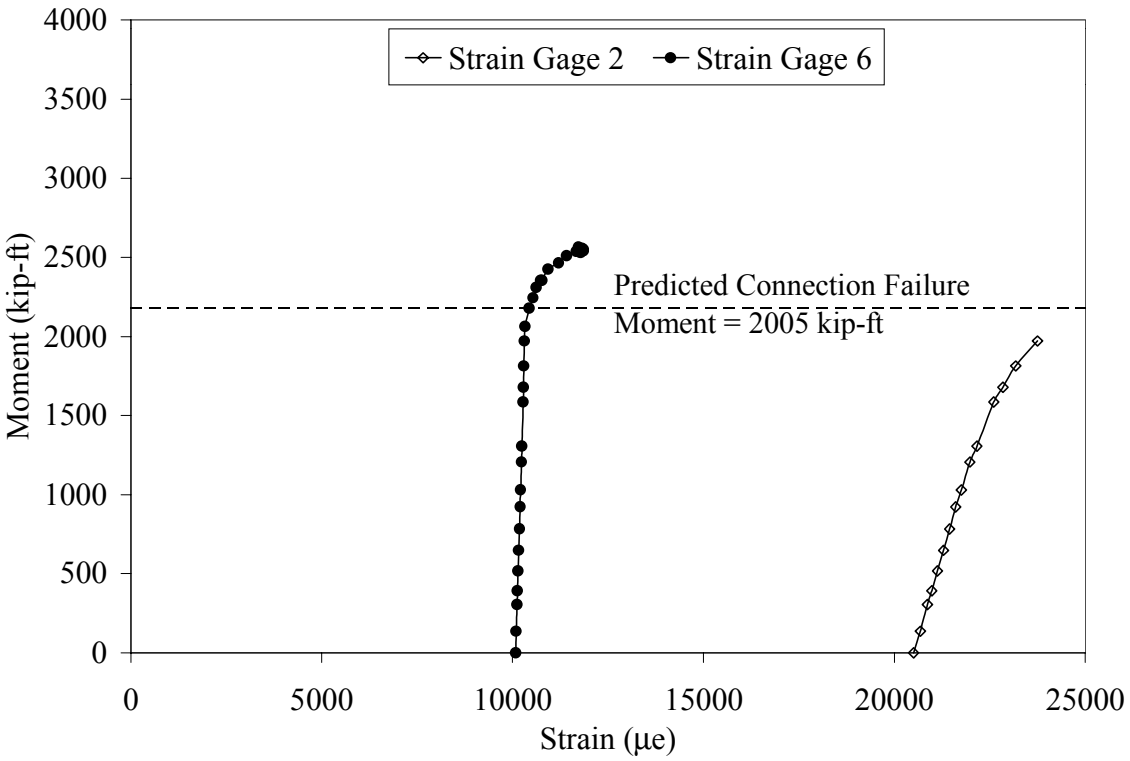

E.16 Applied Moment vs. Web Strain for Cycle 3 in Test F5-$1^{1}/_{4}$-$^{3}/_{4}$-84

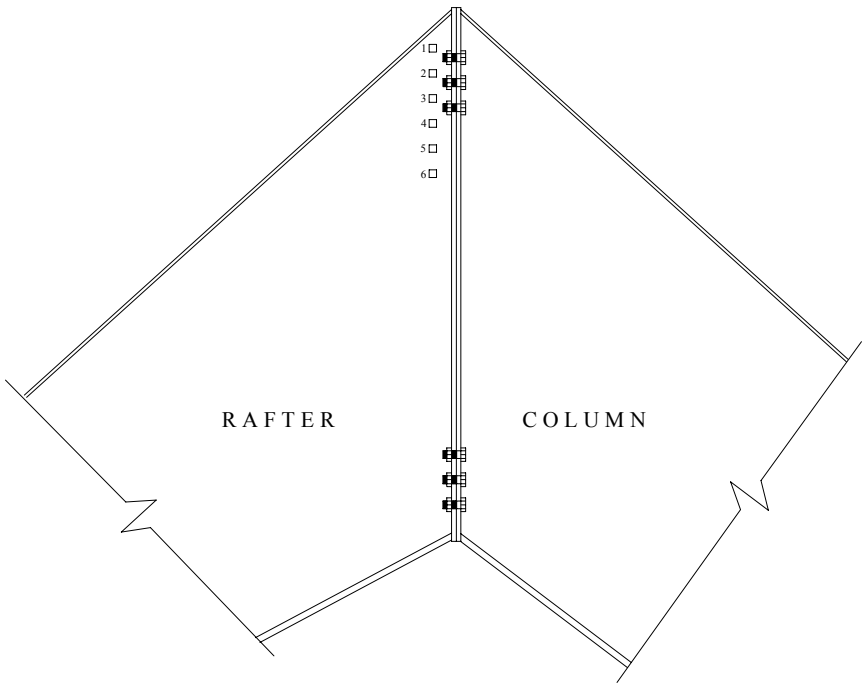

Figure E.17 Strain Gage Locations for Cycle 3 in Test F5-$1^{1}/_{4}$-$^{3}/_{4}$-84

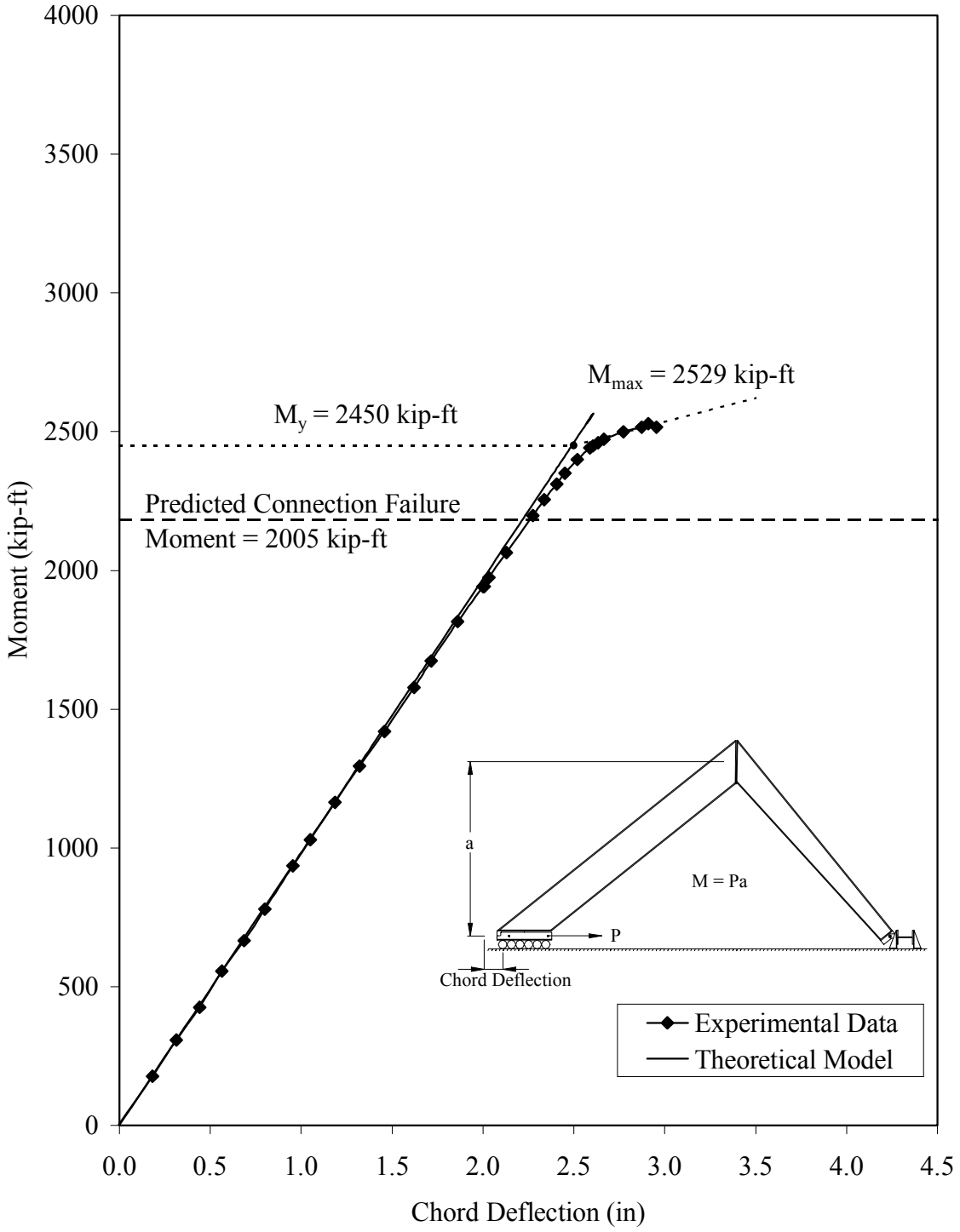

Figure E.18 Applied Moment vs. Chord Deflection for Cycle 4 in Test F5-$1^1/_4$-$^3/_4$-84

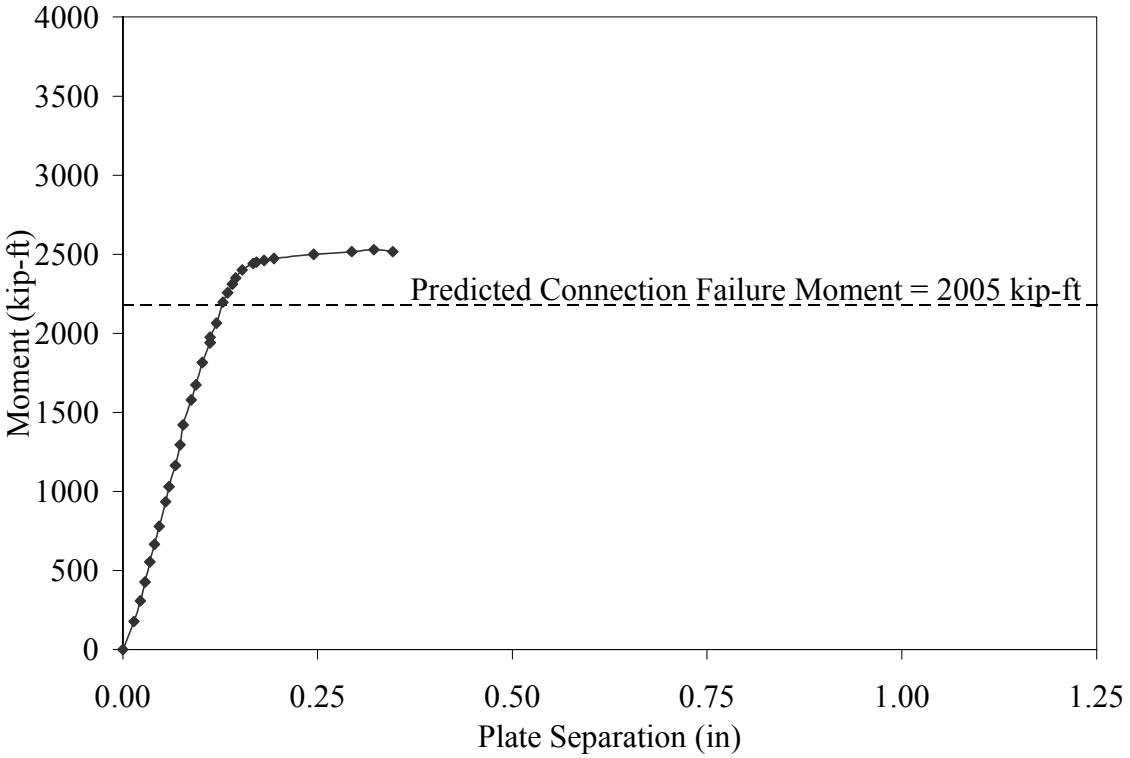

Figure E.19 Applied Moment vs. Plate Separation for Cycle 4 in Test F5-$1^{1}/_{4}$-$^{3}/_{4}$-84

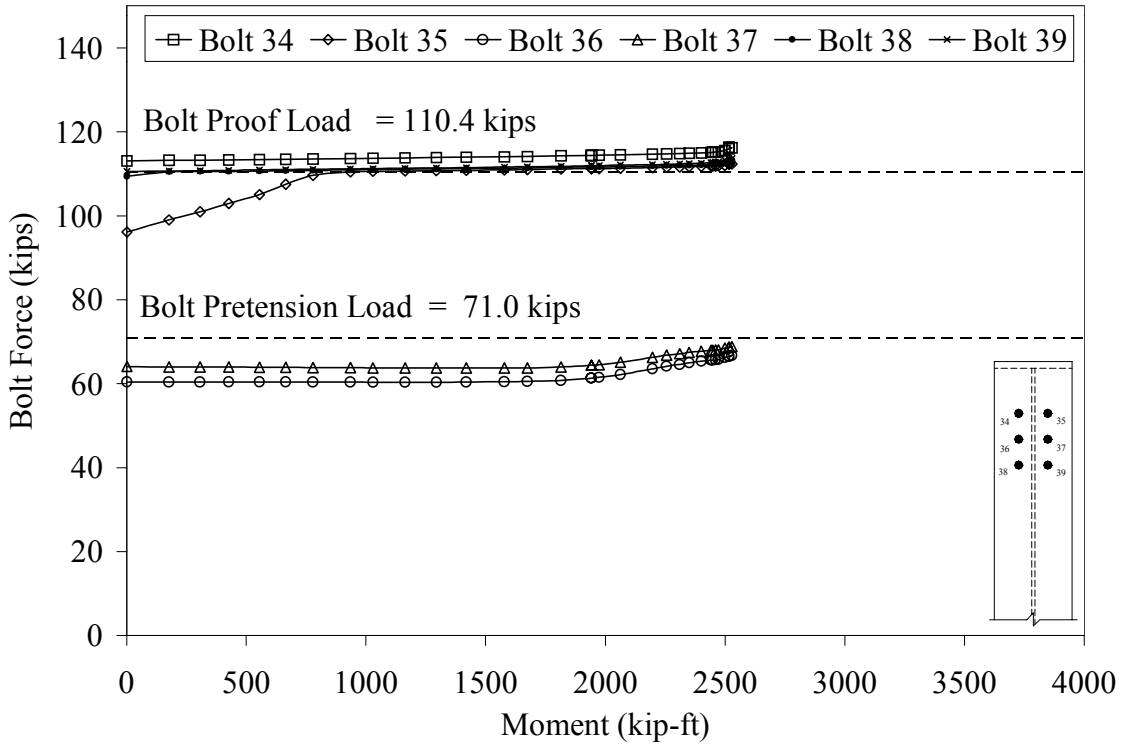

Figure E.20 Bolt Force vs. Applied Moment for Cycle 4 in Test F5-$1^{1}/_{4}$-$^{3}/_{4}$-84

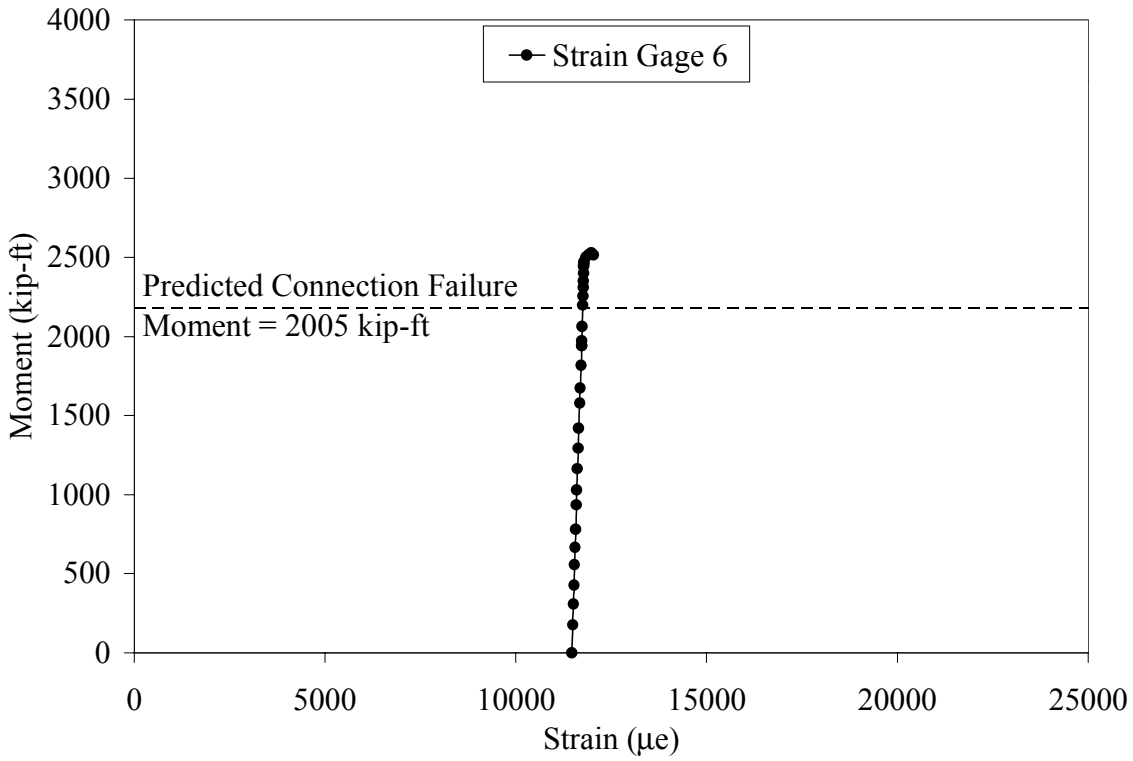

E.21 Applied Moment vs. Web Strain for Cycle 4 in Test F5-$1^{1}/_{4}$-$^{3}/_{4}$-84

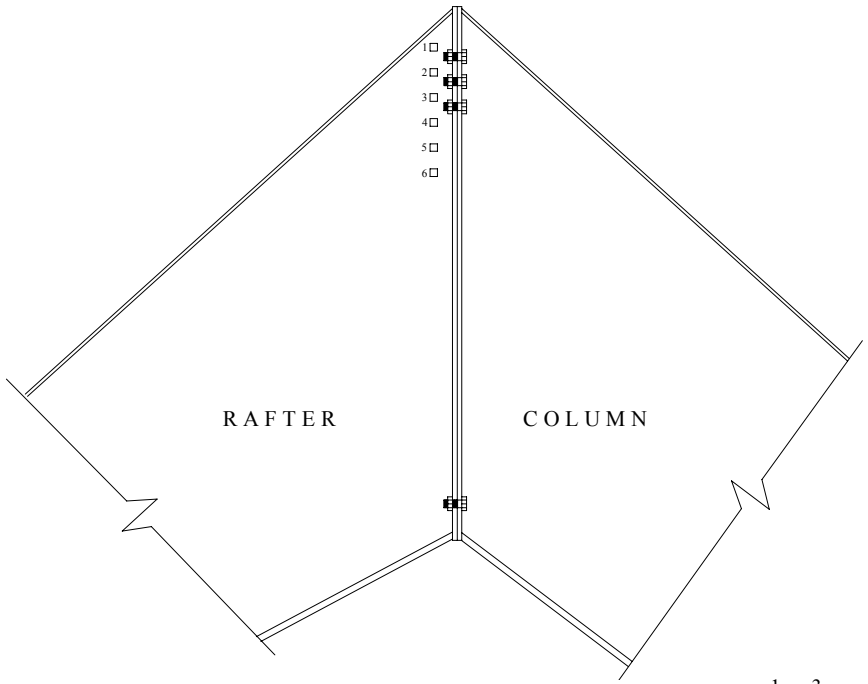

Figure E.22 Strain Gage Locations for Cycle 4 in Test F5-$1^{1}/_{4}$-$^{3}/_{4}$-84

a) Yielding of Column and Rafter End-Plate

b) Yielding of Web on Tension Side

Figure E.23 F5-$1^{1}/_{4}$-$^{3}/_{4}$-84 at end of Test

APPENDIX F

F5S-$1^{1}/_{4}$-$^{3}/_{4}$-84 KNEE TEST RESULTS

TEST NAME: F5S-$1^{1}/_{4}$-$^{3}/_{4}$-84
TEST DATE: March 8, 2000

CONNECTION DESCRIPTION

NOMINAL YIELD STRESS	50 ksi
NUMBER OF TENSION BOLTS	10
NUMBER OF STITCH BOLTS	2
NUMBER OF COMPRESSION BOLTS	6
NOMINAL GAGE	4.5 in
NOMINAL PITCH (see end plate drawing)	4 in / 5 in
NOMINAL END PLATE WIDTH	12 in
NOMINAL END PLATE LENGTH	84 in
NOMINAL END PLATE THICKNESS	0.75 in

BOLT DATA

BOLT DIAMETER	1 1/4 in
BOLT TYPE	A325
BOLT PRETENSION	71 kips

COLUMN DATA

NOMINAL FLANGE WIDTH	12 in
NOMINAL TOP FLANGE THICKNESS	0.5 in
NOMINAL BOTTOM FLANGE THICKNESS	1 in
NOMINAL WEB THICKNESS	0.375 in

RAFTER DATA

NOMINAL FLANGE WIDTH	12 in
NOMINAL TOP FLANGE THICKNESS	0.5 in
NOMINAL BOTTOM FLANGE THICKNESS	1 in
NOMINAL WEB THICKNESS	0.3125 in

EXPERIMENTAL (All values are for an end-plate connection with two rows of tension bolts and a stiffener outside the bolt rows. See Cycle 5 in attached discussion.)

FAILURE LOAD	202.5 kips
MAXIMUM APPLIED END-PLATE MOMENT	2606 kip-ft
FAILURE LOCATION	End Plates
FAILURE MODE	End plate yielding with high bolt strains
PREDICTED CONNECTION FAILURE MOMENT	1742 kip-ft

TEST NAME: F5S-$1^{1}/_{4}$-$^{3}/_{4}$-84
TEST DATE: March 8, 2000

DISCUSSION

The test was divided into five cycles, using four different bolt patterns. The bolts in the two outermost tension rows were not fully tightened to the minimum bolt tension, but to an amount that could be safely attained with the equipment available.

CYCLE 1 & 2(18 BOLTS)

The first two cycles were run using all 18 bolts. The data acquisition system was zeroed, except for the bolts and the web strain gage channels, and the test was started. At approximately 160 kips, some yielding was visible under the rafter compression flange. At 180 kips, yield lines had formed around the upper web stiffeners on the rafter web. The specimen was then loaded to 190 kips. The load was removed to adjust the hydraulic pump. For the second cycle, the specimen was loaded to 200 kips. No failure occurred. The specimen was then unloaded. During cycles one and two, bolt strains increased, with the top two tension bolts having the largest strain increase. Upon unloading, all bolt strains returned to their initial readings (no permanent deformation). The theoretical and measured chord chord deflection correlated for Cycle # 1. For Cycle #2, the measured chord deflection indicated that the specimen was slightly stiffer than the theoretical deflection predicted.

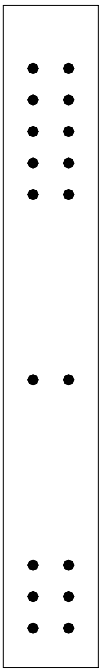

TEST NAME: F5S-$1^{1}/_{4}$-$^{3}/_{4}$-84
TEST DATE: March 8, 2000

DISCUSSION CON'T

CYCLE 3 (14 BOLTS)

The four innermost tension bolts were removed prior to beginning Cycle #3, leaving six bolts on the tension side of the end plate, six bolts on the compression side, and the two stitch bolts. The data acquisition system was zeroed, except for the bolt channels, and the test was started. There was a slight increase in the web yielding of the rafter. The specimen was loaded up to 200 kips without failure and then unloaded. There was an increase in all bolt strains, with the top two tension bolts having the largest strain increase. Upon unloading, all bolt strains returned to their initial readings (no permanent deformation). The measured chord deflection indicated that the specimen was stiffer than the theoretical deflection predicted.

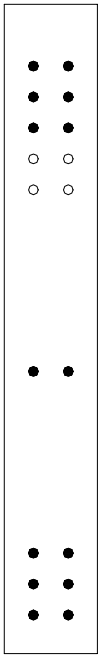

TEST NAME: F5S-$1^{1}/_{4}$-$^{3}/_{4}$-84
TEST DATE: March 8, 2000

DISCUSSION CON'T

CYCLE 4 (12 BOLTS)

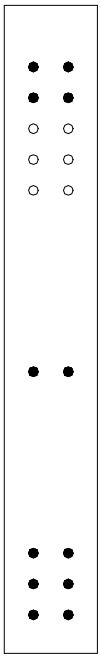

The two more bolts were removed from the tension flange leaving four bolts in tension, six bolts in compression, and two stitch bolts. The data acquisition system was zeroed, except for the bolt channels, and the test was started. There was more substantial yielding of the column and rafter webs and also some end-plate separation. At 200 kips, the specimen had not reached failure and was unloaded. Bolt strains increased significantly during this cycle with some permanent strain remaining. The measured chord deflection indicated that the specimen was slightly stiffer than the theoretical deflection predicted.

TEST NAME: F5S-$1^{1}/_{4}$-$^{3}/_{4}$-84
TEST DATE: March 8, 2000

DISCUSSION CON'T

CYCLE 5 (6 BOLTS)

The two stitch bolts were removed as well as four compression bolts and the two innermost tension bolts. The data acquisition system was zeroed, and the test was started. It was apparent that the stitch bolts and the compression bolts were producing a substantial amount of the end-plate clamping force even when the specimen was unloaded. At 200 kips, there was severe web yielding and end-plate separation. Bolt forces were also very high. As soon as load was applied, it would gradually drop off. Finally, while increasing the load, one of the lateral braces failed and the specimen failed laterally. As expected, the bolt strains were high for this cycle and produced permanent strain in the specimen. The theoretical and measured deflections correlated for this cycle.

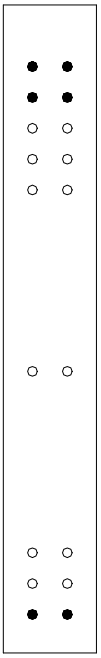

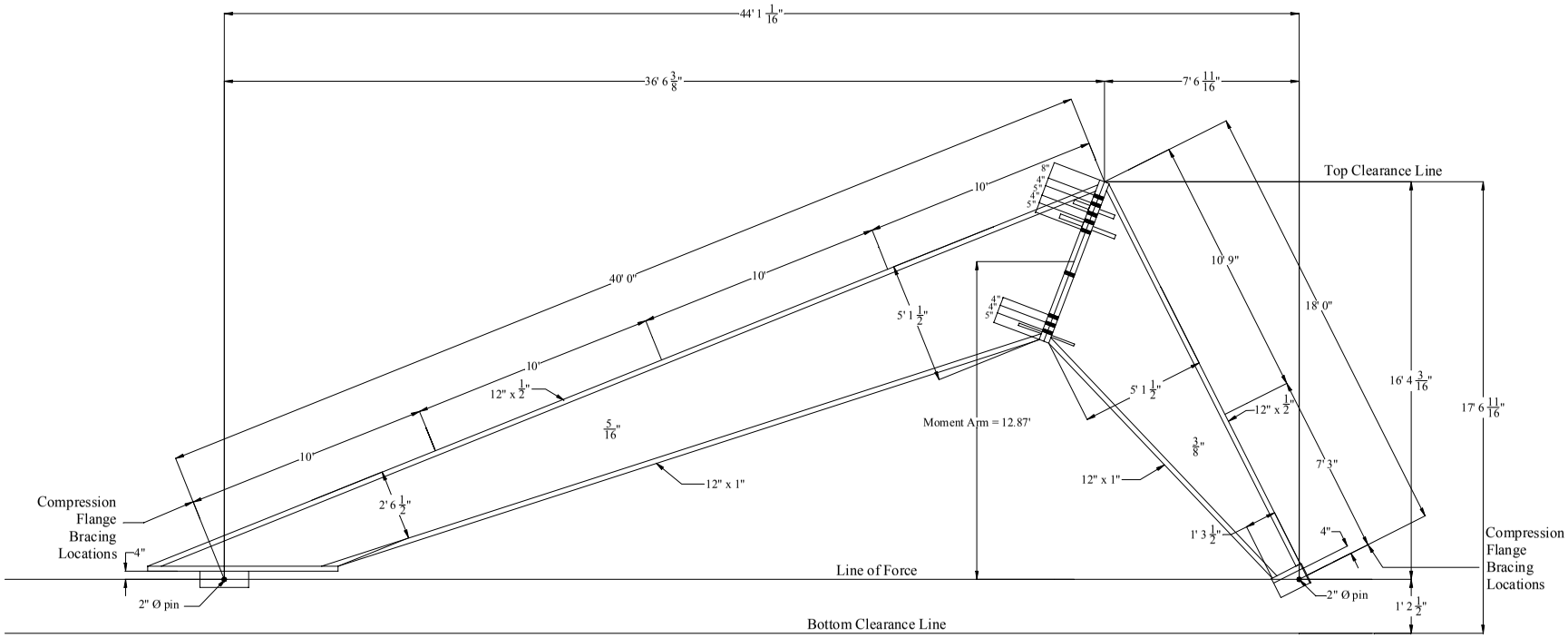

Figure F.1 Specimen Nominal Dimensions for Test F5S-$1^{1}/_{4}$-$^{3}/_{4}$-84

Table F.1 Geometric Dimensions and Material Properties for Test F5S-$1^1/_4$-$^3/_4$-84

	Nominal Specimen Dimensions	Measured Specimen Dimensions	Measured Yield Stress *	Measured Ultimate Stress	% Elongation
Rafter					
Top Flange	$^1/_2$" x 12" x 42' 3 $^{15}/_{16}$"	0.506" x 12" x 42' 6 $^1/_2$"	56.0 ksi	80.6 ksi	26.0 %
Web	$^5/_{16}$"	0.309"	46.0 ksi	66.3 ksi	27.5 %
Bottom Flange	1" x 12" x 30' 10 $^3/_4$"	1.012" x 12" x 30' 11$^1/_2$"	55.6 ksi	84.3 ksi	25.8 %
End Plate	$^3/_4$" x 12" x 7'	0.775" x 12" x 7' $^4/_{16}$"	55.2 ksi	83.3 ksi	26.0 %
Column					
Top Flange	$^1/_2$" x 12" x 17' 5 $^9/_{16}$"	0.506" x 12" x 17' 7 $^1/_2$"	56.6 ksi	80.8 ksi	27.0 %
Web	$^3/_8$"	0.369"	49.2 ksi	68.3 ksi	26.0 %
Bottom Flange	1" x 12" x 13' 3 $^3/_4$"	1.013" x 12" x 13' 5 $^1/_2$"	56.1 ksi	84.7 ksi	27.0 %
End Plate	$^3/_4$" x 12" x 7'	0.774" x 12" x 7'	55.2 ksi	83.3 ksi	26.0 %

* Nominal Yield Stress = 50 ksi

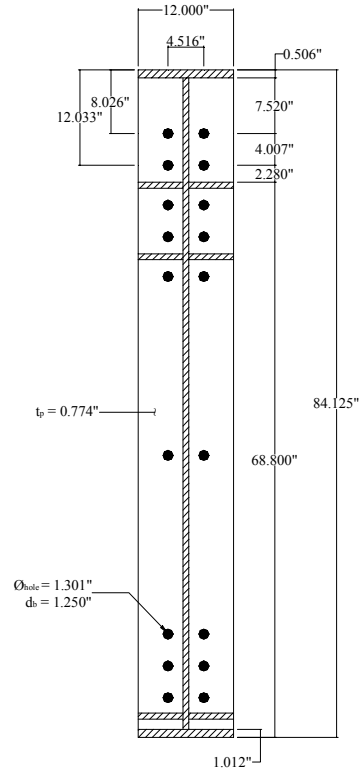

Figure F.2 Average Measured Connection Details for Test F5S-$1^1/_4$-$^3/_4$-84

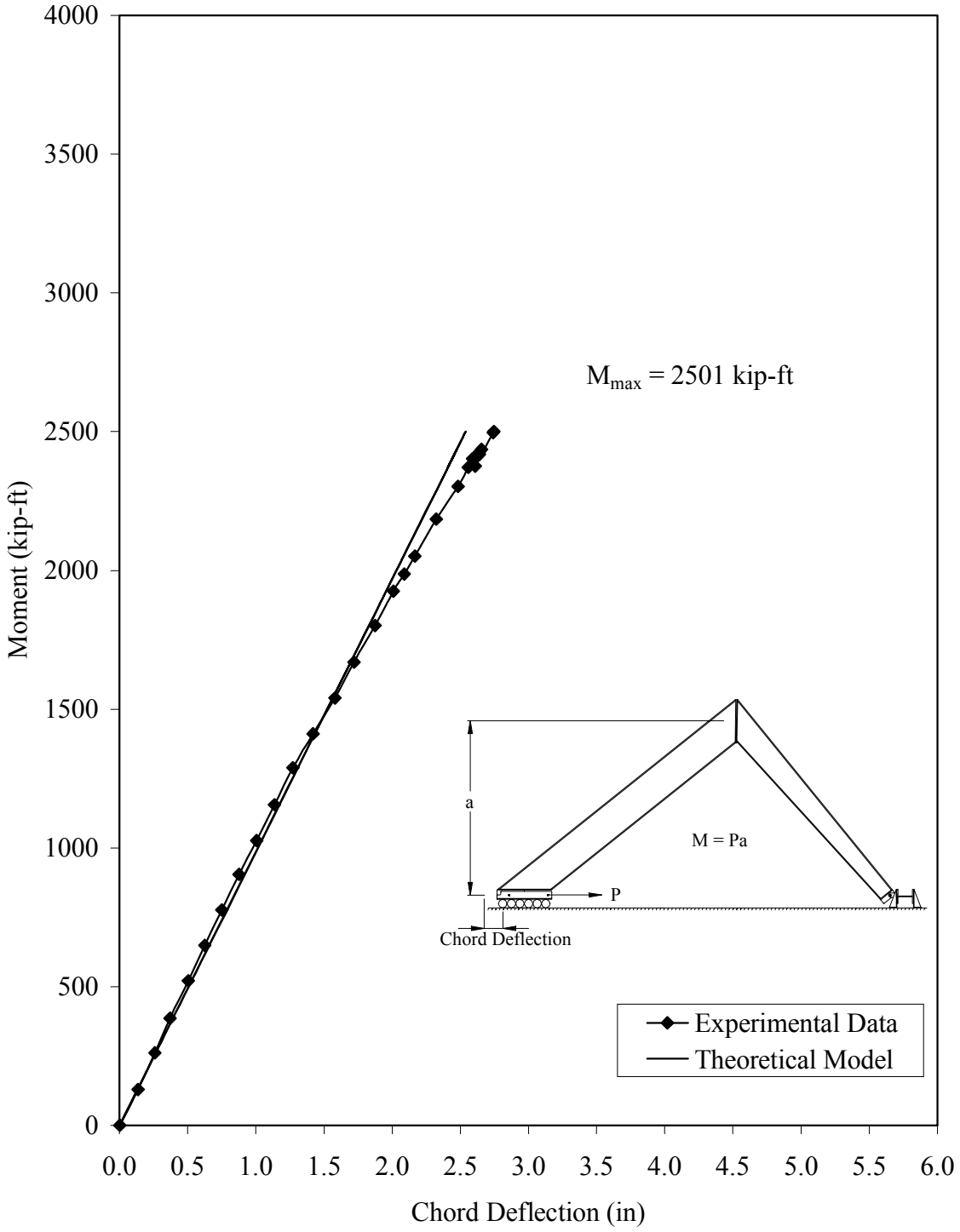

Figure F.3 Applied Moment vs. Chord Deflection for Cycle 1 in Test F5S-$1^{1}/_{4}$-$^{3}/_{4}$-84

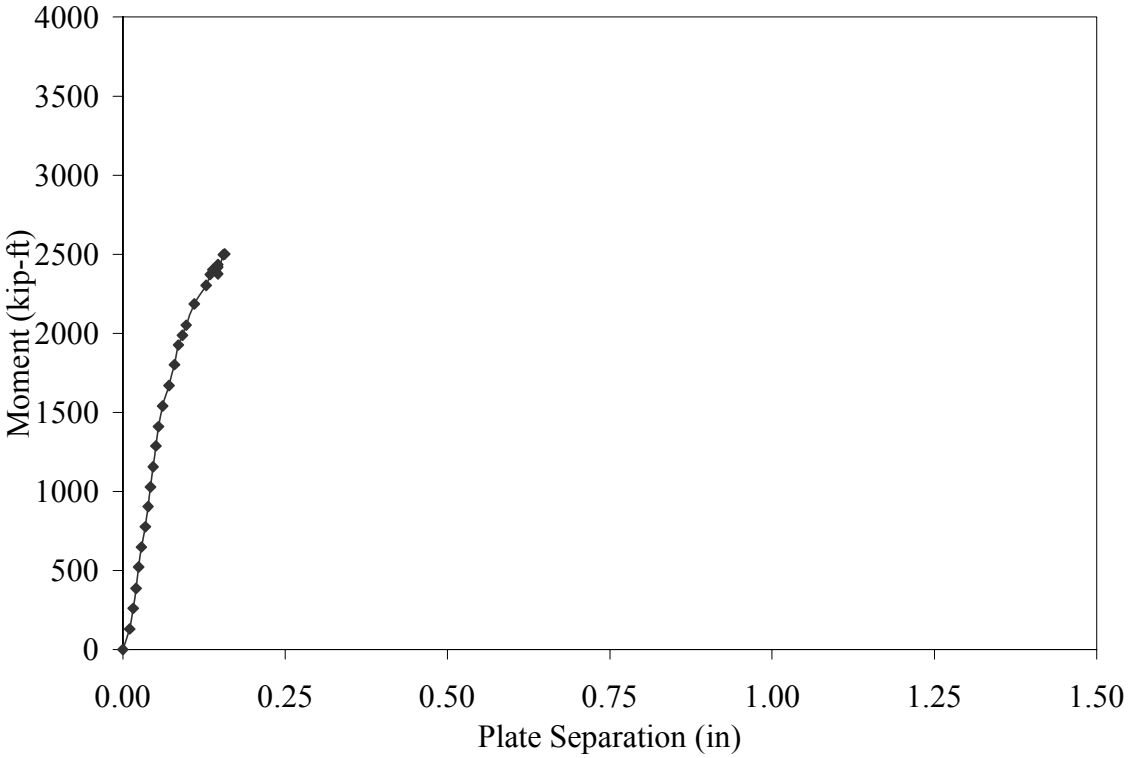

Figure F.4 Applied Moment vs. Plate Separation for Cycle 1 in Test F5S-$1^{1}/_{4}$-$^{3}/_{4}$-84

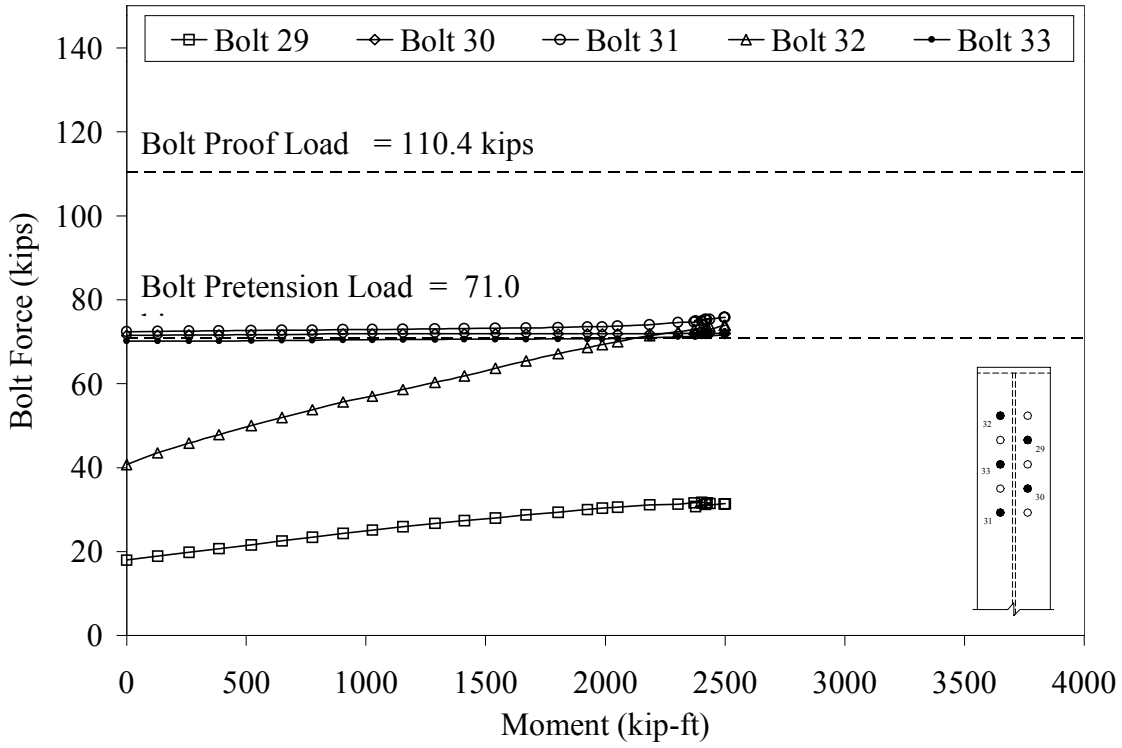

Figure F.5 Bolt Force vs. Applied Moment for Cycle 1 in Test F5S-$1^{1}/_{4}$-$^{3}/_{4}$-84

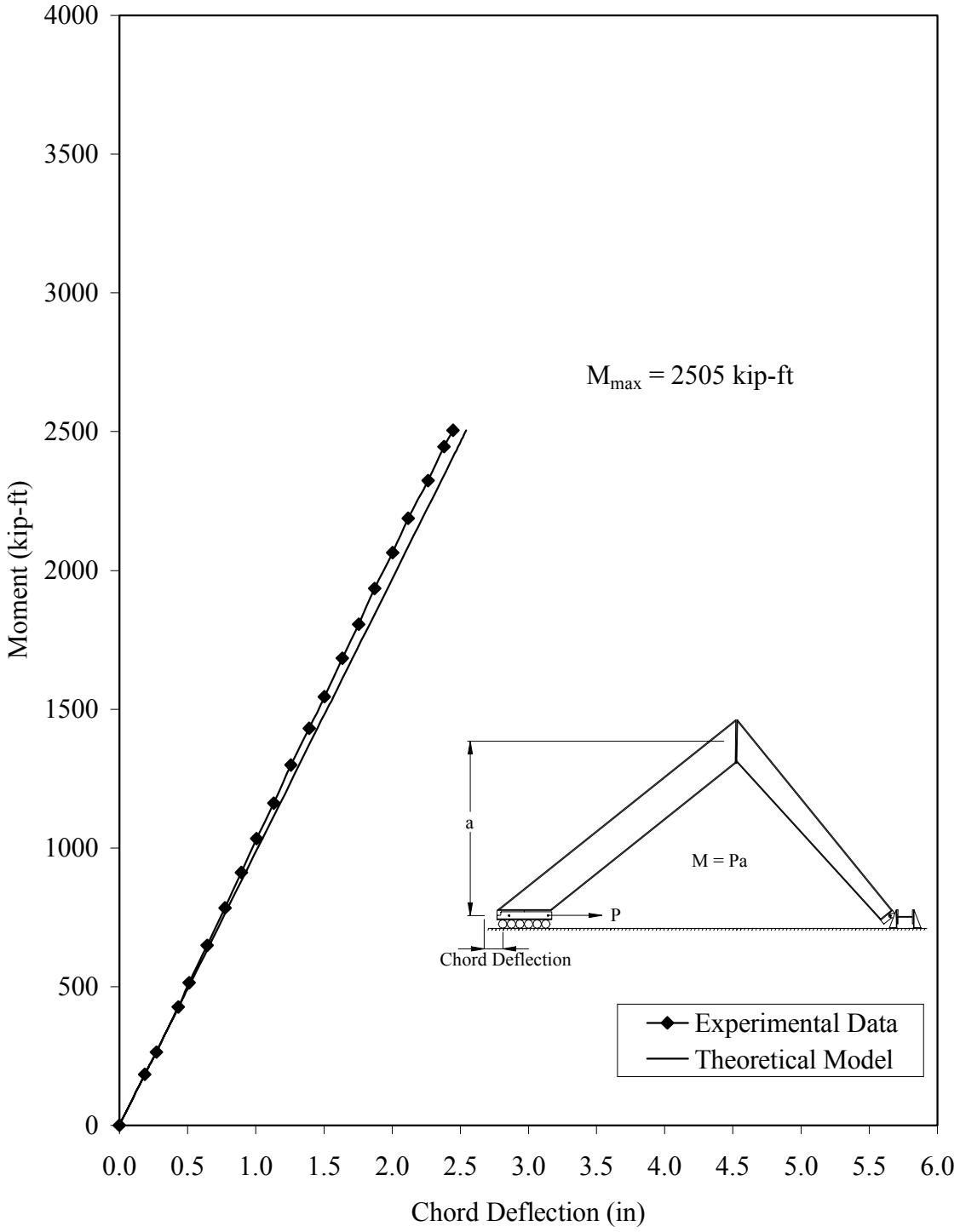

Figure F.6 Applied Moment vs. Chord Deflection for Cycle 2 in Test F5S-$1^{1}/_{4}$-$^{3}/_{4}$-84

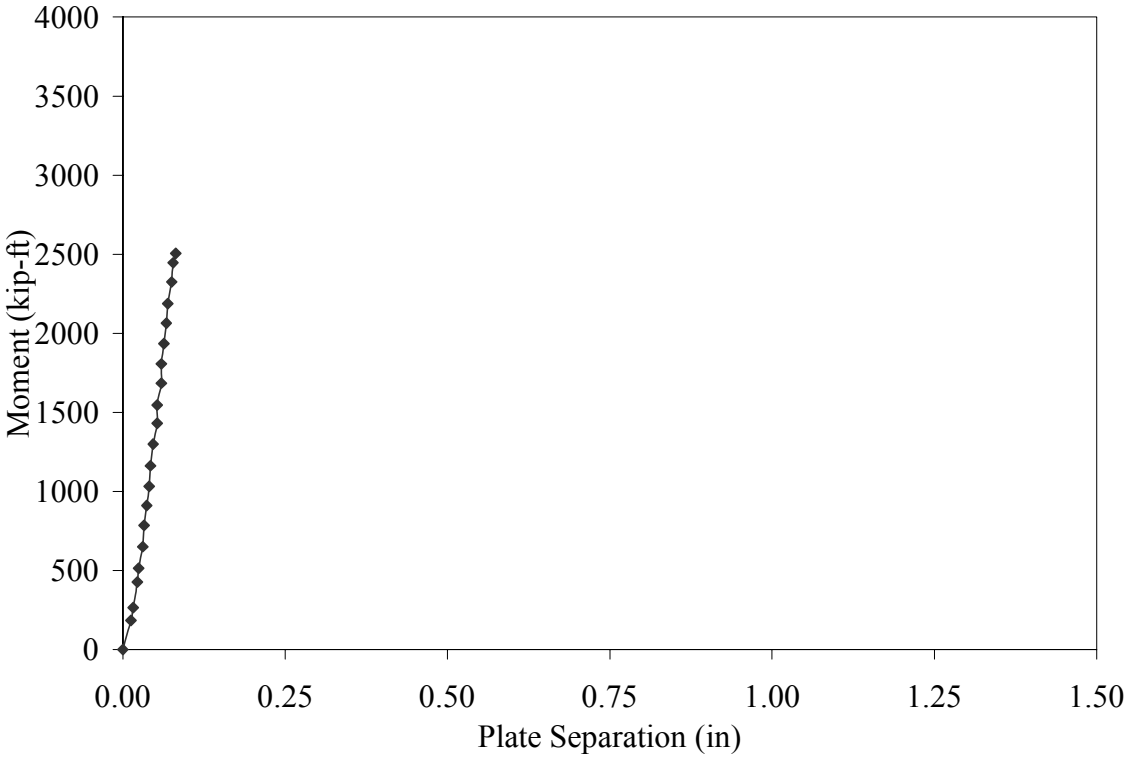

Figure F.7 Applied Moment vs. Plate Separation for Cycle 2 in Test F5S-$1^{1}/_{4}$-$^{3}/_{4}$-84

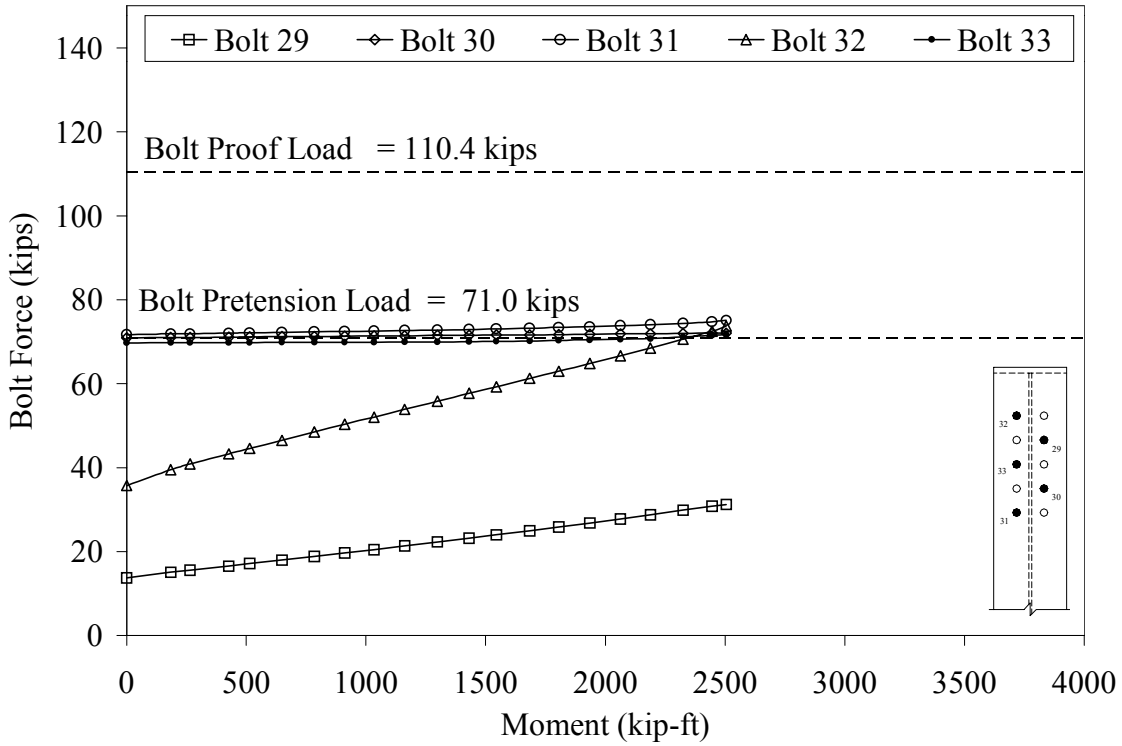

Figure F.8 Bolt Force vs. Applied Moment for Cycle 2 in Test F5S-$1^{1}/_{4}$-$^{3}/_{4}$-84

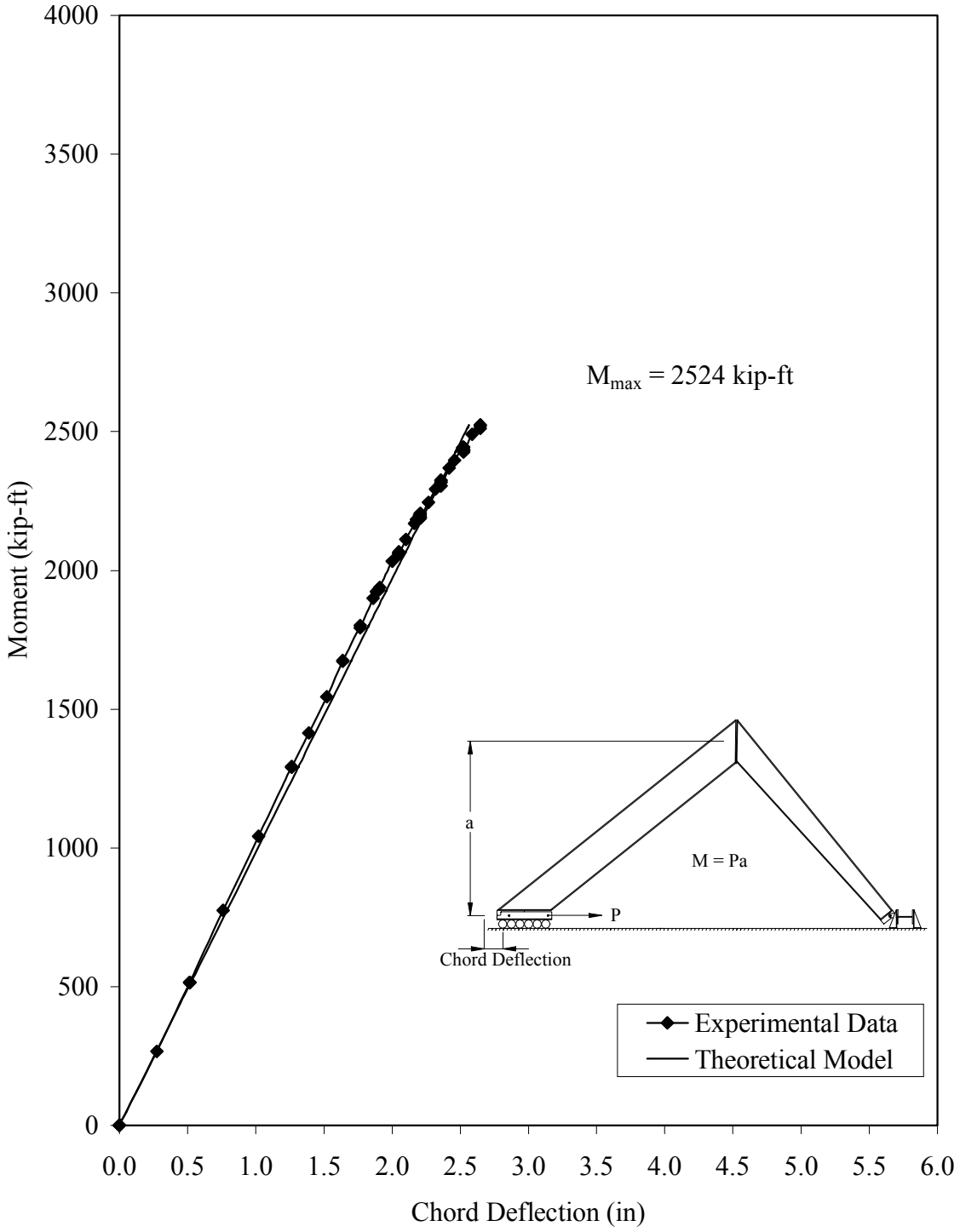

Figure F.9 Applied Moment vs. Chord Deflection for Cycle 3 in Test F5S-$1^{1}/_{4}$-$^{3}/_{4}$-84

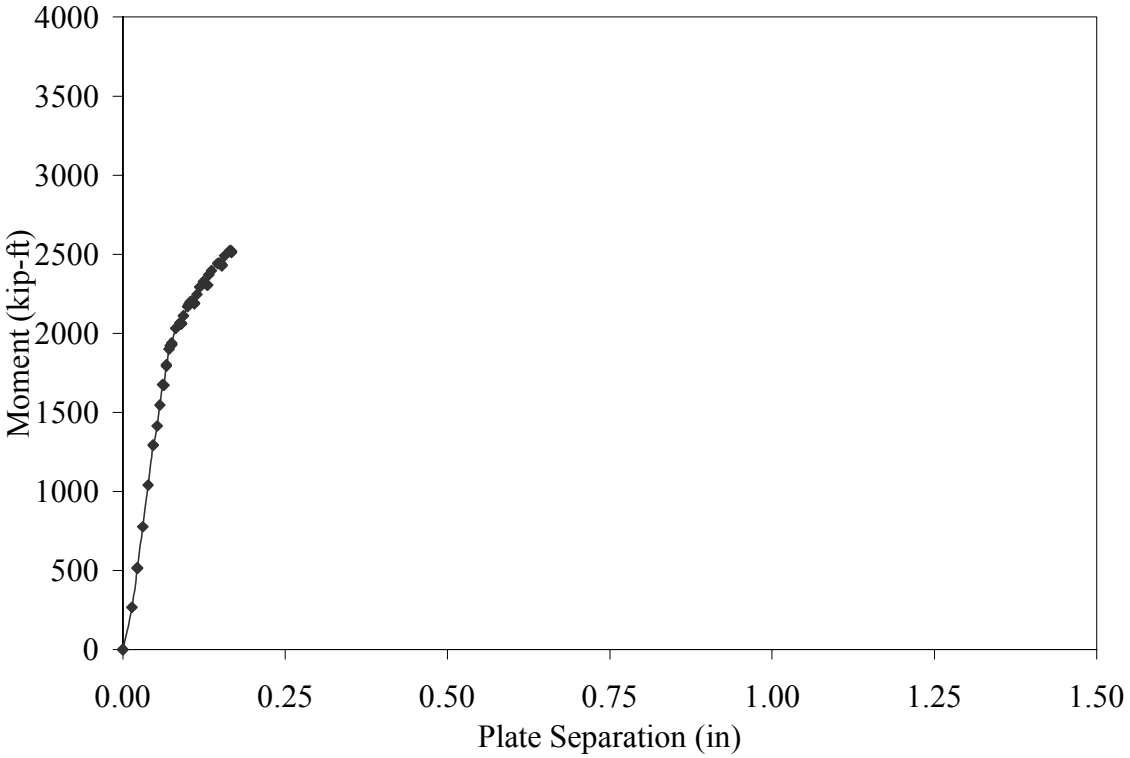

Figure F.10 Applied Moment vs. Plate Separation for Cycle 3 in Test F5S-1$^{1}/_{4}$-$^{3}/_{4}$-84

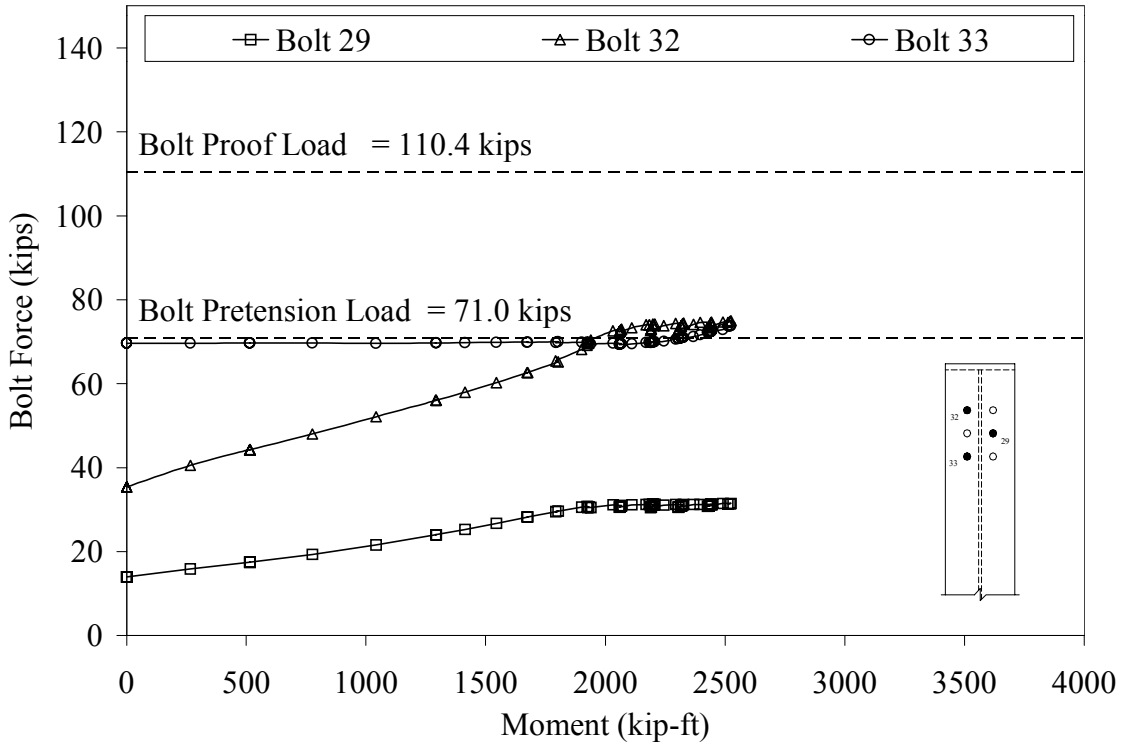

Figure F.11 Bolt Force vs. Applied Moment for Cycle 3 in Test F5S-1$^{1}/_{4}$-$^{3}/_{4}$-84

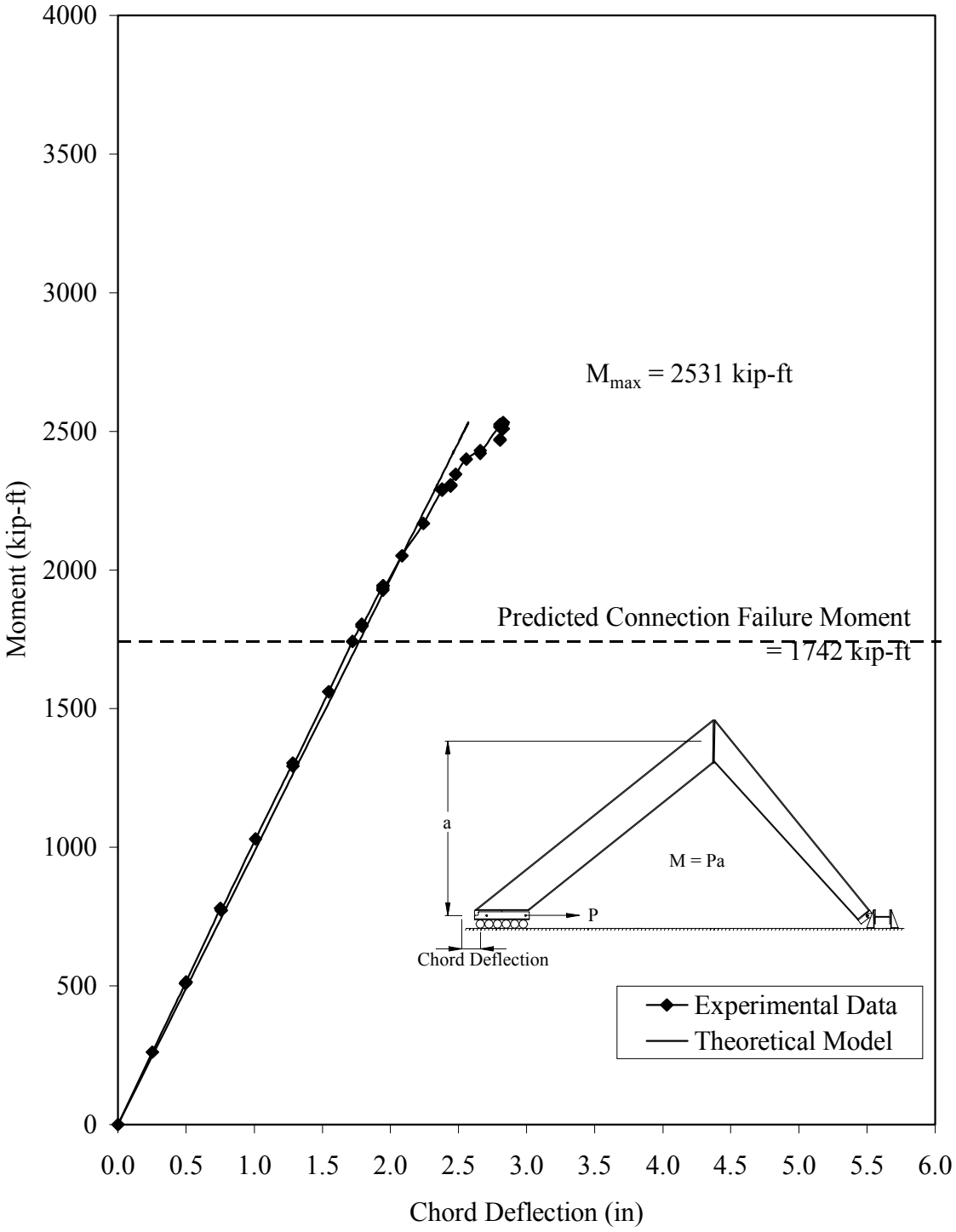

Figure F.12 Applied Moment vs. Chord Deflection for Cycle 4 in Test F5S-$1^{1}/_{4}$-$^{3}/_{4}$-84

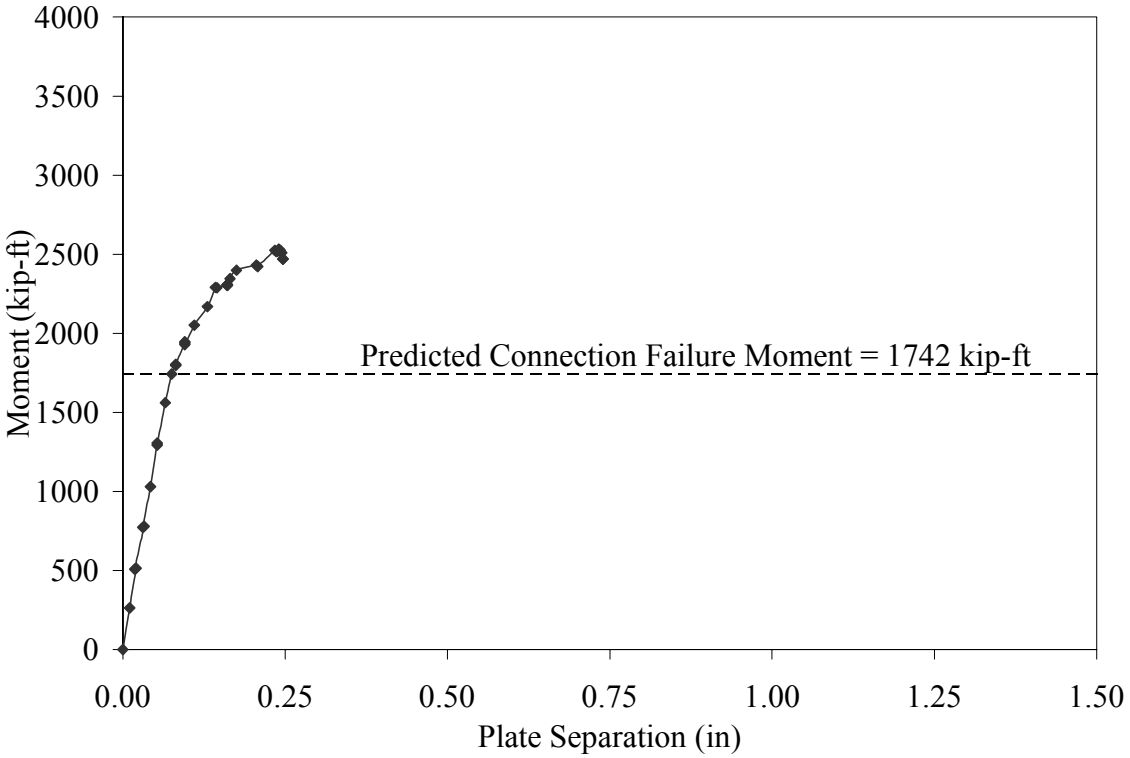

Figure F.13 Applied Moment vs. Plate Separation for Cycle 4 in Test F5S-$1^{1}/_{4}$-$^{3}/_{4}$-84

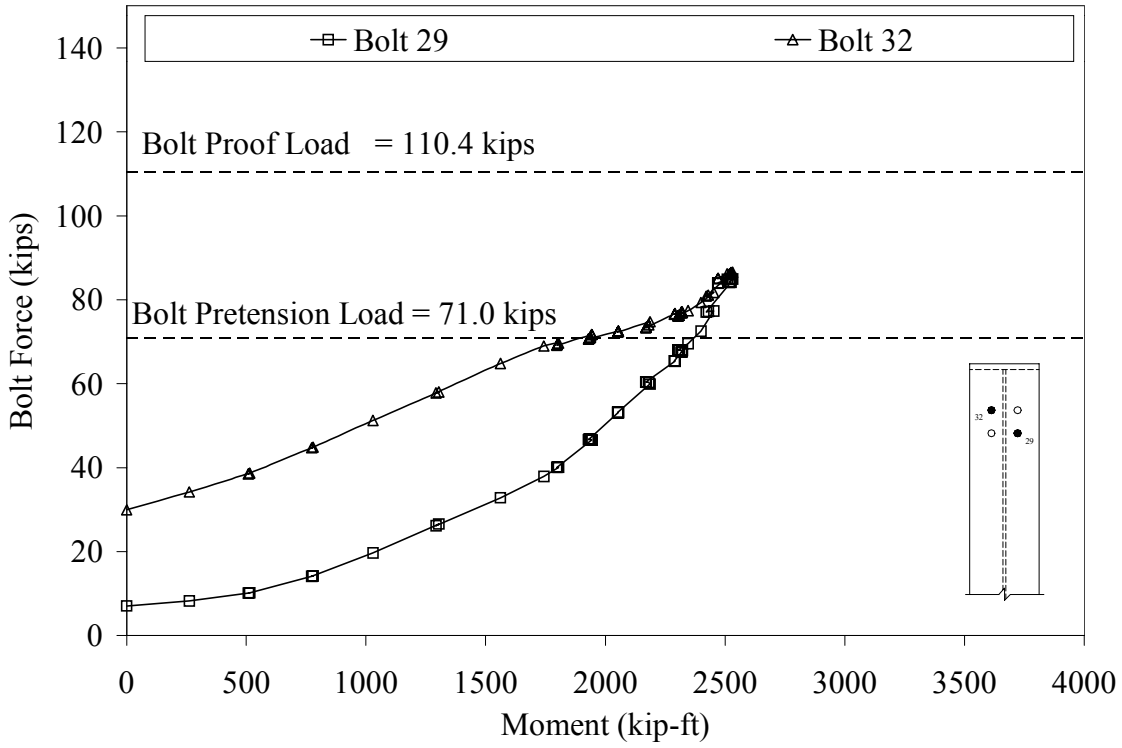

Figure F.14 Bolt Force vs. Applied Moment for Cycle 4 in Test F5S-$1^{1}/_{4}$-$^{3}/_{4}$-84

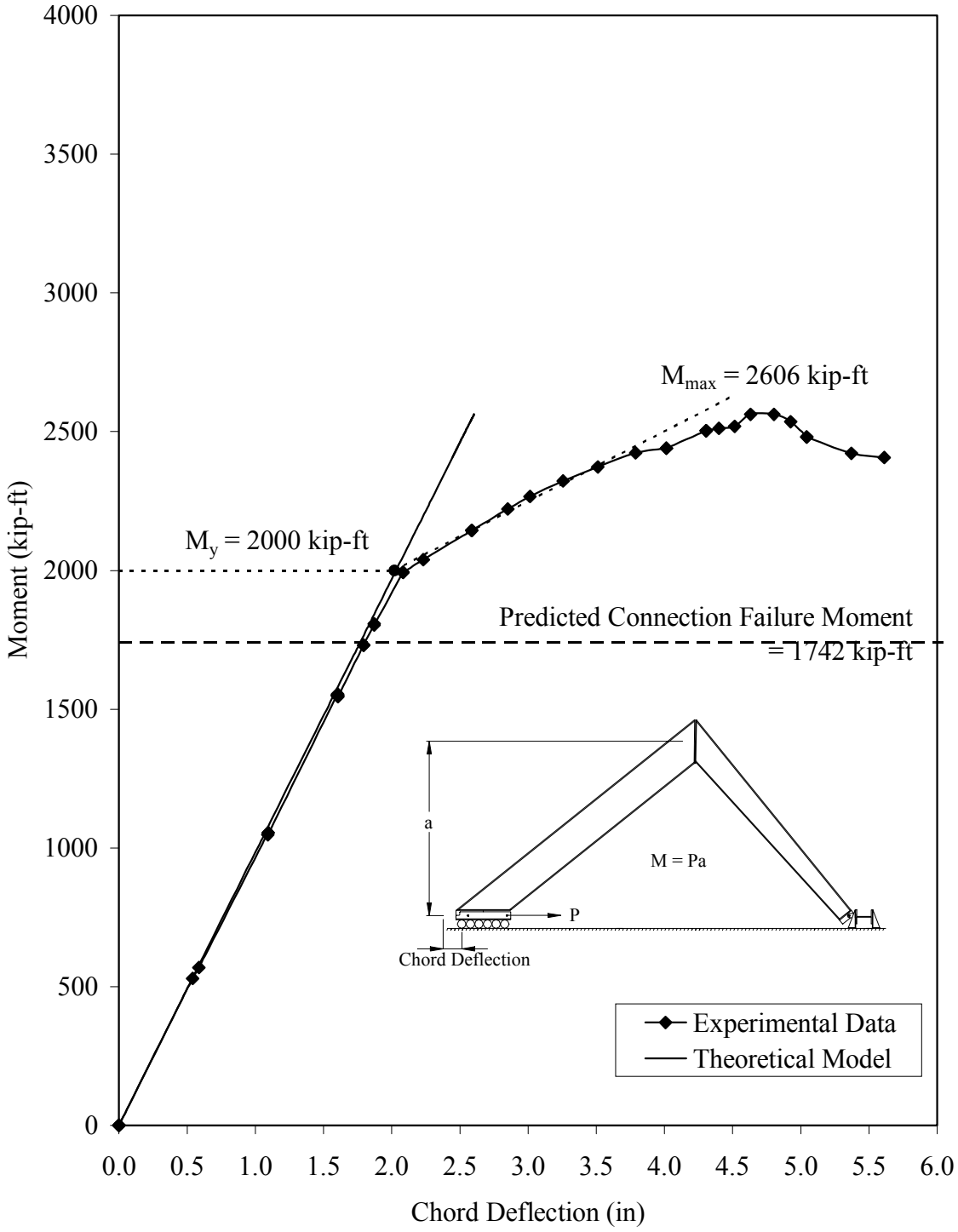

Figure F.15 Applied Moment vs. Chord Deflection for Cycle 5 in Test F5S-$1^1/_4$-$^3/_4$-84

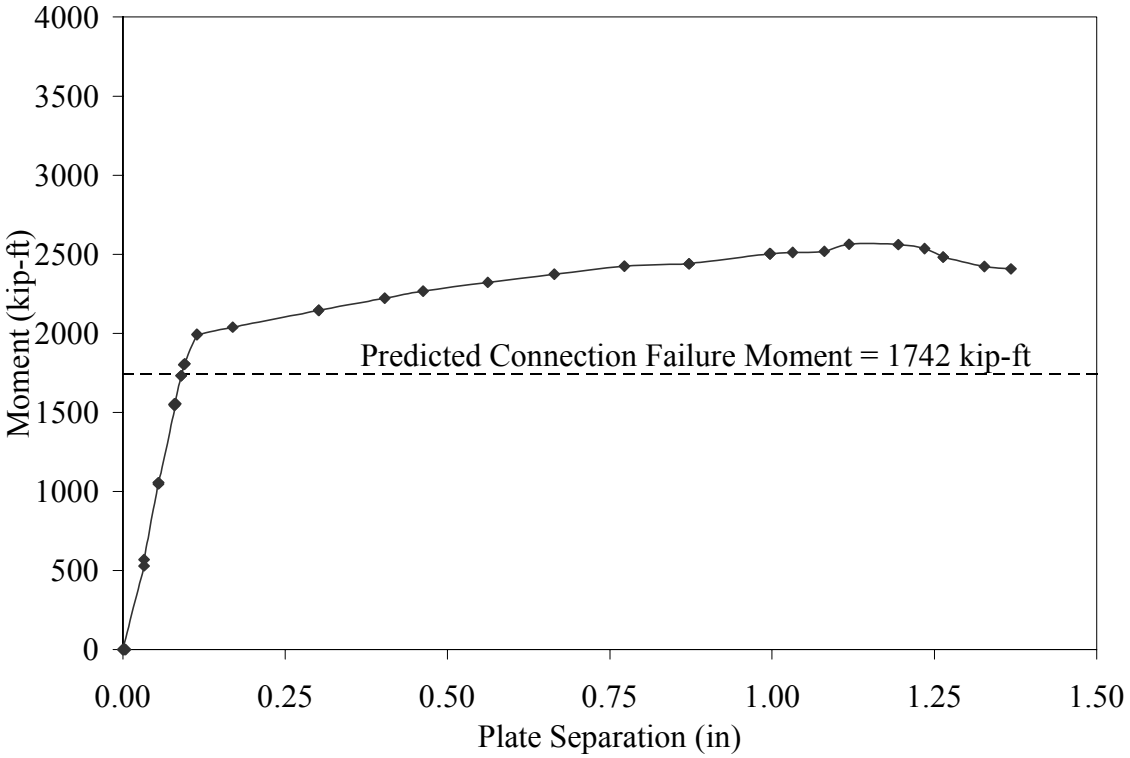

Figure F.16 Applied Moment vs. Plate Separation for Cycle 5 in Test F5S-$1^{1}/_{4}$-$^{3}/_{4}$-84

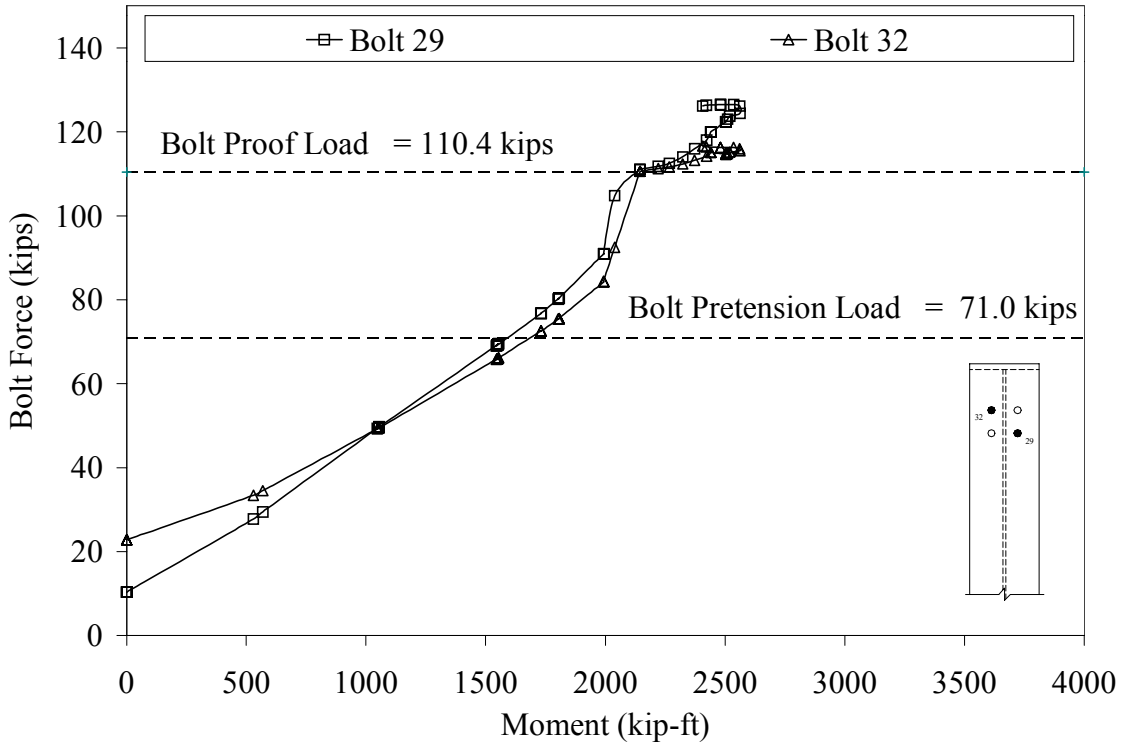

Figure F.17 Bolt Force vs. Applied Moment for Cycle 5 in Test F5S-$1^{1}/_{4}$-$^{3}/_{4}$-84

a) Yielding of Column and Rafter Web

c) Yielding of Rafter Flange

Figure F.18 F5S-$1^{1}/_{4}$-$^{3}/_{4}$-84 at end of Test

APPENDIX G

MRE$^{1}/_{4}$-1$^{1}/_{4}$-1-70$^{1}/_{2}$ GIRDER TEST RESULTS

TEST NAME: MRE$^{1}/_{4}$-1$^{1}/_{4}$-1-70$^{1}/_{2}$
TEST DATE: January 25, 2000

CONNECTION DESCRIPTION

NOMINAL YIELD STRESS	50 ksi
NUMBER OF TENSION BOLTS	10
NUMBER OF STITCH BOLTS	2
NUMBER OF COMPRESSION BOLTS	10
NOMINAL GAGE	4.5 in.
NOMINAL PITCH	4 in.
NOMINAL END PLATE WIDTH	12 in.
NOMINAL END PLATE LENGTH	70.5 in.
NOMINAL END PLATE THICKNESS	1.0 in.

BOLT DATA

BOLT DIAMETER	1 1/4 in.
BOLT TYPE	A325
BOLT PRETENSION	71 kips

PLATE GIRDER DATA

NOMINAL FLANGE WIDTH	12 in.
NOMINAL TOP FLANGE THICKNESS	0.750 in.
NOMINAL BOTTOM FLANGE THICKNESS	0.750 in.
NOMINAL WEB THICKNESS	0.375 in.

EXPERIMENTAL

MAXIMUM APPLIED LOAD	265 kips
MAXIMUM APPLIED END-PLATE MOMENT	3044 kip-ft
FAILURE LOCATION	Specimen did not fail
FAILURE MODE	Specimen did not fail
PREDICTED CONNECTION FAILURE MOMENT	3399 kip-ft

TEST NAME: MRE$^{1}/_{4}$-1$^{1}/_{4}$-1-70$^{1}/_{2}$
TEST DATE: January 25, 2000

DISCUSSION

Before testing, the data acquisition system was zeroed, except for the bolt and web strain gage channels. The load was applied at 10 kip intervals. The bolt strains did not increase until the load reached approximately 100 kips. After that point, the two outermost tension bolts steadily increased in strain with load. The theoretical deflection correlated with the actual deflection up to a load of 50 kips, after which the actual deflection slowly deviated away from the theoretical with load (the specimen lost stiffness). At approximately 140 kips, the web strain gage readings exceeded the yield strain. After 200 kips, there was a steady increase in plate separation. Yielding was visible on both end plates around the tension bolts. There was also slight yielding visible along the top flange, particularly near the connection. The specimen reached a maximum load of 265 kips, at which the strain in Bolt #23 was approximately 15,000 microstrains. The specimen was then unloaded. The specimen did not reach failure. The specimen strength exceeded the capacity of the test setup.

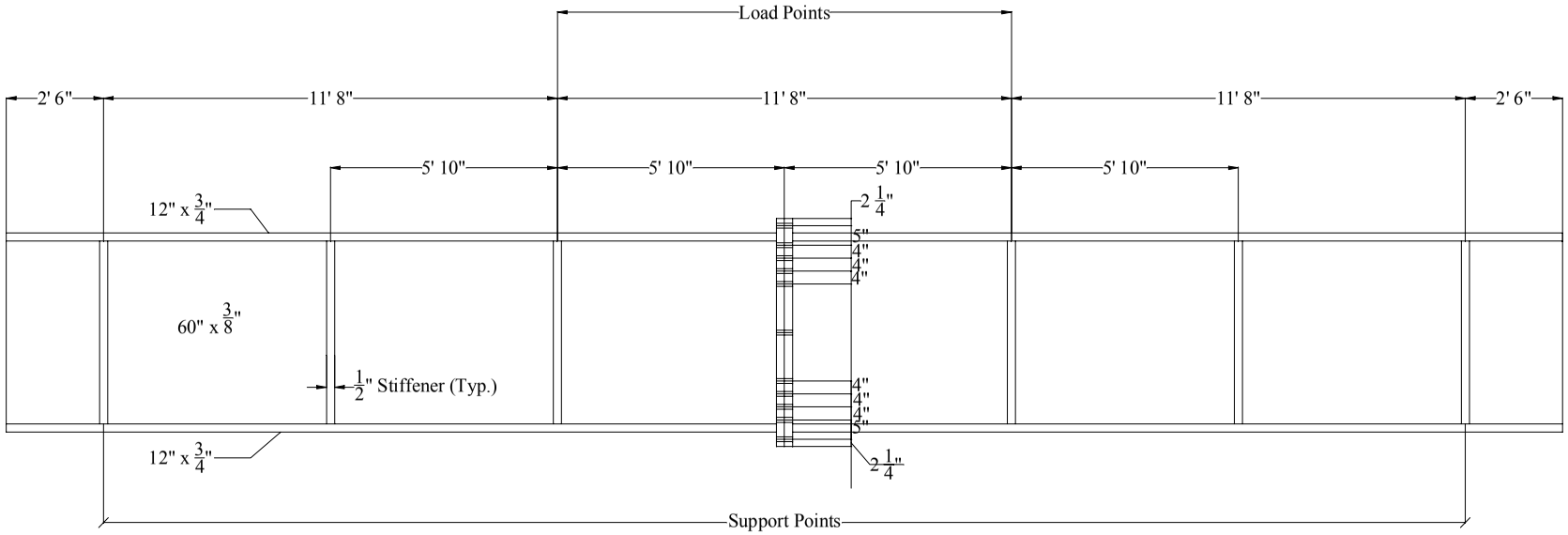

Figure G.1 Specimen Nominal Dimensions for Test MRE$^{1}/_{4}$-1$^{1}/_{4}$-1-70$^{1}/_{2}$

Table G.1 Geometric Dimensions and Material Properties for Test MRE$^{1}/_{4}$-1$^{1}/_{4}$-1-70$^{1}/_{2}$

	Nominal Specimen Dimensions	Measured Specimen Dimensions	Measured Yield Stress *	Measured Ultimate Stress	% Elongation
Plate Girder A					
Top Flange	$^{3}/_{8}$" x 60" x 19' 11"	0.375" x 60" x 19' 11 $^{1}/_{16}$"	**	**	**
Web	$^{3}/_{4}$" x 12" x 19' 11"	0.773" x 12" x 19' 11 $^{1}/_{16}$"	**	**	**
Bottom Flange	$^{3}/_{4}$" x 12" x 19' 11"	0.780" x 12" x 19' 11 $^{1}/_{16}$"	**	**	**
End Plate	1" x 12" x 5' 10 $^{1}/_{2}$"	1.018" x 12" x 5' 10 $^{9}/_{16}$"	54.9 ksi	85.4 ksi	26.0 %
Plate Girder B					
Top Flange	$^{3}/_{8}$" x 60" x 19' 11"	0.375" x 60 $^{1}/_{16}$" x 19' 10 $^{15}/_{16}$"	**	**	**
Web	$^{3}/_{4}$" x 12" x 19' 11"	0.773" x 12" x 19' 10 $^{15}/_{16}$"	**	**	**
Bottom Flange	$^{3}/_{4}$" x 12" x 19' 11"	0.774" x 12" x 19' 10 $^{15}/_{16}$"	**	**	**
End Plate	1" x 12" x 5' 10 $^{1}/_{2}$"	1.025" x 12 " x 5' 10 $^{9}/_{16}$"	54.9 ksi	85.4 ksi	26.0 %

* Nominal Yield Stress = 50 ksi

** No coupons were tested from this specimen

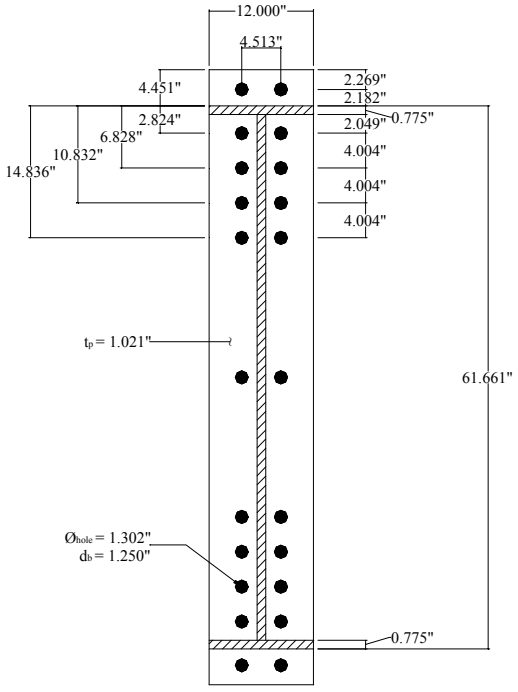

Figure G.2 Average Measured Connection Details for Test MRE$^{1}/_{4}$-1$^{1}/_{4}$-1-70$^{1}/_{2}$

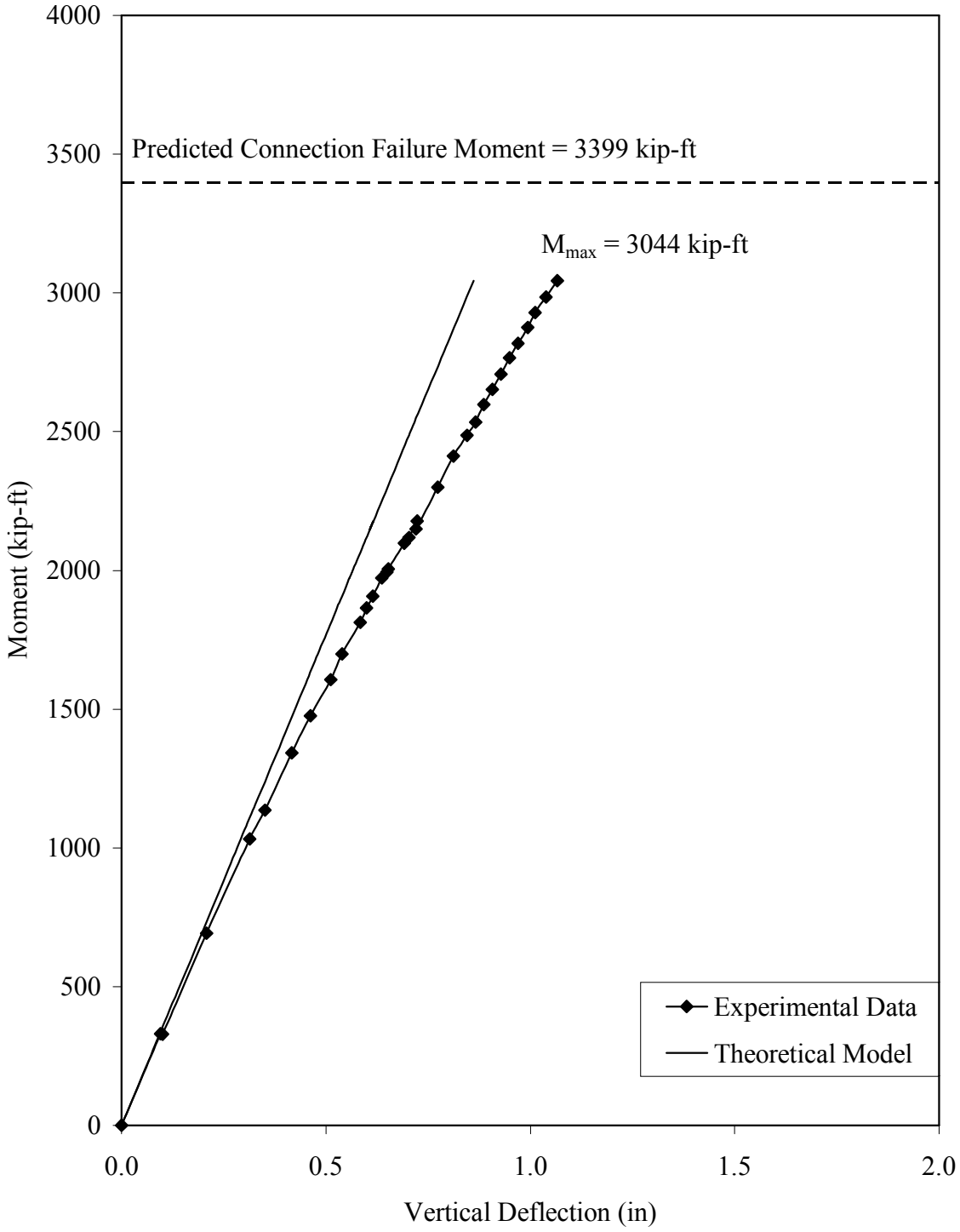

Figure G.3 Applied Moment vs. Average Vertical Deflection at the Load Points for Test MRE$^{1}/_{4}$-1$^{1}/_{4}$-1-70$^{1}/_{2}$

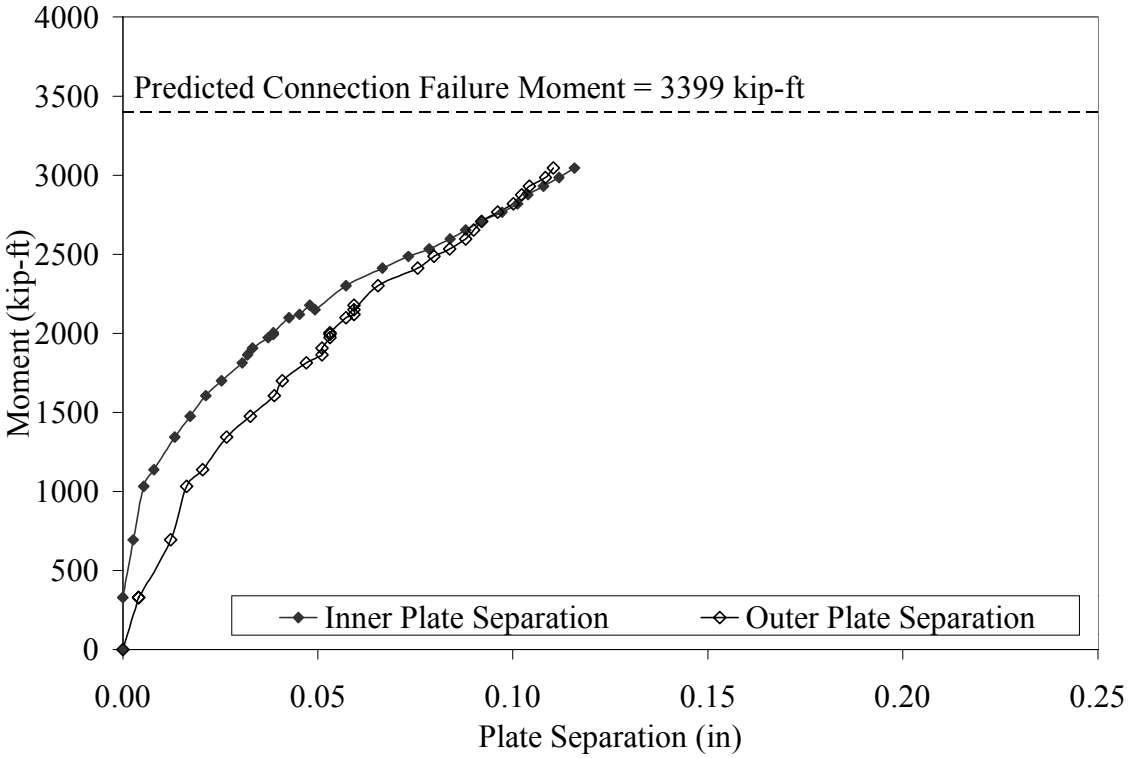

Figure G.4 Applied Moment vs. Plate Separation for Test MRE$^{1}/_{4}$-1$^{1}/_{4}$-1-70$^{1}/_{2}$

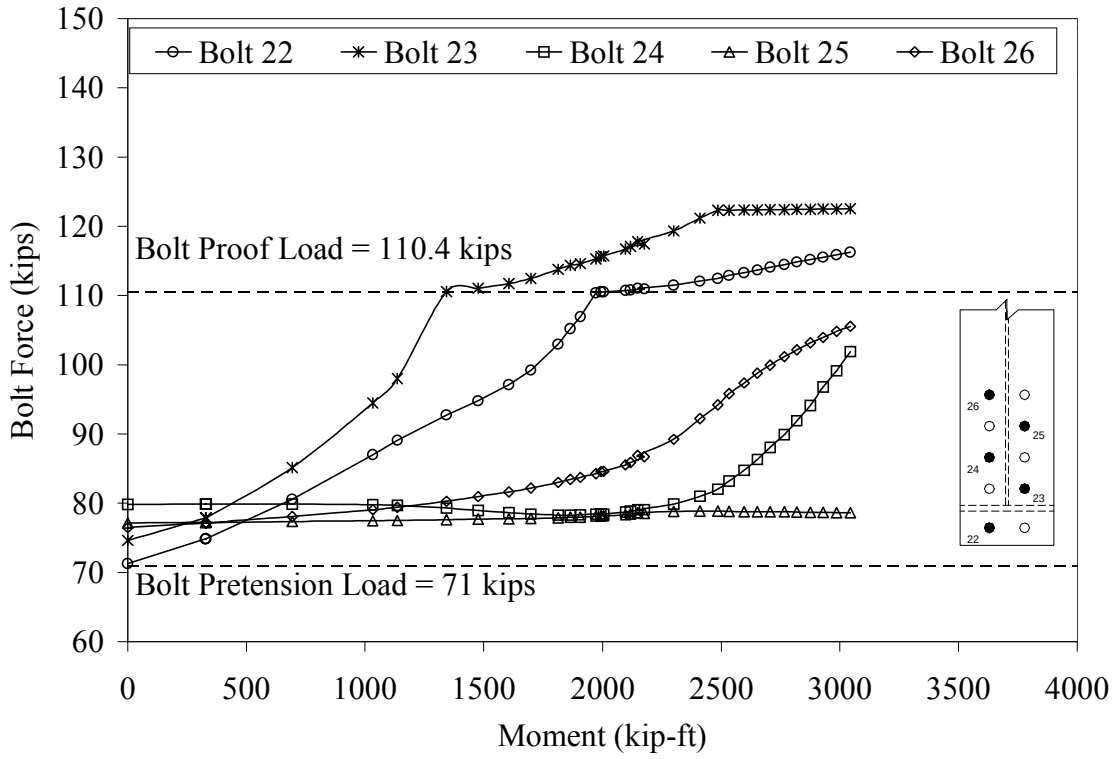

Figure G.5 Bolt Force vs. Applied Moment for Test MRE$^{1}/_{4}$-1$^{1}/_{4}$-1-70$^{1}/_{2}$

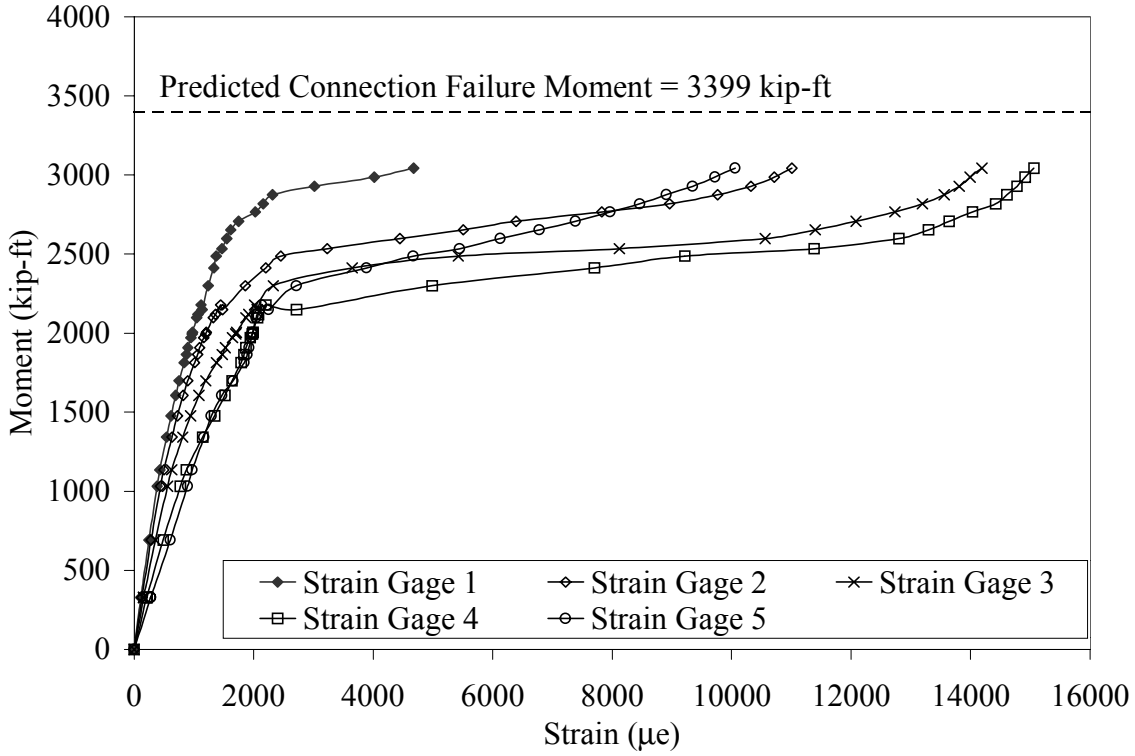

Figure G.6 Applied Moment vs. Web Strain for Test MRE$^{1}/_{4}$-1$^{1}/_{4}$-1-70$^{1}/_{2}$

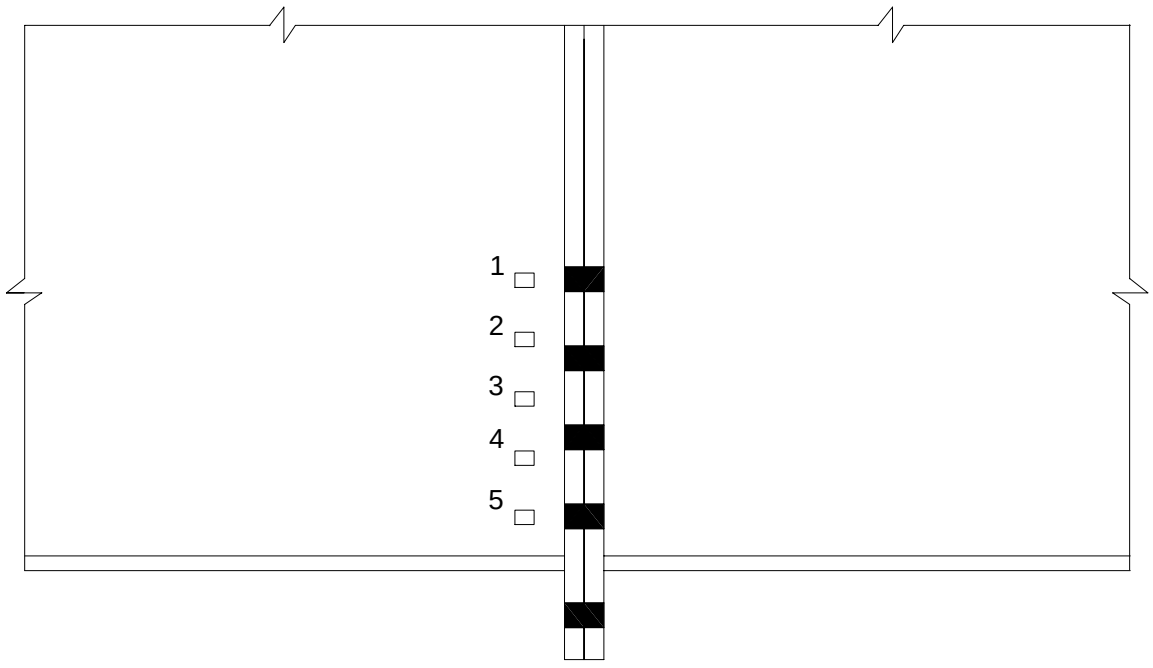

Figure G.7 Strain Gage Locations for Test MRE$^{1}/_{4}$-1$^{1}/_{4}$-1-70$^{1}/_{2}$

a) Connection After Testing

d) Yielding of End-Plate
(Note: Chalk was used to outline where yielding has occurred.)

Figure G.8 MRE$^{1}/_{4}$-1$^{1}/_{4}$-1-70$^{1}/_{2}$ at end of Test

VITA

Vincenza Maria Italiano was born in Elizabeth, New Jersey on February 3, 1976. She graduated from Roselle Catholic High School in Roselle, New Jersey in 1994. In 1998, she graduated from Rutgers University with a Bachelor of Science in Civil Engineering. She worked for a year as an environmental engineering with Najarian Associates in Eatontown, New Jersey. In July 1999, she enrolled in the graduate program in the Structural Engineering and Materials Division at Virginia Polytechnic Institute and State University in Blacksburg, Virginia. She is currently working at Weidlinger Associates located in New York, NY.